Article

STING inhibits the reactivation of dormant metastasis in lung adenocarcinoma

https://doi.org/10.1038/s41586-023-05880-5

Received: 7 December 2021

Accepted: 22 February 2023

Published online: 29 March 2023

Check for updates

Jing Hu[1], Francisco J. Sánchez-Rivera[1,11,12], Zhenghan Wang[1], Gabriela N. Johnson[1], Yu-jui Ho[1], Karuna Ganesh[2,3], Shigeaki Umeda[4], Siting Gan[1], Adriana M. Mujal[5], Rebecca B. Delconte[5], Jessica P. Hampton[1], Huiyong Zhao[6], Sanjay Kottapalli[7], Elisa de Stanchina[6], Christine A. Iacobuzio-Donahue[4,8], Dana Pe'er[7,9,10], Scott W. Lowe[1,10], Joseph C. Sun[5] & Joan Massagué[1,9] ✉

Metastasis frequently develops from disseminated cancer cells that remain dormant after the apparently successful treatment of a primary tumour. These cells fluctuate between an immune-evasive quiescent state and a proliferative state liable to immune-mediated elimination[1–6]. Little is known about the clearing of reawakened metastatic cells and how this process could be therapeutically activated to eliminate residual disease in patients. Here we use models of indolent lung adenocarcinoma metastasis to identify cancer cell-intrinsic determinants of immune reactivity during exit from dormancy. Genetic screens of tumour-intrinsic immune regulators identified the stimulator of interferon genes (STING) pathway as a suppressor of metastatic outbreak. STING activity increases in metastatic progenitors that re-enter the cell cycle and is dampened by hypermethylation of the *STING* promoter and enhancer in breakthrough metastases or by chromatin repression in cells re-entering dormancy in response to TGFβ. STING expression in cancer cells derived from spontaneous metastases suppresses their outgrowth. Systemic treatment of mice with STING agonists eliminates dormant metastasis and prevents spontaneous outbreaks in a T cell- and natural killer cell-dependent manner—these effects require cancer cell STING function. Thus, STING provides a checkpoint against the progression of dormant metastasis and a therapeutically actionable strategy for the prevention of disease relapse.

Metastasis is the principal cause of death from cancer and frequently develops after a period of dormancy lasting for months up to decades depending on the type of tumour[6]. For example, nearly half of cases with an early diagnosis (stage I or II) of lung adenocarcinoma (LUAD) develop metastasis months to years after the treatment of the primary tumour[7]. This implies the existence of disseminated cancer cells that can reinitiate tumour growth after a period of dormancy[8,9]. Persistence of disseminated cancer cells in the bone marrow predicts increased risk for relapse[10]. TGFβ and other growth inhibitory signals in the host tissue cause proliferative quiescence in disseminated cancer cells[1,2,11], but this process is reversible. Immune-mediated elimination has emerged as an important barrier against the progression of dormant cancer cells that re-enter the cell cycle[2,3,5]. During dormancy, quiescent cancer cells downregulate the expression of natural killer (NK) cell-activating ligands and major histocompatibility complex (MHC) class I molecules to evade recognition by NK cells and T cells, respectively[2–4]. Depletion of these immune cells in mice harbouring dormant metastasis leads to macrometastatic outbreaks in multiple organs[2,3]. These observations suggest that disseminated cancer cell populations exist in an equilibrium between a predominant immune-evasive quiescent state and a proliferative state that undergoes elimination by the immune system. In line with this hypothesis, immunosuppressed recipients of organ transplants from donors who had long been cured of melanoma developed donor-derived metastatic disease[12]. A better understanding of the immune mechanisms that suppress the progression of indolent metastasis could be harnessed for improved elimination of dormant cancer cells and the prevention of aggressive disease relapse. Here we report that cancer cell-autonomous signalling by STING, the innate immune sensor of cytosolic double stranded DNA (dsDNA), is a powerful suppressor of reawakened LUAD metastatic cells.

Models of dormancy under immune control

To identify immune suppressors of dormant metastatic outbreak, we used models in which cancer cells derived from early-stage LUAD

[1]Cancer Biology and Genetics Program, Sloan Kettering Institute, Memorial Sloan Kettering Cancer Center, New York, NY, USA. [2]Molecular Pharmacology Program, Sloan Kettering Institute, Memorial Sloan Kettering Cancer Center, New York, NY, USA. [3]Department of Medicine, Memorial Sloan Kettering Cancer Center, New York, NY, USA. [4]Department of Pathology, Memorial Sloan Kettering Cancer Center, New York, NY, USA. [5]Immunology Program, Sloan Kettering Institute, Memorial Sloan Kettering Cancer Center, New York, NY, USA. [6]Antitumor Assessment Core, Memorial Sloan Kettering Cancer Center, New York, NY, USA. [7]Computational and Systems Biology Program, Sloan Kettering Institute, Memorial Sloan Kettering Cancer Center, New York, NY, USA. [8]Human Oncology and Pathogenesis Program, Memorial Sloan Kettering Cancer Center, New York, NY, USA. [9]The Alan and Sandra Gerry Metastasis and Tumor Ecosystems Center, Memorial Sloan Kettering Cancer Center, New York, NY, USA. [10]Howard Hughes Medical Institute, Memorial Sloan Kettering Cancer Center, New York, NY, USA. [11]David H. Koch Institute for Integrative Cancer Research, Massachusetts Institute of Technology, Cambridge, MA, USA. [12]Department of Biology, Massachusetts Institute of Technology, Cambridge, MA, USA. ✉e-mail: massaguj@mskcc.org

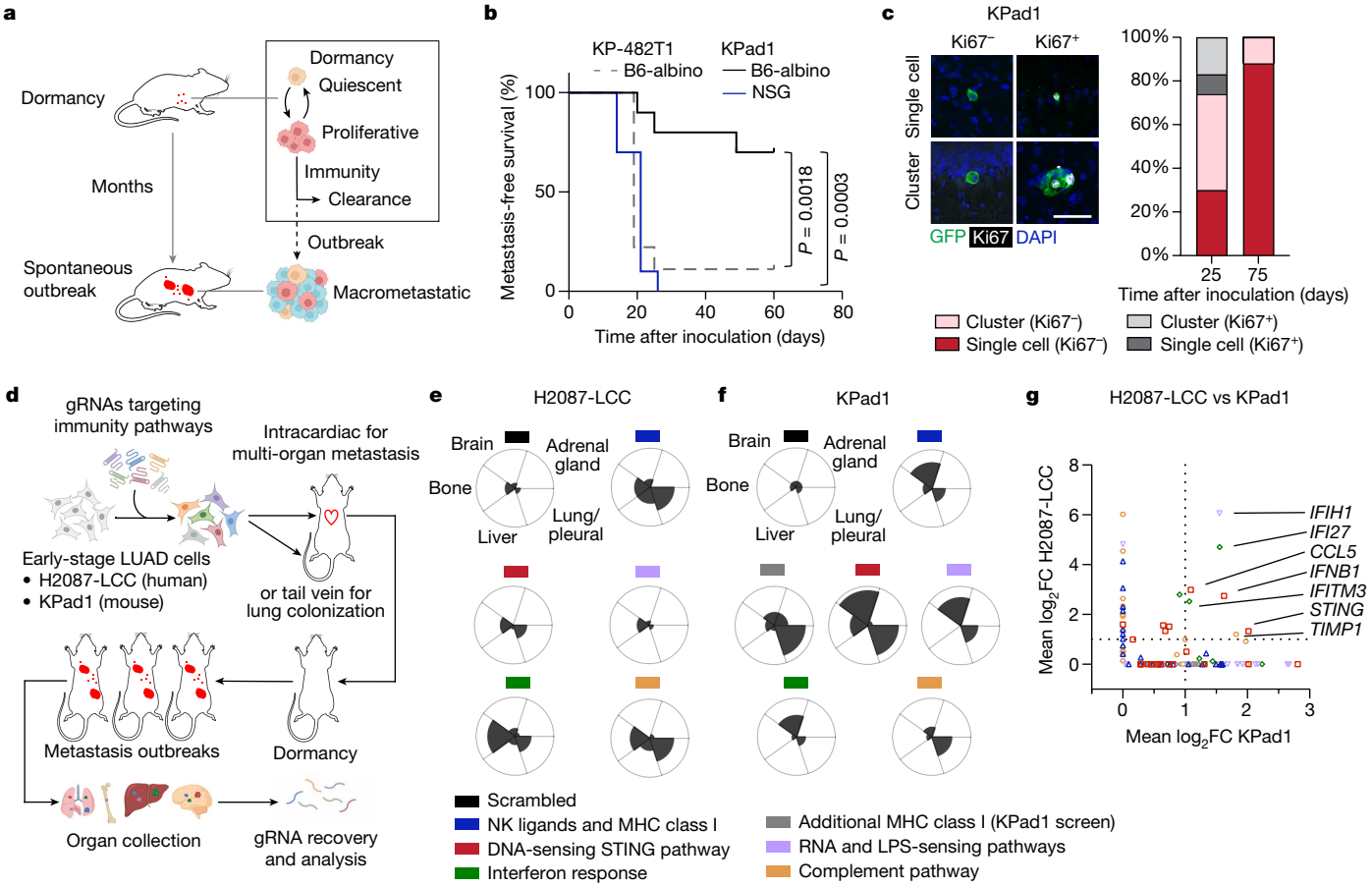

Fig. 1 | Genetic screens identify cell-autonomous immune regulators of dormant metastasis. a, Schematic of experimental models of metastatic dormancy in which disseminated cancer cells fluctuate between an immune-evasive quiescent state and a proliferative state eliminated by the immune system. **b**, Metastasis-free survival Kaplan–Meier plots of immunocompetent B6-albino or immunodeficient NSG mice intracardially inoculated with 2×10^4 KPad1 or KP-482T1 cells. $n = 9$ (KP-482T1) or 10 (KPad1) mice per group; log-rank test. **c**, Representative immunofluorescence (left) and quantification (right) of the proportion of KPad1 single cells and clusters in the brains of B6-albino mice 25 or 75 days after intracardiac inoculation of 2×10^4 cells. Scale bar, 50 µm. $n = 23$ (25 days) or 17 (75 days) single cells or clusters. **d**, Schematic of CRISPR screen design. **e**,**f**, Petal plots of metastasis incidence in specific organs after intracardiac inoculation of 2.5×10^5 H2087-LCC cells in athymic mice (**e**) or KPad1 cells in B6-albino mice (**f**). Cells were transduced with the indicated sgRNA pools. Metastasis progression was monitored by bioluminescence imaging (BLI) for 106 (**e**) or 62 days (**f**) after inoculation. The radius of each black petal represents the proportion of mice developing metastases in the indicated organ from 8–12 mice per pool (**e**) or 7–9 mice per pool (**f**). **g**, Enrichment of sgRNAs in multi-organ metastases from H2087-LCC and KPad1 cells after intracardiac inoculation into athymic mice or B6-albino mice, respectively. Genes with average $\log_2$ fold change ($\log_2$FC) > 0 are plotted. Genes targeted by the top enriched sgRNAs in both screens are listed. Owing to non-homology of genes encoding NK cell-activating ligands and MHC class I in human and mouse, these genes were scored in the H2087-LCC screen or the KPad1 screen but not both. See also Extended Data Figs. 1 and 2.

tumours are inoculated into the arterial circulation of mice to populate different organs, where metastases remain dormant for several months with few spontaneous outbreaks (Fig. 1a). We previously isolated and characterized one such model, H2087-LCC, derived from H2087 stage I human LUAD cells[2]. When inoculated into *Foxn1*^{nu} athymic nude mice, which lack T cells, H2087-LCC cells populate the lungs, liver, bone marrow and adrenal glands, remaining as quiescent single cells and small proliferative clusters that rarely form large tumours[2]. This phenotype is in stark contrast to that produced by the aggressive late-stage LUAD cell line H2030, which gives rise to aggressive multi-organ metastases (Extended Data Fig. 1a). Although only a small proportion of H2087-LCC-harbouring mice developed metastases, nearly all developed multi-organ metastases when treated with anti-asialo-GM1 antibody to deplete NK cells (Extended Data Fig. 1a–c). We previously showed that NK cells selectively eliminate proliferative H2087-LCC early-stage progenitors[13]. To develop a fully immunocompetent model of dormant metastasis, we initiated LUAD tumours in *Kras*$^{LSL\text{-}G12D/+}$;*Trp53*$^{flox/flox}$ (KP) mice by intranasal delivery of Cre recombinase[14] and derived a cell culture population from an early-stage LUAD lesion (KPad1 cells). When injected into syngeneic immunocompetent C57BL/6 mice or C57BL/6 derived B6-albino mice, KPad1 cells showed an indolent metastatic phenotype compared with cells derived from an aggressive KP LUAD tumour (KP-482T1 cells[14]) (Fig. 1b). Disseminated KPad1 cells remained as single cells or small clusters (<20 cells), a majority of which were quiescent as determined by Ki67 staining 25 or 75 days after inoculation (Fig. 1c). Notably, KPad1 cells rapidly formed multi-organ metastatic disease in B6-albino mice that were depleted of NK cells, CD4$^+$ T cells, or CD8$^+$ T cells by antibody treatment (Extended Data Fig. 1e,f) and in NOD–SCID gamma-null (NSG) mice, which lack NK cells and mature T and B cells (Fig. 1b and Extended Data Fig. 1d,f). Thus, immune surveillance restricted the progression of dormant metastases in both the H2087-LCC and the KPad1 models.

Screen to uncover metastasis suppressors

To identify cell-autonomous suppressors of exit from dormant metastasis, we conducted focused CRISPR screens in vivo using single guide RNA (sgRNA) libraries targeting various immunity activating factors in H2087-LCC and KPad1 cells (Fig. 1d). As NK cell-activating ligands[15]

and MHC class I molecules are implicated in the regulation of dormant metastasis, we designed and constructed libraries to target these genes. To identify new immune regulators of metastasis, we queried our previously published single-cell RNA-sequencing (scRNA-seq) datasets comparing dormant H2087-LCC cells that were induced to proliferate in culture versus cultures of H2087-LCC that had grown in vivo as spontaneous outbreaks under immune surveillance[13]. Gene set enrichment analysis (GSEA) comparing reawakened cells with those from spontaneous outbreaks revealed a selective enrichment for transcriptional signatures associated with immune regulation, including interferon-α (IFNα), IFNγ and complement pathways in the reawakened cells (Extended Data Fig. 1g and Supplementary Table 1). Genes from these pathways were included in the screen. As expression of IFNα and IFNβ lies downstream of pathways that sense dsDNA (the STING pathway), RNA and lipopolysaccharides[16], we also included components from these immune-sensing pathways in the screen. In all, our libraries targeted 220 genes belonging to these classes of immune regulators (102 from H2087-LCC cells and 118 from KPad1 cells) (Supplementary Tables 2 and 3). To maximize library representation in vivo, we divided the libraries into sub-pools targeting 20 genes each (5 sgRNAs per gene) followed by library transduction and selection of sgRNA-expressing cancer cells. To mitigate against the high attrition that cancer cells suffer during dissemination[17], we inoculated 10–12 athymic nude mice or 7–10 B6-albino mice per pool with 2.5×10^5 cells to ensure high sgRNA representation in vivo. We injected library-transduced H2087-LCC and KPad1 cells intracardially into the arterial circulation of recipient mice for dissemination to multiple organs. To assess lung-colonization activity, library-transduced KPad1 cells were separately injected into the tail vein of recipient mice. Cells expressing a neutral safe-targeting sgRNA were inoculated as controls. Metastatic disease development was monitored longitudinally using luciferase bioluminescence imaging, and brain, lung, liver, bone and adrenal gland tissues were collected individually from mice showing overt metastases (Fig. 1d).

Several sgRNA pools enhanced the metastatic activity of H2087-LCC and KPad1 cells to multiple organs, suggesting that loss of function of one or more genes in these pathways is sufficient to allow the metastatic progression of reawakened dormant cancer cells (Fig. 1e,f, Extended Data Fig. 1h–j and Supplementary Table 4). To identify candidate sgRNAs that fuel this metastatic outbreak, we isolated genomic DNA from individual organs, followed by next-generation sequencing to quantify sgRNA enrichment. Consistent with previous studies showing that NK cells and T cells suppress the reawakening of dormant metastasis[2,3], sgRNAs targeting specific NK activating ligands and MHC class I molecules were among the top enriched guides across all screens, supporting the robustness of our screening platform and results. Of note, multiple genes associated with the STING pathway (*STING*, *IFNB1* and *CCL5*) and interferon-responsive genes downstream of STING (*IFI27* and *IFITM3*) were among the top-ranked sgRNA targets in the H2087-LCC and KPad1 screens (Fig. 1g, Extended Data Figs. 1k,l and 2 and Supplementary Table 5). These sgRNAs were enriched in liver metastases from H2087-LCC, brain and adrenal metastases from KPad1, and bone and lung metastases from both models (Extended Data Fig. 2). sgRNAs targeting the STING and IFNα pathways also scored in the KPad1 lung-colonization screen (Extended Data Fig. 1m), further pointing at these pathways as candidate suppressors of exit from dormant metastasis in LUAD.

STING activation in reawakened cells

The STING pathway triggers innate immune responses to cytosolic dsDNA in cancer cells and cells infected with viruses or bacteria[18]. Cytosolic dsDNA binds to cyclic GMP–AMP synthase (cGAS), which produces the second messenger cGAMP. cGAMP binding induces STING to stimulate kinase-mediated activation of IRF3 and NF-κB transcriptional drivers of type I interferon and pro-inflammatory chemokine expression[19]. Cancer cells contain significant levels of cytosolic dsDNAs and cGAMP, probably owing to genomic instability[20,21]. Notably, immunostaining of mouse lung or brain sections harbouring disseminated H2087-LCC or KPad1 cells demonstrated higher levels of STING and the STING-induced chemokine CCL5 in single proliferative metastatic cells and small clusters compared with quiescent single cells, whereas the levels of STING and CCL5 in macrometastases were closer to those of dormant cells (Fig. 2a and Extended Data Fig. 3a–c), indicating increased STING expression and pathway activity in recently reawakened metastatic cells.

We analysed STING and CCL5 expression in lymph nodes from patients with stage II or stage III LUAD harbouring small clusters of disseminated cancer cells. STING and CCL5 immunofluorescence intensities were higher in proliferative ($Ki67^{high}$) disseminated cancer cells than in quiescent cells (Fig. 2b and Extended Data Fig. 3d), whereas patient-derived macrometastases showed lower STING and CCL5 expression than their matched primary tumour (Fig. 2c,d and Extended Data Fig. 3e–g), all of which are consistent with our findings in the dormant metastasis mouse model.

We previously showed that cancer cells in patient-derived LUAD metastasis samples and H2087-LCC-derived metastatic colonies comprise a developmental continuum spanning from stem-like lung epithelial regenerative progenitors expressing the transcription factor SOX2, through intermediate developmental stages expressing FOXA2 and NKX2-1, and late-stage alveolar progenitors expressing SOX9 (ref. 13). These distinct stages exhibit differential sensitivities to immune surveillance, with $SOX2^+$ progenitors being constrained by NK cell-mediated killing whereas $SOX9^+$ cells are more resistant to NK cell surveillance[13]. Disseminated H2087-LCC cells and small clusters predominantly include $SOX2^+$ cells both in situ[2] and upon isolation and placement in culture[13], while spontaneous H2087-LCC metastases are enriched in $SOX9^+$ cells[13]. Thus, LUAD metastatic tumours include a heterogeneous continuum of developmental stages from $SOX2^+$ to $SOX9^+$ differentially recognized by the immune system.

To verify that STING upregulation selectively occurs in early-stage $SOX2^+$ metastatic progenitors, we compared scRNA-seq datasets derived from H2087-LCC cells that were isolated as dormant populations in mice and then placed in culture to reawaken their proliferation, with H2087-LCC cell populations that had spontaneously grown as large outbreaks in vivo and were then placed in culture[13]. When stimulated to resume proliferation under culture conditions, dormancy-derived $SOX2^+$ cells expressed higher levels of *STING* compared with macrometastasis-derived $SOX9^+$ cells (Fig. 2e and Extended Data Fig. 3h,i). STING activation leads to expression of canonical immune-stimulatory genes, including type I interferons and their targets, which are anti-tumorigenic, and expression of non-canonical NF-κB target genes, which promote growth in tumours with chromosomal instability[22,23]. Canonical STING target genes[24–26] and IFNα response genes (GSEA hallmark gene set) were more highly expressed in the reawakened dormant cells than in macrometastasis-derived populations (Extended Data Figs. 3h and 4a and Supplementary Table 6). NF-κB targets were similarly expressed in both reawakened STING-high cells and macrometastasis-derived STING-low cells, consistent with previous reports[22,23] (Extended Data Fig. 3h).

Analysis of scRNA-seq data from patient-derived LUAD macrometastases[13] showed that the $SOX2^+$ early-stage progenitors present in these lesions express high levels of *STING*, canonical STING targets, IFNα response genes and NF-κB target genes, compared with $SOX9^+$ cells from the same lesions (Extended Data Figs. 3j,k and 4b). We observed no downregulation of *STING* in $SOX9^+$ progenitors in H2087-LCC metastases formed after NK cell depletion (Extended Data Fig. 3l), and H2087-LCC metastasis samples from spontaneous outbreaks exhibited lower levels of *STING* mRNA and protein compared to outbreaks after depletion of NK cells (Extended Data Fig. 3m,n), suggesting that the decline in *STING* expression is tied to development of the lesions under

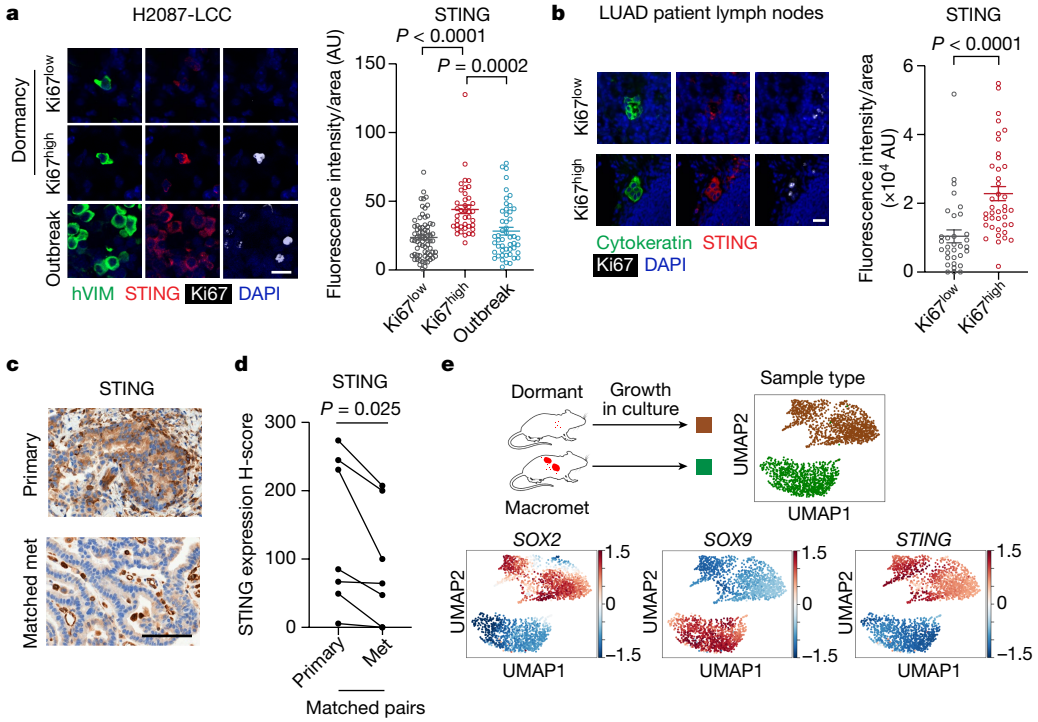

Fig. 2 | STING activation in metastatic progenitors re-entering the cell cycle. a, Left, representative immunofluorescence of H2087-LCC cells in lungs of athymic mice inoculated with 1×10^5 cells. Organs were collected 4 weeks after inoculation to capture the dormant state, and 10–13 weeks after inoculation to capture spontaneous outbreaks. hVIM, human vimentin. Disseminated cancer cells were present as single quiescent ($Ki67^{low}$) and proliferative cells ($Ki67^{high}$) during dormancy. Right, the signal intensity of STING in vimentin-positive cells was quantified and plotted. Scale bar, 10 µm. $n = 70$ cells ($Ki67^{low}$), 40 cells ($Ki67^{high}$), or 50 regions (outbreaks), from 5 mice per group. Mean ± s.e.m., two-sided unpaired *t*-test. **b**, Left, representative images of micrometastatic cells (cytokeratin AE1 and AE3 (cytokeratin)) in lymph nodes from patients with stage II or stage III LUAD. Right, the signal intensity of STING in cytokeratin-positive cells was quantified and plotted. Scale bar, 20 µm. $n = 32$ ($Ki67^{low}$) or 40 ($Ki67^{high}$) regions from 14 lymph nodes of 9 patients. Mean ± s.e.m., two-sided unpaired *t*-test. **c**,**d**, Immunohistochemistry (**c**) and quantification (**d**) of STING expression (H-score) in patient-derived LUAD metastases compared with matched primary tumours. Scale bar, 50 µm. $n = 7$ matched pairs, two-tailed paired *t*-test. **e**, Uniform manifold approximation and projection (UMAP) plots showing imputed and *z*-normalized expression of *STING*, *SOX2* and *SOX9* in H2087-LCC cells isolated from dormant metastases or spontaneous macrometastases in athymic mice and placed in growth-promoting culture conditions. $n = 2{,}245$ cells isolated from 3 mice. See also Extended Data Figs. 3 and 4. AU, arbitrary units.

immune surveillance. Collectively, these data suggest that the transition of metastatic $SOX2^+$ progenitors from dormancy to a proliferative state is accompanied by heightened STING activity, and the more differentiated $SOX9^+$ progenitors downregulate STING as macrometastases develop under immune selective pressure.

STING activation suppresses metastasis

To determine the effect of STING on metastasis progression, we performed necessity and sufficiency experiments in the H2078-LCC and KPad1 models, as well as their aggressive counterparts H2030 and KP-482T1, respectively. Knockout of *STING* in H2087-LCC cells using sgRNAs different from those used in the original screen accelerated the incidence of metastatic outbreaks and worsened metastasis-free survival in mice inoculated with these cells (Fig. 3a and Extended Data Fig. 5a). Cells derived from spontaneous metastatic outbreaks (H2087-LCC-SO cells) showed low *STING* expression and no induction of *IFNB1* expression by exogenous cGAMP compared with parental H2087-LCC cells (Extended Data Fig. 5b–d). Conversely, in H2087-LCC-SO cells with doxycycline-inducible overexpression of STING (Extended Data Fig. 5e), doxycycline administration 7 days after inoculation of these cells into athymic mice increased the metastasis-free survival time (Fig. 3b and Extended Data Fig. 5f).

STING and cGAMP-induced *IFNB1* expression levels in H2087 human LUAD cells were similar to those in human bronchial epithelial cells and higher than those in the aggressively metastatic H2030 and A549 LUAD cell lines[27,28] (Extended Data Fig. 5g,h), although H2030 and A549 cells expressed high levels of *IFNB1* in response to polyinosinic-polycytidylic acid (poly(I:C)), a STING-independent agonist (Extended Data Fig. 5i). Since overexpression of wild-type STING in H2030 did not robustly activate the STING pathway, we transduced these cells with a constitutively active STING V155M mutant[29], which inhibited their metastatic activity in athymic mice (Extended Data Fig. 5j). *Sting* expression and cGAMP responsiveness were higher in KPad1 cells compared with the aggressive counterpart KP-482T1 (Extended Data Fig. 6a,b). *Sting* knockout in KPad1 cells increased their metastatic activity in immunocompetent mice (Fig. 3c and Extended Data Fig. 6c), whereas *STING* overexpression suppressed the strong metastatic activity of KP-482T1 cells (Fig. 3d). We labelled wild-type KPad1 cells with RFP and *Sting*-knockout KPad1 cells with GFP, then mixed the cells at different ratios and intracardially inoculated them into mice. Macrometastases largely consisted of *Sting*-knockout cells even when these cells were only 10% of the inoculum (Extended Data Fig. 6d). *STING* knockout promoted metastasis in multiple organs including bone, brain and lung in H2087-LCC cells, and bone, brain, lung and adrenal glands in KPad1 cells (Fig. 3e). Of note, *STING* knockout or overexpression did not affect the proliferation of these models in vitro, as measured by an EdU uptake assay (Extended Data Figs. 6e,f and 7a,b), their initial survival in mice, as measured by quantitative bioluminescence imaging one to seven days after intracardiac inoculation (Extended Data Figs. 6g,h and 7c,d), or expression of SOX2 or SOX9 (Extended Data Fig. 7e,f), as measured by immunofluorescence analysis of macrometastatic lesions.

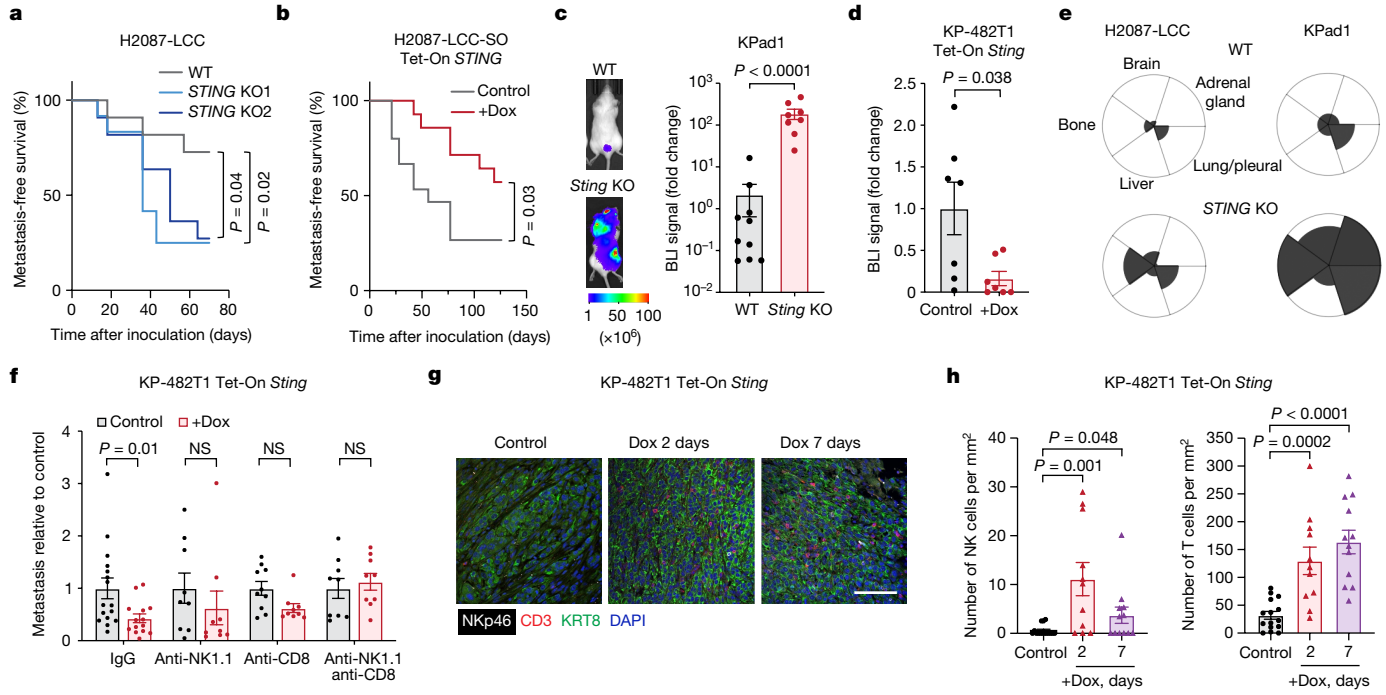

Fig. 3 | Metastasis suppression by tumour-intrinsic STING. a, Metastasis-free survival plots of athymic mice intracardially inoculated with 1×10^5 wild-type (WT) or *STING*-knockout (KO1 and KO2) H2087-LCC cells. $n = 11$ (WT and KO2) or 12 (KO1) mice per group; log-rank test. **b**, Metastasis-free survival plots of athymic mice intracardially inoculated with 1×10^5 H2087-LCC cells derived from spontaneous outbreaks and inducibly overexpressing STING following doxycycline (Dox) treatment. $n = 15$ (control) or 14 (doxycycline) mice; log-rank test. **c**, Metastases 26 days after intracardiac inoculation of 2.5×10^5 WT or *Sting*-KO KPad1 cells in B6-albino mice. Mean ± s.e.m. $n = 10$ (WT) or 8 (KO) mice. Two-sided Mann–Whitney *U*-test. **d**, Metastases 21 days after inoculation of 5×10^4 KP-482T1 cells with doxycycline-inducible STING expression in C57BL/6J mice. $n = 7$ mice per group. Mean ± s.e.m., two-sided Mann–Whitney *U*-test. **e**, Metastasis incidence in specific organs after intracardiac inoculation of 1×10^5 WT or *STING*-KO H2087-LCC cells into 11 athymic mice (left) or 2.5×10^5 KPad1 cells into 8–10 B6-albino mice (right). Metastasis monitored for 12 (H2087-LCC) or 7 (KPad1) weeks after inoculation. **f**, Metastases by KP-482T1 cells with doxycycline-inducible expression of STING after inoculation of 2×10^4 cells into B6-albino mice. Mice were treated with the indicated antibodies. BLI results are plotted relative to values without doxycycline per treatment group. $n = 16$ (control/IgG), 14 (doxycycline/IgG), 10 (control/anti-CD8) or 9 (other groups) mice per group. Mean ± s.e.m., two-sided Mann–Whitney *U*-test. **g**,**h**, Representative immunofluorescence (**g**) and quantification (**h**) of NKp46$^+$ NK cells or CD3$^+$ T cells in femoral metastases in C57BL/6J mice. Mice were intracardially inoculated with 1×10^5 KP-482T1-Tet-On *Sting* cells and placed on a doxycycline diet 1 week later for 2 days or 7 days. Femurs were collected 14 days after cell inoculation. Scale bar, 100 µm. $n = 15$ (control), 11 (2 days) or 12 (7 days) lesions, from 4–8 mice per group. Mean ± s.e.m., two-sided unpaired *t*-test. See also Extended Data Figs. 5–8. NS, not significant.

The inhibitory effect of STING on KP-482T1 metastasis was dependent on both NK cells and CD8$^+$ T cells, as antibody-mediated depletion of these cell populations in mice eliminated the effect of STING (Fig. 3f). Analysis of cell culture supernatants confirmed that STING overexpression in KP-482T1 cells induced the secretion of CCL5, CCL20, CXCL10 and other pro-inflammatory factors[26,30] (Extended Data Fig. 6i), which are implicated in the recruitment and activation of innate and adaptive immune cells[18,31–33].

We performed immune phenotyping of KP-482T1 metastasis-bearing bones after short-term (two-day or seven-day) induction of STING expression from a doxycycline-inducible vector (Extended Data Fig. 8a). STING overexpression increased the number of immune cells, including NK cells, CD4$^+$ T cells, CD8$^+$ T cells and conventional type 1 dendritic cells (cDC1), in metastasis-bearing femurs (Extended Data Fig. 8b and Supplementary Fig. 2), while not affecting degranulation or production of effector cytokines of NK and CD8$^+$ T cells (Extended Data Fig. 8c–f). Immunofluorescence analysis of NK cells (anti-NKp46 staining) and T cells (anti-CD3 staining) in KP-482T1 metastases showed an increased proportion of infiltrated NK cells and T cells in response to *STING* overexpression (Fig. 3g,h). In the H2087-LCC model, *STING* knockout did not affect the efficacy of NK cell-mediated direct killing (Extended Data Fig. 8g), but suppressed the migration ability of NK cells (Extended Data Fig. 8h). Collectively, these results suggest that cancer cell-intrinsic STING activation suppresses LUAD metastasis by promoting infiltration of NK cells and T cells.

Basis for STING downregulation

Hypermethylation of the *STING* promoter has been reported in *KRAS–LKB1*-mutant lung cancer cell lines[34]. To examine if *STING* expression is regulated by DNA methylation during metastasis progression, we first conducted chromatin immunoprecipitation with sequencing (ChIP–seq) analysis of histone marks in H2087-LCC cells, the spontaneous outbreak derivative line H2087-LCC-SO1, and the aggressive metastatic counterpart H2030, identifying the promoter region (marked by H3K4me3) and a 3′ enhancer region (marked by H3K4me1) in *STING* (Extended Data Fig. 9a). We observed DNA hypermethylation on the *STING* promoter and 3′ enhancer in two independent H2087-LCC spontaneous outbreak cell populations (SO1 and SO2), as well as in H2030 and A549 cells compared to H2087-LCC cells, as determined by immunoprecipitation of 5-methylcytosine on the *STING* promoter and 3′ enhancer (Fig. 4a). DNA methylation was associated with reduced or absent establishment of the 3′ enhancer marked by H3K4me1 and reduced enhancer activity marked by H3K27ac in H2087-LCC-SO1 or H2030 cells, respectively (Extended Data Fig. 9a). Chromatin immunoprecipitation with PCR (ChIP–PCR) analysis of DNA methyltransferase (DNMT) binding showed higher DNMT3B binding on

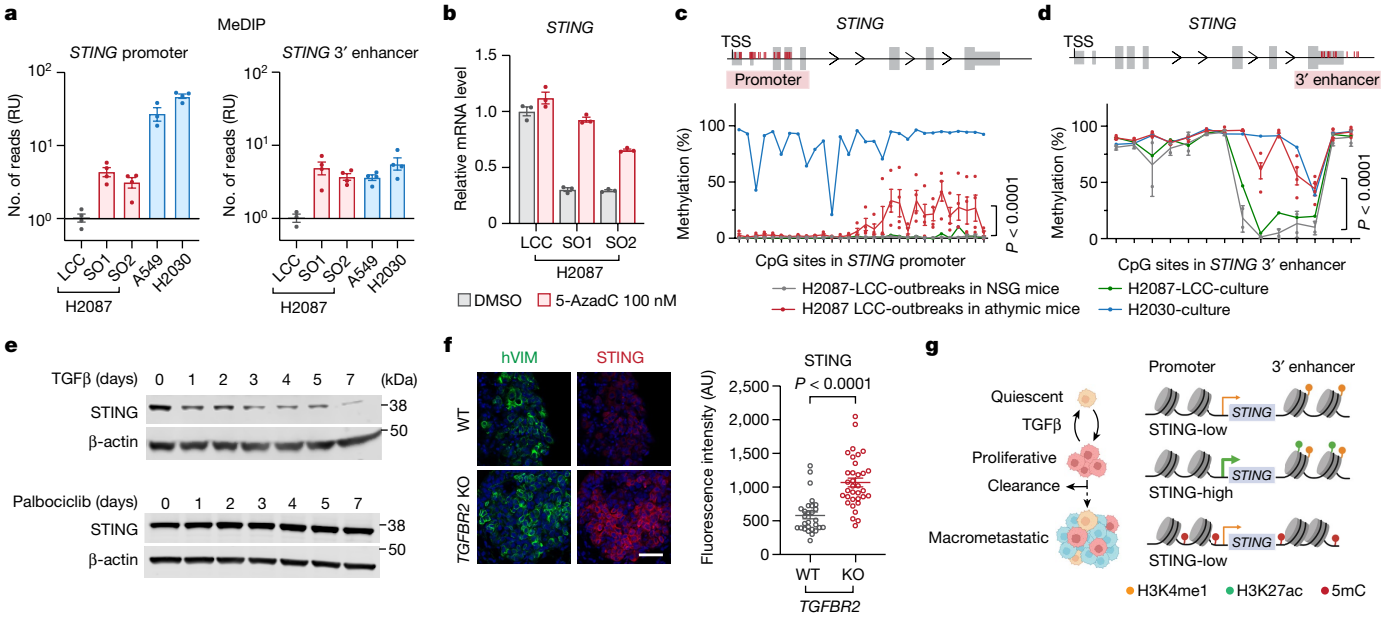

Fig. 4 | STING downregulation during dormancy and metastatic progression. a, PCR-based quantification of *STING* promoter (left) or 3′ enhancer (right) reads in methylated DNA immunoprecipitation (MeDIP) samples from parental H2087-LCC, two spontaneous metastasis outbreaks (SO1 and SO2), and the aggressive cell lines A549 and H2030. Mean ± s.e.m., representative of two independent experiments. Each dot represents a technical replicate of the assay. **b**, Quantitative PCR with reverse transcription (RT–qPCR) analysis of *STING* mRNA levels after 3-day treatment of the indicated cell lines with 100 nM 5-aza-2′-deoxycytidine (5-azadC). Mean ± s.e.m., representative of two independent experiments. Each dot represents a technical replicate of the assay. **c**,**d**, Schematic of the *STING* locus and the locations of 30 CpG sites analysed in the *STING* promoter (**c**) and 14 sites in the *STING* 3′ enhancer (**d**), and the percentage of methylation on each CpG site as determined by bisulfite sequencing of H2087-LCC cells freshly sorted from 4 metastatic outbreaks in 2 athymic mice or 2 outbreaks in 2 NSG mice, and H2087-LCC and H2030 cells in culture. Organs were collected 5–7 weeks after intracardiac inoculation of 1×10^5 H2087-LCC cells. $n = 4$ (athymic) or 2 (NSG) outbreaks. Mean ± s.e.m., two-way ANOVA. **e**, Western blot analysis of STING in H2087-LCC cells treated with TGFβ or the CDK4/6 inhibitor palbociclib for the indicated time periods, representative of 2 independent experiments. For gel source data, see Supplementary Fig. 1. **f**, Left, immunofluorescence staining of human vimentin and STING in lung metastases generated 7 weeks after intravenous inoculation of 1×10^5 WT or *TGFBR2*-knockout (KO) H2087-LCC cells in NSG mice. Right, the staining intensity of STING in vimentin-positive areas was quantified. Scale bar, 50 µm. $n = 28$ (WT) or 34 (*TGFBR2*-knockout) lesions from 6 mice. Mean ± s.e.m., two-sided unpaired *t*-test. **g**, Schematic summary of epigenetic mechanisms regulating *STING* expression during dormancy and metastasis progression. 5mc, 5-methylcytosine. See also Extended Data Figs. 9 and 10.

the *STING* promoter and 3′ enhancer in H2087-LCC-SO1 and SO2 as well as in H2030 and A549 cells (Extended Data Fig. 9b). Treatment of H2087-LCC-SO1, H2087-LCC-SO2, H2030 and A549 cells with the DNMT inhibitor 5-aza-2′-deoxycytidine (decitabine) rescued *STING* expression in these cells (Fig. 4b and Extended Data Fig. 9c).

To validate these observations in vivo, we freshly isolated H2087-LCC tumour cells from spontaneous outbreaks and conducted targeted next-generation bisulfite sequencing analysis on the *STING* promoter and 3′ enhancer. Approximately half of the CpG sites in these regions showed higher levels of DNA methylation in cells sorted from spontaneous outbreaks in athymic nude mice compared to outbreaks in NSG mice or to H2087-LCC cells in culture (Fig. 4c,d, Extended Data Fig. 9d and Supplementary Table 7).

To investigate the basis for *STING* downregulation in dormant cells, we examined the response of H2087-LCC cells to TGFβ, an inducer of metastatic dormancy in breast, and head and neck carcinomas[1,11,35,36]. TGFβ causes growth inhibition as a part of broader response programmes[37,38]. We treated H2087-LCC cells with TGFβ or palbociclib, a CDK4/6 inhibitor which specifically induces cell cycle arrest. Both TGFβ and palbociclib inhibited cell proliferation (Extended Data Fig. 10a), but only TGFβ caused a decrease in STING expression and STING-dependent *IFNB1* and *CCL5* expression (Fig. 4e and Extended Data Fig. 10b,c). TGFβ had limited effects on cGAS or cGAMP levels (Extended Data Fig. 10d,e). ChIP–seq analysis of histone modification marks showed that TGFβ causes a loss of the H3K27ac activation mark in the *STING* 3′ enhancer but does not affect enhancer establishment as marked by H3K4me1 (Extended Data Fig. 10f) or enhancer DNA methylation (Extended Data Fig. 10g).

We next examined whether TGFβ also regulates the expression of STING and CCL5 in H2087-LCC cells in vivo. H2087-LCC cells engineered with a TGFβ and a *SMAD*-dependent mCherry transcriptional reporter (Extended Data Fig. 10h) exhibited TGFβ signalling activity as dormant metastatic cells in the lungs after inoculation into athymic mice (Extended Data Fig. 10i). TGFβ receptor 2 (*TGFBR2*) knockout in H2087-LCC cells prevented canonical gene responses (induction of *SMAD7* and *SNAI1*) and *STING* downregulation by TGFβ (Extended Data Fig. 10j). When inoculated via the tail vein into NSG mice, used here to avert the interference of immune surveillance, *TGFBR2*-knockout H2087-LCC cells showed accelerated lung metastasis (Extended Data Fig. 10k) and increased expression of STING and CCL5 compared to control (Fig. 4f and Extended Data Fig. 10l). Collectively, these results demonstrate a role of TGFβ in downregulating STING expression by enhancer inhibition during dormancy, and a role of promoter and enhancer DNA methylation in the downregulation of *STING* expression in metastatic outbreaks (Fig. 4g).

Leveraging STING to prevent metastasis

We tested the hypothesis that pharmacologic activation of STING in mice harbouring dormant metastasis would deplete disseminated cancer cells by enhancing STING-dependent elimination of metastatic cells re-entering the cell cycle (Extended Data Fig. 11a). To this end, we treated mice harbouring disseminated KPad1 or H2087-LCC cells with a STING agonist followed by either collecting the brains and lungs to quantify disseminated tumour entities (DTEs) which include single cells, small

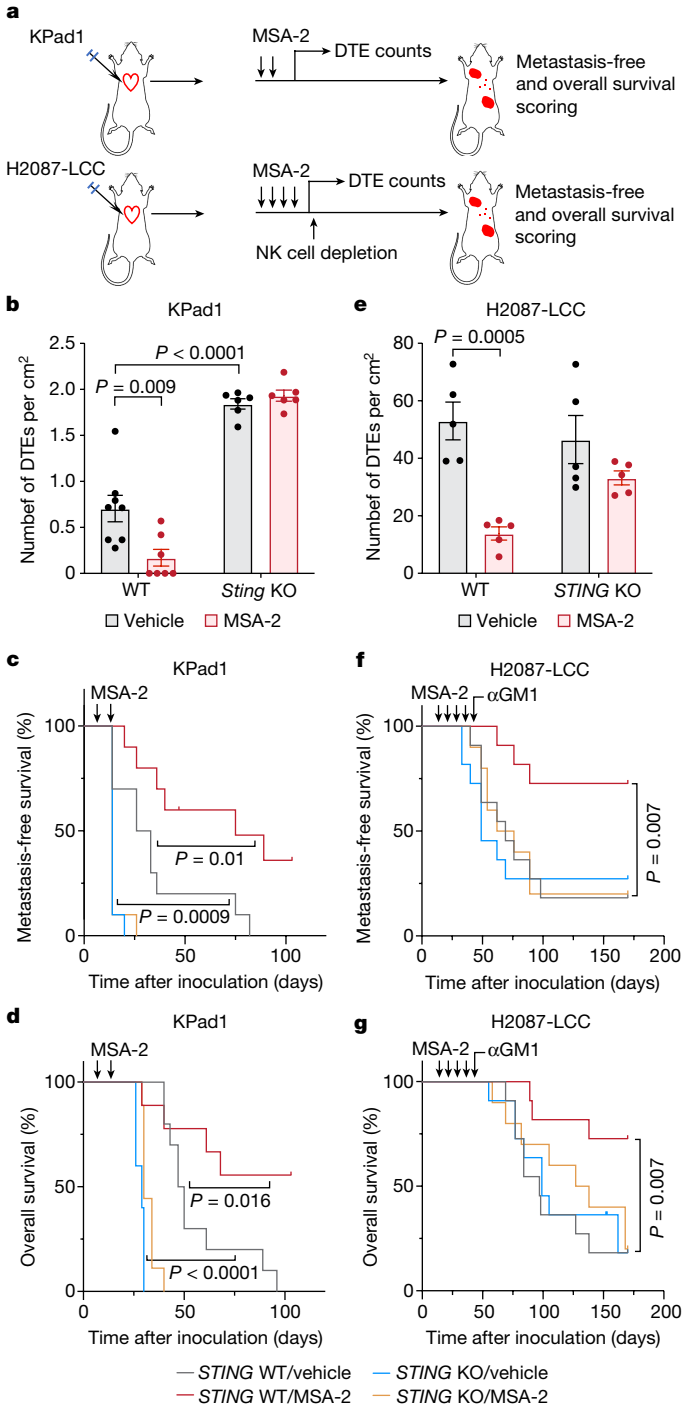

Fig. 5 | STING-agonist depletion of disseminated cancer cells to prevent metastasis. a, Schematic of the experimental design. **b**, B6-albino mice were intracardially inoculated with 1×10^5 WT or *Sting*-KO KPad1 cells and treated with vehicle or MSA-2 (50 mg per kg (body weight)) once weekly at weeks 2 and 3. Brains were collected 5 weeks after inoculation and the number of DTEs was counted. DTEs included single cells and small cell clusters, except in the case of *Sting*-knockout KPad1 cells, which included mostly micro- and macrometastases. $n = 8$ (WT/vehicle), 7 (WT/MSA-2), or 6 (*Sting*-knockout/vehicle and *Sting*-knockout/MSA-2) mice per group. Mean ± s.e.m., two-sided unpaired *t*-test. **c**,**d**, Kaplan–Meier plots of metastasis-free survival (**c**) or overall survival (**d**) of B6-albino mice that were intracardially inoculated with 2.5×10^5 WT or *Sting*-KO KPad1 cells, treated as in **b** and tracked for metastasis formation and for survival. $n = 10$ mice per group. Log-rank test. **e**, Athymic mice were inoculated with 1×10^5 WT or *STING*-KO H2087-LCC cells via the tail vein and treated with vehicle or MSA-2 (50 mg per kg(body weight)) once weekly for 4 weeks starting 2 weeks after inoculation. Lungs were collected six weeks after inoculation and the number of DTEs was counted. DTEs included single cells and small cell clusters. $n = 5$ mice per group. Mean ± s.e.m., two-sided unpaired *t*-test. **f**,**g**, Kaplan–Meier plots of metastasis-free survival (**f**) and overall survival (**g**) of athymic mice intracardially inoculated with 1×10^5 WT or *STING*-KO H2087-LCC cells and treated as in **e**. Anti-asialo-GM1 treatment started six weeks after cell inoculation. $n = 11$ (WT/vehicle, WT/MSA-2 and *STING*-knockout/vehicle) or 10 (*STING*-knockout/MSA-2) mice per group. Log-rank test. See also Extended Data Fig. 11.

cell clusters and metastases or allowing the mice to proceed until spontaneous metastasis emerged (Fig. 5a). We used benzothiophene oxobutanoic acid (MSA-2), a non-nucleotide STING agonist with anti-tumour effects[39]. MSA-2 treatment in vitro increased the expression of *STING* target genes *CXCL10* and *CCL5* in wild-type (but not *STING*-knockout) KPad1 and H2087-LCC cells (Extended Data Fig. 11b,c).

We intracardially inoculated wild-type or *STING*-knockout KPad1 cells into syngeneic immunocompetent mice and H2087-LCC cells into athymic nude mice, allowed one week (KPad1) or two weeks (H2087-LCC) for disseminated cells to settle in distant organs, and then started weekly treatments with MSA-2 for two weeks (KPad1) or four weeks (H2087-LCC) during the dormancy period in each model (Fig. 5a). Treatment with MSA-2 led to a STING-dependent depletion of disseminated KPad1 cancer cells, with *Sting*-knockout KPad1 cells accumulating at higher levels compared to *Sting*-proficient cells (Fig. 5b).

Moreover, MSA-2 increased metastasis-free and overall survival of mice inoculated with *Sting*-proficient (but not *Sting*-knockout) KPad1 cells (Fig. 5c,d). The incidence of metastasis was proportional to the number of disseminated KPad1 cells in the various conditions (compare Fig. 5b with Fig. 5c,d).

The metastasis-suppression effect of MSA-2 required STING activity in the cancer cells, as well as the presence of NK cells, $CD4^+$ T cells and $CD8^+$ T cells, as depletion of these cells in the mice abolished the effect (Extended Data Fig. 11f–j). Pre-treatment of KPad1 cells with MSA-2 in vitro before inoculation in mice did not affect metastatic progression (Extended Data Fig. 11k). Moreover, treatment with MSA-2 led to the depletion of disseminated H2087-LCC cells, and this effect was absent in *STING*-knockout H2087-LCC cells (Fig. 5e). Since spontaneous outbreaks are infrequent in the H2087-LCC model, we depleted NK cells one week after the last MSA-2 dose to allow metastasis formation by cancer cells remaining after MSA-2 treatment, which serves as another readout of the residual burden of metastasis-initiating H2087-LCC cells. MSA-2 treatment decreased the incidence of metastasis, an effect that was also dependent on *STING* in the cancer cells (Fig. 5f,g).

We also tested ADU-S100 (ref. 40) (also known as ML-RR-S2 CDA), an earlier-generation STING-activating cyclic di-adenosine mimic of cGAMP. ADU-S100 treatment of KPad1 and H2087-LCC cells in vitro increased the expression of *CXCL10* and *CCL5* in a STING-dependent manner (Extended Data Fig. 11d,e). As ADU-S100 is unstable after systemic administration[41], we delivered the drug locally through intratracheal instillation in mice harbouring KPad1 or H2087-LCC cells in the lungs. Consistent with our findings using MSA-2, ADU-S100 treatment inhibited the formation of metastatic outbreaks in mice harbouring *Sting* wild-type (but not *Sting*-knockout) KPad1 cells (Extended Data Fig. 11l). In the H2087-LCC model, ADU-S100 treatment reduced the number of disseminated cancer cells in the lungs (Extended Data Fig. 11m).

Discussion

Our results reveal a role of STING signalling in the interaction between dormant disseminated LUAD cells and anti-tumour immunity, preventing the progression of these cancer cells from an indolent state to aggressive metastasis. The ability of STING agonists to eliminate disseminated cancer cells and suppress relapse when administered during

the indolent phase of metastasis is in line with our genetic screens identifying cancer cell-intrinsic STING as a target of interest. This effect of STING agonists requires cancer cell STING and depends on NK cells, $CD4^+$ T cells and $CD8^+$ T cells. The precise mechanism leading to STING activation in dormant $SOX2^+$ LUAD cells re-entering the cell cycle and in proliferative $SOX2^+$ subpopulations in patient-derived metastasis samples remains to be fully elucidated. It is worth noting that micronuclei arising from chromosomal instability in cancer cells accumulate through mitosis and activate the cGAS–STING pathway[21,42,43].

Current clinical trials with STING agonists are in the setting of advanced tumours, in which this pathway plays a complex role, promoting anti-tumour immune responses[40,44,45], cancer cell senescence and apoptosis[46–48], as well as inducing pro-tumorigenic effects[20,49] through NF-κB signalling in some models[22,23] but not in others[50]. These disparate roles may complicate the outcome of STING-agonist trials in established tumours. However, the dormant metastasis microenvironment is very different from that of the advanced metastases. Targeting specific vulnerabilities of dormant metastasis in the adjuvant setting may provide unique opportunities to prevent metastasis. Our observations warrant further investigation towards rationally harnessing the immune system in the adjuvant setting.

Online content

Any methods, additional references, Nature Portfolio reporting summaries, source data, extended data, supplementary information, acknowledgements, peer review information; details of author contributions and competing interests; and statements of data and code availability are available at https://doi.org/10.1038/s41586-023-05880-5.

1. Goddard, E. T., Bozic, I., Riddell, S. R. & Ghajar, C. M. Dormant tumour cells, their niches and the influence of immunity. *Nat. Cell Biol.* **20**, 1240–1249 (2018).
2. Malladi, S. et al. Metastatic latency and immune evasion through autocrine inhibition of WNT. *Cell* **165**, 45–60 (2016).
3. Pommier, A. et al. Unresolved endoplasmic reticulum stress engenders immune-resistant, latent pancreatic cancer metastases. *Science* **360**, eaao4908 (2018).
4. Pantel, K. et al. Frequent down-regulation of major histocompatibility class I antigen expression on individual micrometastatic carcinoma cells. *Cancer Res.* **51**, 4712–4715 (1991).
5. Eyles, J. et al. Tumor cells disseminate early, but immunosurveillance limits metastatic outgrowth, in a mouse model of melanoma. *J. Clin. Invest.* **120**, 2030–2039 (2010).
6. Massagué, J. & Ganesh, K. Metastasis-initiating cells and ecosystems. *Cancer Discov.* **11**, 971–994 (2021).
7. Consonni, D. et al. Lung cancer prognosis before and after recurrence in a population-based setting. *JNCI* **107**, djv059 (2015).
8. Willis, R. A. *The Spread of Tumours in the Human Body* (J. & A. Churchill, 1934).
9. Hadfield, G. The dormant cancer cell. *Br. Med. J.* **2**, 607–610 (1954).
10. Janni, W. et al. Persistence of disseminated tumor cells in the bone marrow of breast cancer patients predicts increased risk for relapse—a European pooled analysis. *Clin. Cancer Res.* **17**, 2967–2976 (2011).
11. Sosa, M. S., Bragado, P. & Aguirre-Ghiso, J. A. Mechanisms of disseminated cancer cell dormancy: an awakening field. *Nat. Rev. Cancer* **14**, 611–622 (2014).
12. Xiao, D. et al. Donor cancer transmission in kidney transplantation: a systematic review. *Am. J. Transplant.* **13**, 2645–2652 (2013).
13. Laughney, A. M. et al. Regenerative lineages and immune-mediated pruning in lung cancer metastasis. *Nat. Med.* **26**, 259–269 (2020).
14. Winslow, M. M. et al. Suppression of lung adenocarcinoma progression by Nkx2-1. *Nature* **473**, 101–104 (2011).
15. Marcus, A. et al. Recognition of tumors by the innate immune system and natural killer cells. *Adv. Immunol.* **122**, 91–128 (2014).
16. McNab, F., Mayer-Barber, K., Sher, A., Wack, A. & O'Garra, A. Type I interferons in infectious disease. *Nat. Rev. Immunol.* **15**, 87–103 (2015).
17. Kienast, Y. et al. Real-time imaging reveals the single steps of brain metastasis formation. *Nat. Med.* **16**, 116–122 (2010).
18. Barber, G. N. STING: infection, inflammation and cancer. *Nat. Rev. Immunol.* **15**, 760–770 (2015).
19. Ablasser, A. & Chen, Z. J. cGAS in action: expanding roles in immunity and inflammation. *Science* **363**, eaat8657 (2019).
20. Chen, Q. et al. Carcinoma–astrocyte gap junctions promote brain metastasis by cGAMP transfer. *Nature* **533**, 493–498 (2016).
21. Mackenzie, K. J. et al. cGAS surveillance of micronuclei links genome instability to innate immunity. *Nature* **548**, 461–465 (2017).
22. Bakhoum, S. F. et al. Chromosomal instability drives metastasis through a cytosolic DNA response. *Nature* **553**, 467–472 (2018).
23. Hong, C. et al. cGAS–STING drives the IL-6-dependent survival of chromosomally instable cancers. *Nature* **607**, 366–373 (2022).
24. Konno, H., Konno, K. & Barber, G. N. Cyclic dinucleotides trigger ULK1 (ATG1) phosphorylation of STING to prevent sustained innate immune signaling. *Cell* **155**, 688–698 (2013).
25. Ishikawa, H. & Barber, G. N. STING is an endoplasmic reticulum adaptor that facilitates innate immune signalling. *Nature* **455**, 674–678 (2008).
26. Chen, H. et al. Activation of STAT6 by STING is critical for antiviral innate immunity. *Cell* **147**, 436–446 (2011).
27. Nguyen, D. X. et al. WNT/TCF signaling through LEF1 and HOXB9 mediates lung adenocarcinoma metastasis. *Cell* **138**, 51–62 (2009).
28. Luis-Ravelo, D. et al. Tumor–stromal interactions of the bone microenvironment: in vitro findings and potential in vivo relevance in metastatic lung cancer models. *Clin. Exp. Metastasis* **28**, 779–791 (2011).
29. Jeremiah, N. et al. Inherited STING-activating mutation underlies a familial inflammatory syndrome with lupus-like manifestations. *J. Clin. Invest.* **124**, 5516–5520 (2014).
30. Abe, T. et al. STING recognition of cytoplasmic DNA instigates cellular defense. *Mol. Cell* **50**, 5–15 (2013).
31. Dufour, J. H. et al. IFN-gamma-inducible protein 10 (IP-10; CXCL10)-deficient mice reveal a role for IP-10 in effector T cell generation and trafficking. *J. Immunol.* **168**, 3195–3204 (2002).
32. Appay, V. & Rowland-Jones, S. L. RANTES: a versatile and controversial chemokine. *Trends Immunol.* **22**, 83–87 (2001).
33. Schutyser, E., Struyf, S. & Van Damme, J. The CC chemokine CCL20 and its receptor CCR6. *Cytokine Growth Factor Rev.* **14**, 409–426 (2003).
34. Kitapma, S. et al. Suppression of STING associated with LKB1 loss in KRAS-driven lung cancer. *Cancer Discov.* **9**, 34–45 (2019).
35. Bragado, P. et al. TGF-β2 dictates disseminated tumour cell fate in target organs through TGF-β-RIII and p38α/β signalling. *Nat. Cell Biol.* **15**, 1351–1361 (2013).
36. Ghajar, C. M. et al. The perivascular niche regulates breast tumour dormancy. *Nat. Cell Biol.* **15**, 807–817 (2013).
37. David, C. J. & Massagué, J. Contextual determinants of TGFβ action in development, immunity and cancer. *Nat. Rev. Mol. Cell Biol.* **19**, 419–435 (2018).
38. Su, J. et al. TGF-β orchestrates fibrogenic and developmental EMTs via the RAS effector RREB1. *Nature* **577**, 566–571 (2020).
39. Pan, B. S. et al. An orally available non-nucleotide STING agonist with antitumor activity. *Science* **369**, eaba6098 (2020).
40. Corrales, L. et al. Direct activation of STING in the tumor microenvironment leads to potent and systemic tumor regression and immunity. *Cell Rep.* **11**, 1018–1030 (2015).
41. Flood, B. A., Higgs, E. F., Li, S. Y., Luke, J. J. & Gajewski, T. F. STING pathway agonism as a cancer therapeutic. *Immunol. Rev.* **290**, 24–38 (2019).
42. Harding, S. M. et al. Mitotic progression following DNA damage enables pattern recognition within micronuclei. *Nature* **548**, 466–470 (2017).
43. Chen, J. et al. Cell cycle checkpoints cooperate to suppress DNA- and RNA-associated molecular pattern recognition and anti-tumor immune responses. *Cell Rep.* **32**, 108080 (2020).
44. Deng, L. F. et al. STING-dependent cytosolic DNA sensing promotes radiation-induced type I interferon-dependent antitumor immunity in immunogenic tumors. *Immunity* **41**, 843–852 (2014).
45. Woo, S. R. et al. STING-dependent cytosolic DNA sensing mediates innate immune recognition of immunogenic tumors. *Immunity* **41**, 830–842 (2014).
46. Dou, Z. et al. Cytoplasmic chromatin triggers inflammation in senescence and cancer. *Nature* **550**, 402–406 (2017).
47. Gluck, S. et al. Innate immune sensing of cytosolic chromatin fragments through cGAS promotes senescence. *Nat. Cell Biol.* **19**, 1061–1070 (2017).
48. Zierhut, C. et al. The cytoplasmic DNA sensor cGAS promotes mitotic cell death. *Cell* **178**, 302–315.e323 (2019).
49. Ahn, J. et al. Inflammation-driven carcinogenesis is mediated through STING. *Nat. Commun.* **5**, 5166 (2014).
50. Vasudevan, A. et al. Single-chromosomal gains can function as metastasis suppressors and promoters in colon cancer. *Dev. Cell* **52**, 413–428.e6 (2020).

Methods

Clinical samples

Human specimens were obtained and approved under Memorial Sloan Kettering Cancer Center Institutional Review Board biospecimen research protocol 17–239. Lung cancer primary tumour and metastatic samples were obtained from patients with confirmed stage II, III or IV lung cancer. Patients were both male and female, with an age range of 56–81 years at recruitment. Four pairs of tissues from primary tumour and metastases were collected at autopsy (non-human subject by NIH definition). All patients provided pre-procedure informed consent.

Animal studies

All animal experiments were performed in accordance with protocols approved by the Memorial Sloan Kettering Cancer Center Institutional Animal Care and Use Committee (IACUC). Athymic nude (*Foxn1*^{nu}, stock 069) mice were obtained from Envigo. NSG (NOD.Cg-Prkdc^{scid}IL2rg^{tm1Wjl}/SzJ, stock 005557), C57BL/6J (stock 000664), and B6(Cg)-*Tyr*$^{c-2J}$/J (B6-albino, stock 000058) mouse strains were obtained from The Jackson Laboratory. Female mice from 6 to 8 weeks of age were used for these studies. Animals were housed under the following conditions: temperatures of 21.1–22.2 °C (70–72 °F), 30–70% humidity, 10–15 fresh air exchanges hourly, and a 12:12 h light:dark cycle (lights were on from 06:00–18:00).

For multi-organ metastasis assays, 0.2–2.5 × 10^5 cells were resuspended in 100 µl phosphate-buffered saline solution (PBS) and inoculated into the right cardiac ventricle of mice with a 26-gauge needle syringe. Lung-colonization assays were performed by injecting 1.0–2.5 × 10^5 cells in the lateral tail vein of mice with a 28-gauge needle syringe[2]. Metastatic burden of luciferase-transduced cancer cells was monitored by BLI of luciferase activity using retro-orbital injection of D-luciferin (150 mg kg^{-1}) and an IVIS Spectrum Xenogen instrument (PerkinElmer). Data were analysed using Living Image software (PerkinElmer, v 4.5.0). The black fur of the C57BL/6J strain interferes with bioluminescence imaging. Therefore, metastasis formation experiments with KPad1 and KP-482T1 cells were conducted in B6(Cg)-*Tyr*$^{c-2J}$/J (B6-albino) mice, which are C57BL/6J mice that carry a mutation in the tyrosinase gene (*Tyr*$^{c-2J}$), resulting in loss of pigment from skin, hair and eyes. Human cancer cells were inoculated in athymic nude mice. For ex vivo imaging of metastases-bearing organs at experimental end points, mice were anaesthetized with 100 mg kg^{-1} ketamine and 10 mg kg^{-1} xylazine and retro-orbitally injected with D-luciferin prior to organ isolation. Isolated organs were analysed using the IVIS Spectrum Xenogen instrument and Living Image software. Cell clusters or metastatic lesions were classified according to the size of the lesion and the number of cells contained. Cell clusters were defined as clusters containing fewer than 20 cells (<10^3 µm^2) from BLI negative organs; micrometastases were defined as lesions containing approximately between 500 and 2,500 cells (>10^3 µm^2 to 5 × 10^4 µm^2) from organs with weak BLI signal (intensity <10-fold over background); macrometastases were defined as lesions containing more than 2,500 cells (>5 × 10^4 µm^2) from organs with strong BLI signals (intensity >10-fold of signal from background, refer to Extended Data Fig. 10k). To score metastasis-free survival, metastasis onset was defined when whole-body BLI signal intensity reaches to 10-fold over background. In accordance with protocols approved by the IACUC, animals were killed when tumour burden exceeded 1,000 mm^3 (or 1.5 cm in diameter), or if the mass of the tumour exceeded more than 10% of the animal's mass. If animals showed any signs of respiratory distress or other signs of illness, such as hunched posture, reduced and/or erratic movement, greater than 10–15% weight loss, diminished appetite or failure to groom, the animals were euthanized prior to the end point. These limits were not exceeded in any of the experiments.

For NK cell depletion assays in athymic nude mice, 33 µg anti-asialo-GM1 antibody (Wako Chemical, 986–10001) was injected intraperitoneally once every 5 days[2]. For NK, CD4 or CD8 T cell depletion in C57BL/6J and B6(Cg)-*Tyr*$^{c-2J}$/J mice, 200 µg InVivoMab anti-mouse NK1.1 antibody (clone PK136, BioXCell, BE0036), CD4 antibody (clone GK1.5, BioXCell, BE0003-1), CD8α antibody (clone 53-6.7, BioXCell, BE0004-1) or IgG2a control (clone 2A3, BioXCell, BE0089) was injected intraperitoneally once weekly[51]. Immune cell depletion started on the same day as cell inoculation unless otherwise indicated.

For inducible STING overexpression experiments, mice were maintained on a diet of doxycycline food pellets (2,500 mg kg^{-1}, Envigo). For experiments with H2087-LCC cells, STING induction started 7 days after cell inoculation. For experiments with KP-482T1 cells, STING induction started on the same day or one day after cell inoculation, unless otherwise indicated.

For experiments with *Sting*-knockout KPad1 cells, cells were mixed 1:1 from two cell lines in which STING was knocked out by two different sgRNAs. For STING-agonist treatment assays, MSA-2 (MedChemExpress, HY-136927) was dissolved in PBS with mild pH adjustment and injected subcutaneously (50 mg kg^{-1}) once weekly[39]. ADU-S100 ammonium salt (MedChemExpress, HY-12885B)[40] was intratracheally delivered (25–125 µg per mouse in 50 µl water) once weekly.

Cell culture

For establishment of the KPad1 cell line, 2.5 × 10^6 adenovirus expressing Cre recombinase (Ad5CMVCre-mCherry, University of Iowa, VVC-U of Iowa-649) was delivered to *Kras*$^{LSL\text{-}G12D/+}$;*Trp53*$^{flox/flox}$ mice through intranasal inhalation, as described[52]. Lung tumours were isolated 18 weeks later. Tissues were washed in PBS, chopped into small pieces using a sterile razor blade, and resuspended in 30 ml digestion buffer containing 5% fetal bovine serum (FBS), 2 mM L-glutamine, 100 IU ml^{-1} penicillin/streptomycin, 40 µg ml^{-1} gentamicin, 250 µg ml^{-1} type III collagenase (Worthington Biochemical, LS004208), 0.0625 U ml^{-1} dispase solution, and 0.05 mg ml^{-1} DNase, in DMEM. After incubation at 37 °C for 30 min, tissue was passed through a 70 µm strainer, spun down, and plated in DMEM supplemented with 10% FBS for cell culture.

Mouse lung cancer cell line KP-482T1 was a gift from T. Jacks[14]. Human bronchial/tracheal epithelial cells (NHBE) were purchased from Lonza (CC-2540). A549 cells were purchased from ATCC (CCL-185). H2087 (ATCC, CRL-5922)-LCC derivatives and the H2030 (ATCC, CRL-5914)-BrM derivative were isolated as described[2,27]. H2087-LCC derived spontaneous outbreak cell lines were generated from spontaneous metastases in mice inoculated intracardially with H2087-LCC cells. KPad1 and KP-482T1 cell lines were genotyped to verify the presence of *Kras*^{G12D} and *Tp53* mutations using PCR amplification. A549, H2087-LCC, and H2030-BrM cells were authenticated with STR profiling. NHBE cells were not authenticated.

H2030-BrM, KP-482T1, and KPad1 were cultured in RPMI 1640 medium supplemented with 10% FBS, 2 mM glutamine, 100 IU ml^{-1} penicillin/streptomycin, and 1 µg ml^{-1} amphotericin B. A549 cells were cultured in DMEM with the same supplements. 293T cells were cultured in DMEM supplemented with 10% FBS and 2 mM L-glutamine. Normal human bronchial epithelial cells were cultured in BEGM bronchial epithelial cell growth basal medium supplemented with SingleQuots (Lonza, CC-3170). H2087-LCC cells and outbreak derivatives were cultured in RPMI 1640 medium supplemented with 10% FBS, 2 mM glutamine, 100 IU ml^{-1} penicillin/streptomycin, 1 µg ml^{-1} amphotericin B, 0.5 mM sodium pyruvate, 10 mM HEPES, 50 nM hydrocortisone, 25 nM sodium selenite, 20 µg ml^{-1} insulin, 10 µg ml^{-1} transferrin, 0.5% bovine serum albumin (BSA), and 1 ng ml^{-1} recombinant human epidermal growth factor. All cell lines tested negative for mycoplasma prior to use in experiments.

Cell culture treatments

Treatment of cell cultures with 2′,3′-cyclic GMP–AMP (cGAMP) or poly(I:C) was performed as previously described[53,54]. For cGAMP treatment, cells were incubated in digitonin permeabilization buffer (50 mM

HEPES pH 7.3, 100 mM KCl, 3 mM $MgCl_2$, 0.1 mM DTT, 85 mM sucrose, 0.2% BSA, and 1 μg ml^{-1} digitonin) for 30 min, then fresh medium was added with 0.5 μg ml^{-1} or 4 μg ml^{-1} cGAMP (Invivogen, tlrl-nacga23) or no additions. For poly(I:C) treatment, cells were incubated with control or 0.5 μg ml^{-1} poly(I:C) (Invivogen, tlrl-picw) and Lipofectamine 2000 transfection reagent (Thermo Fisher Scientific, 11-668-027). Cell lysates were collected 4 h after treatment and processed for RNA isolation.

For other treatments, 50 μM ADU-S100 (MedChemExpress, HY-12885B), 33 μM MSA-2 (MedChemExpress, HY-136927) or vehicle was added to the medium for 4 to 6 h. 100 nM 5-aza-2′-deoxycytidine (Millipore Sigma, A3656-5MG) or DMSO vehicle was added to the medium for 3 days. TGFβ1 (100 pM, R&D Systems) or TGFβ receptor inhibitor SB-505124 (2.5 μM, Millipore Sigma, S4696-5MG) was added in 2% FBS supplemented medium for the indicated time. Two micromolar CDK4/6 inhibitor palbociclib (PD-0332991) (Selleckchem, S1116) was added to the medium for 5–8 days. 20 ng ml^{-1} or 1 μg ml^{-1} doxycycline was added to the medium for 1–2 days. RNA extraction followed all these incubations.

CRISPR screen

Plasmids and sgRNA cloning. To generate stable Cas9-expressing cell lines, lentiCas9-Blast (Addgene, 52962) was used. To express sgRNAs, pUSEPR (U6-sgRNA-EFS-Puro-P2A-TurboRFP) was used[55]. In brief, pUSEPR vector was linearized with BsmBI (NEB) or Esp3I (NEB) and ligated with BsmBI and Esp3I-compatible annealed and phosphorylated oligonucleotides encoding sgRNAs, using high-concentration T4 DNA ligase (NEB). All sgRNA sequences used are listed in Supplementary Tables 2 and 3.

Design and cloning of focused CRISPR libraries. sgRNA sequences (five per gene) targeting genes of interest were designed using a combination of the Broad Institute sgRNA Designer tool[56] and the Vienna Bioactivity CRISPR score[57] (Supplementary Tables 2 and 3). sgRNAs were divided into small pools of libraries, and oligonucleotide pools were synthesized by Agilent Technologies. Libraries were cloned into pUSEPR using a modified version of the protocol published by Doench et al.[56] to ensure a library representation of >10,000-fold[58]. In brief, each library was selectively amplified using uniquely barcoded forward and reverse primers that append cloning adapters at the 5′ and 3′ ends of the sgRNA insert (Supplementary Table 8a), purified using the QIAquick PCR Purification Kit (Qiagen), and ligated into BsmBI/Esp3I-digested and dephosphorylated pUSEPR, using high-concentration T4 DNA ligase (NEB). A total of 1.2 μg of ligated pUSEPR-CRISPR Library plasmid DNA was then electroporated into Endura electrocompetent cells (Lucigen). Competent cells were recovered for 1 h at 37 °C, plated across four 15 cm LB-carbenicillin plates (Teknova), and incubated at 37 °C for 16 h. The total number of bacterial colonies per sub-pool was quantified using serial dilution plates, to ensure a library representation of >10,000-fold. The next morning, bacterial colonies were scraped and briefly expanded for 4 h at 37 °C in 500 ml of LB-carbenicillin. Plasmid DNA was isolated using the Plasmid Plus Maxi Kit (Qiagen). A validated control sgRNA targeting a neutral region in mouse chromosome 8 (ref. 59) was cloned into the pUSEPR backbone and spiked into each of these libraries at a defined fraction to achieve equimolarity between sgRNAs in the library and the control. To assess sgRNA distribution, the sgRNA target region was amplified using primers that append Illumina sequencing adapters on the 5′ and 3′ ends of the amplicon, as well as a random nucleotide stagger and unique demultiplexing barcode on the 5′ end (Supplementary Table 8b). Library amplicons were size-selected on a 2.5% agarose gel, purified using the QIAquick Gel Extraction Kit (Qiagen), and sequenced on an Illumina NextSeq instrument (75 nt single-end reads).

Focused CRISPR–Cas9 genetic screening. To ensure that most cells harbour a single sgRNA integration event, the volume of viral supernatant that would achieve a multiplicity of infection of ~0.3 upon spinfection of a population of Cas9-expressing cancer cells was determined. In brief, cells were plated at 1×10^6 per well in 12-well plates along with increasing volumes of master pool viral supernatant and 10 μg ml^{-1} polybrene (EMD Millipore). Cells were then centrifuged at 1,500 rpm for 2 h at 37 °C and incubated at 37 °C overnight. Viral infection efficiency was determined by the percentage of TurboRFP+ cells assessed by flow cytometry on an LSRFortessa (BD Biosciences) instrument 72 h post infection. The volume of viral supernatant that achieved 30% infection rate was utilized in the screen. To ensure a representation of 1000X at the transduction step, the appropriate number of cells in 12-well plates was spinfected with viral supernatant. Twenty-four hours after infection, cells were pooled into two 150 mm tissue culture plates (Corning) per infection replicate and selected with 2.5 μg ml^{-1} puromycin (Gibco) for 4 days. Subsequently, 5×10^5 puromycin-selected cells were pelleted and stored at 20 °C (cumulative population doubling T0, input population). For H2087-LCC, 2.5×10^5 cells expressing individual pool of library were intracardially injected into 10–12 athymic nude mice (cumulative population doubling T3, input population). For KPad1, 2.5×10^5 cells per mouse were intracardially or intravenously injected into 7-10 B6-albino mice (cumulative population doubling T9, input population). This ensured high representation of sgRNAs (500×) in disseminated cancer cells, as a majority of circulating cancer cells perish and only a small percentage of cells (<10%) survive during colonization[17,60]. Metastasis progression was monitored weekly through BLI.

Isolation of genomic DNA from cells. Genomic DNA (gDNA) was extracted from cells using the DNeasy Blood and Tissue Kit (Qiagen) following the manufacturer's instructions. Cell pellets containing 5×10^5 cells were processed in parallel and resulting gDNA was resuspended in 100 μl of 10 mM Tris-Cl with 0.5 mM EDTA, pH 9.0.

Isolation of genomic DNA from tumour tissues. At the end point, mice were killed and tissues containing metastases were collected. gDNA was extracted from tissues using the DNeasy Blood and Tissue Kit (Qiagen) following the manufacturer's instructions. Tissues were either processed immediately by finely mincing the tissue and incubating overnight in a lysis buffer containing proteinase K following the manufacturer's instructions, or snap-frozen in liquid nitrogen and stored at −80 °C until the day of processing. Resulting gDNA was resuspended in 100–200 μl of 10 mM Tris-Cl with 0.5 mM EDTA, pH 9.0, and samples from common tissue or tumour fragments were pooled at the gDNA level, measured using a NanoDrop 2000 (Thermo Fisher), and normalized before performing sequencing deconvolution.

Deconvolution of CRISPR screens. The library was amplified from gDNA by a modified two-step PCR version of the protocol published by Doench et al.[56] All in vivo gDNA was sampled over two-step PCR reactions. In brief, an initial 'enrichment' PCR was performed, whereby the integrated sgRNA cassettes were amplified from gDNA (PCR1), followed by a second PCR to append Illumina sequencing adapters on the 5′ and 3′ ends of the amplicon, as well as a random nucleotide stagger and unique demultiplexing barcode on the 5′ end (PCR2). Each PCR1 reaction contained 25 μl of Q5 High-Fidelity 2× Master Mix (NEB), 2.5 μl of Nuc PCR1 Fwd Primer (10 μM), 2.5 μl of Nuc PCR1 Rev Primer (10 μM), and a maximum of 5 μg of gDNA in 20 μl of water. PCR1 amplicons were purified using the QIAquick PCR Purification Kit (Qiagen) and used as template for PCR2 reactions. Each PCR2 reaction contained 25 μl of Q5 High-Fidelity 2× Master Mix (NEB), 2.5 μl of a unique Nuc PCR2 Fwd Primer (10 μM), 2.5 μl of Nuc PCR2 Rev Primer (10 μM), and 300 ng of PCR1 product in 20 μl of water. Two PCR2 reactions were run per PCR1 product. Library amplicons were size-selected on a 2.5% agarose gel, purified using the QIAquick Gel Extraction Kit (Qiagen) followed by normalization, pooling, purification using AMPure XP beads (Beckman Coulter), and sequencing on an Illumina NextSeq500 instrument (75 nt single-end reads). All primer sequences are available in Supplementary

Table 8b. PCR settings for PCR1 and PCR2 were: initial denaturation at 98 °C for 30 s; then 98 °C for 10 s, 65 °C for 30 s, 72 °C for 30 s for 24 cycles; followed by extension at 72 °C for 2 min.

Analysis of CRISPR–Cas9 genetic screen data. FASTQ files were processed and trimmed to retrieve sgRNA target sequences followed by alignment to the reference sgRNA library file. Raw sequencing read counts were quantified for each sgRNA, and samples were pooled at the organ level for downstream analyses (reads from the same organ across multiple mice were pooled). Reads were normalized to the total read counts per sample, and input samples were used as references to calculate log2 fold change values per sgRNA using a combination of MAGeCK (v 0.5.9.4) and custom R (v 4.0.5) scripts. Enriched fold change ($\log_2$FC > 0) values were used to average across all samples to generate average fold changes. For each library, the most enriched sgRNA for each gene was identified, and the corresponding genes were rank-ordered based on average fold change enrichments, as previously described[61]. See Supplementary Table 5 for all screening data.

Knockout and overexpression constructs

CRISPR-mediated knockouts were generated by cloning sgRNAs into the Guide-it CRISPR–Cas9 vector (Red, TaKaRa, 632602), transfecting the construct into cells, then isolating and expanding the cells with knockouts from single cell colonies. Sequences of sgRNA oligonucleotides are: hSTING.sg1 (forward CCGGGCTGGGACTGCTGTTAAACG; reverse AAACCGTTTAACAGCA GTCCCAGC), mSTING.sg1 (forward CCGGTTGATCCCCCGGAAATCGGG; reverse AAACCCC GATTTC CGGGGGATCAA), mSTING.sg2 (forward CCGGTTAGAGGAATTCGGAG TGCG; reverse AAACCGCACTCCGAATTCCTCTAA), hTGFBR2 (forward CCGGAACGTGCGGTGGG ATCGTGC; reverse AAACGCACGATCCCA CCGCACGTT).

To overexpress wild-type STING or STING(V155M), human wild-type *STING* was amplified by PCR from pUNO1-hSTING-HA3x (Invivogen, puno1ha-hsting). The V155M mutation was introduced in *STING* by PCR. Mouse wild-type *Sting* was amplified by PCR from pUNO1-mSTINGwt-HA3x (Invivogen, puno1ha-mstingwt). PCR amplified products were ligated to pLVX-Tight-Puro (Takara, 632162), a tetracycline-inducible lentiviral expression vector.

To generate a TGFβ reporter system, DNA sequences containing 12 SMAD-binding elements (SBE, 5′-AGCCAGACA-3′) and a minimal CMV promoter[62] were subcloned into pLenti CMV rtTA3 Hygro (w785-1) vector (Addgene, #26730) replacing the original CMV promoter. The mCherry coding sequence was subcloned into pLenti CMVtight eGFP Puro (w771-1) vector (Addgene, #26431) replacing eGFP, to generate a Tet-inducible expression vector expressing mCherry. Both pLenti CMV rtTA3 Hygro and pLenti CMVtight eGFP Puro vectors were gifts from E. Campeau.

scRNA-seq data analysis

We used our previously reported scRNA-seq dataset from human LUAD specimens (GSE123904)[13]. The normalized, imputed gene expression generated by Laughney et al.[13] was used as the input. Metastatic tumour cells were ranked by average lung epithelial development score and assigned to different stages[13]. A gene signature of STING pathway targets (*IFNA2*, *IFNB1*, *CCL5*, *CXCL10*, *TNF*, *OASL*, *IRF1*, *IRF6*, *IRF7*, *IRF9*, *ADAR*, *CCL2*, *CCL26* and *IL33*) was assembled by integrating STING regulated genes in human or mouse cells (Extended Data Fig. 3h,j) from previous reports[24–26,63]. *Z*-normalized, imputed expression of genes or gene signatures was plotted on heat maps using the seaborn.heatmap (v 0.11.2) function in Python (v3.8.8). Violin plots were generated using the seaborn.violinplot (v 0.11.2) function. The gene signature 'STING targets' in the violin plots represents average *z*-scores of the constituent genes in the signature.

We reprocessed the scRNA-seq dataset of H2087 cells derived from Laughney et al.[13], consisting of 3 samples and 2,245 cells in total, including: 351 cells and 892 cells grown in culture from the dormant metastasis stage of mice M4585 and M4587, respectively; and 1,002 cells grown in culture from multiple macrometastases of mouse M4770. The raw sequencing results were aligned and pre-processed by SEQC (v 0.2.1) to human reference genome build GRCh38. The SEQC output was filtered to remove apoptotic cells (that is, cells with more than 20% of mitochondrial gene transcripts), and further filtered to exclude empty droplets (that is, with small library size or lacking gene–gene correlation structure) as well as mitochondrial genes, ribosomal genes, and genes detected in fewer than 10 cells. The filtered counts of three samples were then merged and normalized by the library size. Phenograph clustering was conducted on 258 principal components accounting for a total of 70% variance of the merged normalized expression. The expression was further imputed by running MAGIC (v 0.1.1)[64] with $t = 3$.

For the mouse data heat map (Extended Data Fig. 3h), cells were first sorted by their pseudotime as computed by Palantir (v 1.0.0)[64]. The *z*-scored expression of the displayed genes and/or gene signatures was then plotted using seaborn.heatmap, without hierarchical clustering or moving average smoothing. The *z*-scored expression was also visualized by violin plots using seaborn.violinplot. Clustered heat map (Extended Data Fig. 3i) was computed in Python (v3.8.8) using the normalized dataset from Laughney et al.[13] without any further processing, and using the seaborn.clustermap function, with the method parameter set to "Ward" and the metric parameter kept as the default "euclidean" distance. UMAP plots were generated using scanpy (v 1.8.1)[65]. Genes differentially expressed between the Phenograph (v 1.5.2) clusters were determined by running MAST (v 1.0.1)[66] using default parameters, with normalized counts as the input. Genes with FDR (false discovery rate)-corrected *P* values < 0.01 and absolute $\log_2$FC > 1.2 were considered significantly different. GSEA[67,68] was run to identify significantly enriched gene signatures among differentially expressed genes using hallmark gene sets[69]. Additional open-source algorithms used were Pandas (v 1.4.3), Numpy (v 1.21.5), Scipy (v 1.7.3), Scikit-learn (v 1.1.1) and Matplotlib (v3.5.1).

Flow cytometry analysis of cell surface and intracellular protein expression

For immune phenotyping of metastases-bearing femurs, tissues were washed in PBS, then chopped into small pieces using a sterile razor blade and resuspended in 5 ml of digestion buffer containing 1 mg ml^{-1} collagenase D (Millipore Sigma, 11088866001) and 0.05 mg ml^{-1} DNase in RPMI medium. After incubation at 37 °C for 40 min, the tissue sample was passed through a 70-µm strainer, spun down, and processed in 1× eBioscience 10× red blood cell lysis buffer (Thermo Fisher Scientific, 00-4300-54).

Cells were washed and resuspended with stain medium (PBS supplemented with 2% FBS) that contained fixable viability dye eFluor 506 (Thermo Fisher Scientific, 65-0866-14, 1:400), anti-mouse CD16/32 antibodies (clone 2.4G2, BioXCell, BE0307, 1:1,000) and antibodies specific for proteins of interest. Cells were stained for surface proteins for 25 min at 4 °C, washed, and stained for intracellular proteins according to the FoxP3/Transcription Factor Staining Buffer Set instructions (Thermo Fisher Scientific, 00-5523-00). Stained cells were washed, resuspended in stain medium that contained a known number of 123count eBeads (Thermo Fisher Scientific, 01-1234-42) to calculate absolute cell number, and analysed on a Cytek Aurora (Cytek Biosciences). Flow cytometry data were further analysed using FlowJo software (BD Biosciences, v 10.6.2).

The following antibodies were from Biolegend: anti-mouse NKp46 (clone 29A1.4, 137612, 1:50), anti-mouse CD44 (clone IM7, 103057, 1:400), anti-mouse XCR1 (clone ZET, 148220, 1:100), anti-mouse TCRβ (clone H57-597, 109220, 1:400), anti-mouse CD11c (clone N418, 117318, 1:400), anti-mouse CD19 (clone 6D5, 115530, 1:400), anti-mouse TNF (clone MP6-XT22, 506308, 1:100). The following antibodies were from BD Biosciences: anti-mouse CD49b (clone HMa2, 741523, 1:200),

anti-mouse NK1.1 (PK136, 741926, 1:200), anti-mouse CD8α (53-6.7, 748535, 1:200), anti-mouse CD4 (GK1.5, 565974, 1:200). The following antibodies were from Thermo Fisher Scientific: anti-mouse IFNγ (clone XMG1.2, 48-7311-82, 1:100). Anti-mouse TCRβ (clone H57-597, 1785-16, 1:200) was from Southern Biotech and anti-mouse CD45 (30-F11, 80-0451-U100, 1:200) was from Tonbo.

Ex vivo cytokine stimulation assay

Approximately 1.5 x 10^6 cells were resuspended in Iscove's modified Dulbecco's medium (IMDM) supplemented with 10% FBS, 1% penicillin/streptomycin, 2 mM L-glutamine, 55 μM 2-mercaptoethanol, 1 mM sodium pyruvate, and 1× non-essential amino acids. Cells were cultured with 10 ng ml^{-1} phorbol 12-myristate 13-acetate (Millipore Sigma), 1 μg ml^{-1} ionomycin (Millipore Sigma), 10 μg ml^{-1} brefeldin A (Millipore Sigma), BD GolgiStop containing monensin (BD Biosciences) according to vendor instructions, and anti-mouse CD107a (clone 1D4B, Biolegend, 121624, 1:100) for 4 h at 37 °C. Cells were washed and processed for staining and flow cytometric analysis.

NK cell sorting and expansion

To purify NK cells prior to sorting, spleens from athymic nude mice were collected and dissociated through a 100-μm strainer. Single-cell suspensions were then incubated with rat antibodies against mouse Ly6G, CD19, CD3ε, CD8α, CD4 and Ter-119 antibodies (Bio X Cell, clones 1A8, 1D3, 17A2, 2.43, GK1.5 and TER-119, respectively, 1:100), washed twice in PBS supplemented with 2% FBS, then incubated with BioMag goat anti-rat IgG beads (Qiagen, 310107, 5mg per spleen) to remove antibody-bound cells. Purified NK cells were stained with antibodies against NK1.1 (PK136, Tonbo, 65-5941, 1:100), CD49b (DX5, BioLegend, 108918, 1:100), and NKp46 (29A1.4, BioLegend, 137604, 1:100) in the presence of purified rat anti-mouse CD16/CD32 (BD Biosciences, 553142, 1:1,000) to block non-specific Fc binding and Fixable Viability Dye eFluor 506 (Thermo Fisher Scientific, 65-0866-14, 1:400) to distinguish dead cells. Cell sorting was performed on an Aria III cytometer (BD Biosciences). Sorted NK cells were expanded by culturing in Iscove's modified Dulbecco's medium supplemented with 10% FBS, 2 mM L-glutamine, 55 μM 2-mercaptoethanol, 1% penicillin/streptomycin, and recombinant human IL-15 (50 ng ml^{-1}; Miltenyi Biotec, 130-095-765).

NK cell cytotoxicity assay

Cytotoxicity assays were performed as described previously[70]. In brief, sorted NK cells were resuspended in NK cell medium (phenol-red free RPMI 1640 containing 10% FBS, 1× non-essential amino acids, 2 mM L-glutamine and 1 mM sodium pyruvate). Indicated target cells were labelled with 15 μM calcein-AM (Thermo Fisher Scientific, C1430) for 30 min at 37 °C, washed twice and resuspended in NK cell medium. Effector and target cells were combined at indicated ratios in triplicate wells of a round-bottom 96-well plate. Maximum and spontaneous lysis controls were generated by combining target cells with 2% Triton X-100 or medium alone in place of effector cells, respectively. Cells were incubated at 37 °C for 4 h. Calcein release was quantified by carefully transferring 100 μl of cell-free supernatant to opaque 96-well plates and measuring fluorescent emission using the EnVision Robot Plate Reader (PerkinElmer) set to excitation 485 ± 9 nm and emission 525 ± 15 nm.

In vitro Transwell NK migration assay

NK migration assays were performed as previously described[71]. To prepare conditioned medium from cancer cells, cells were cultured in 6-well plates, washed twice with PBS and switched to serum-free medium 16 h before medium collection. On the day of experiment, NK cells were washed twice and resuspended in serum-free medium. In total, 2.5 × 10^5 NK cells in 100 μl medium were plated on the upper compartment of a Transwell permeable chamber (6.5 mm diameter insert and 5 μm pore size, Corning, 3421). Six-hundred microlitres of serum-free medium or conditioned medium from cancer cells were plated in the bottom chamber. After incubation at 37 °C for 4 h, non-adherent and migrated NK cells from the bottom chamber were collected, mixed with 123count eBeads Counting beads and counted using flow cytometry.

Immunohistochemistry and immunofluorescence

For staining of 5 μm sections, human tissue samples were fixed in formalin and mouse metastatic tissue samples were fixed in 4% paraformaldehyde for 24 h prior to paraffin embedding. Sections were deparaffinized using Histo-Clear (National Diagnostics, HS-200), rehydrated, and incubated with hydrogen peroxide to quench endogenous peroxidase activity, followed by antigen retrieval in antigen unmasking solution, citrate-based (Vector Laboratories, H-3300) in a steamer for 30 min. For vimentin immunohistochemistry, after antigen retrieval, sections were incubated with 2.5% normal horse serum (Vector Labs) and then anti-vimentin antibody (Abcam, ab8069, 1:200) overnight at 4 °C. ImmPRESS horseradish peroxidase (HRP) anti-mouse IgG and ImmPACT DAB Peroxidase (Vector Labs) were used for detection. For immunofluorescence staining, sections were incubated with 10% normal goat serum (Life Technologies, 50062Z) or 10% normal donkey serum (Millipore Sigma, D9663-10ML) supplemented with 2% BSA (Fisher Scientific, BP9706100) and 0.25% Triton X-100. Sections were then incubated in primary antibodies overnight at 4 °C. After washing in PBS with 0.25% Triton X-100 (PBS-Tr), sections were incubated in fluorophore-conjugated secondary antibodies for 2 h, followed by washing and staining with nuclear dye Hoechst 33342 (Thermo Fisher Scientific, H3570, 1:5,000). Tissue sections were then dehydrated in 70–100% ethanol and Histo-Clear, followed by mounting in Vectashield mounting medium (immunohistochemistry) (Vector Laboratories, H100010) or ProLong diamond antifade mountant (immunofluorescence) (Life Technology, P36970). For STING immunohistochemistry, sections were stained with anti-STING antibody (D2P2F, Cell Signaling Technology, 13647, 1:500) via standardized automated protocols, on a Ventana Discovery XT instrument.

For immunofluorescence of thick metastases samples, organs were fixed in 4% paraformaldehyde overnight at 4 °C and then washed twice with 1× PBS. Organs were cryo-protected by sequential immersion in 15% w/v and 30% w/v sucrose, then mounted using Tissue-Tek Optimal Cutting Temperature Compound (Sakura, 4583) on a sliding microtome with a platform freezing unit (Thermo Scientific, Microm KS-34 and Microm HM-450). 80 μm sections were cut and stored in anti-freezing solution (40% w/v ethylene glycol and 30% v/v glycerol in PBS) at −20 °C. Floating sections representative of the entire organ were permeabilized by washing with PBS-Tr 3 times, followed by incubation for 1 h in blocking buffer containing 10% normal goat or donkey serum, supplemented with 2% BSA and 0.25% Triton X-100. Sections were then incubated in primary antibodies diluted in blocking buffer, overnight at 4 °C. After washing with PBS-Tr 6 times, sections were incubated in fluorophore-conjugated secondary antibodies for 2 h. Sections were washed with PBS-Tr and then PBS three times each, followed by staining with nuclear dye Hoechst 33342 for 5 min, and three additional washes in PBS. Sections were transferred onto slides and mounted using ProLong diamond antifade mountant.

For immunofluorescence of NK and T cells in bone metastases samples, bone tissues were fixed in 4% paraformaldehyde overnight at 4 °C and washed twice with 1× PBS. Bone decalcification was achieved by incubating the bone tissue in EDTA-based decalcification solution containing 140 g EDTA L^{-1} (pH 7.4, Millipore Sigma) for 1 to 2 weeks at 4 °C with agitation, changing decalcification solution every other day. Bone tissues were then washed with water for 1 h to remove EDTA, re-fixed in 4% PFA overnight at 4 °C, washed twice in PBS, and incubated in 70% ethanol overnight at 4 °C. After paraffin embedding, tissue blocks were cut into 5 μm sections. Sections were deparaffinized, rehydrated, incubated with hydrogen peroxide, followed by antigen retrieval in antigen unmasking solution, citrate-based. For NK cell staining, the

Alexa Fluor 594 Tyramide SuperBoost kit, streptavidin (Thermo Fisher Scientific, B40935) was applied. Sections were blocked with normal donkey serum, then incubated with the avidin/biotin blocking kit (Vector Laboratories, SP-2001), followed by incubation in goat anti-mouse NKp46/NCR1 (R&D systems, AF2225, 1:250) overnight at 4 °C. Sections were then washed with PBS-Tr and incubated with donkey anti-goat IgG, biotin (Thermo Fisher Scientific, A16009, 1:500) at room temperature for 2 h. After washes with PBS-Tr and PBS, sections were incubated with HRP-conjugated streptavidin for 1 h at room temperature, followed by three washes with PBS. Sections were then incubated with tyramide reagent for 5 min and stop reagent for 5 min. After NK cell staining, sections were stained for T cells and cancer cells by incubating with primary antibodies against CD3ε (D4V8L, Cell Signaling Technologies, 99940S, 1:200) or cytokeratin 8 (TROMA-1, Millipore Sigma, MABT329, 1:100), followed by washes and incubation in fluorophore-conjugated secondary antibodies (Thermo Fisher Scientific) and nuclear staining in Hoechst 33342. Sections were mounted using ProLong diamond antifade mountant.

For quantification of immunohistochemistry, slides were scanned by the Mirax Scanner (Carl Zeiss). A STING immunohistochemistry intensity score was assigned to each tumour lesion based on the scoring levels depicted in Extended Data Fig. 3e, and the tumour area was measured by ImageJ (v 2.1.0). H-score for metastases from each organ was calculated using the following formula: [1 × (per cent tumour area 1+) + 2 × (per cent tumour area 2+) + 3 × (per cent tumour area 3+)], where 1+, 2+, or 3+ refers to the immunohistochemistry staining intensity level. For quantification of immunofluorescence staining, images were acquired with an SP5 confocal microscope (Leica Microsystems) or a Zeiss Imager.Z1 fluorescence microscope (Carl Zeiss). Fluorescence intensity was analysed with ImageJ software (v 2.1.0/1.53c). The following commercial antibodies were used: rat anti-Ki67 (Invitrogen, 14-5698-80, 1:100), mouse anti-Vimentin (Abcam, ab8069, 1:500 (immunofluorescence), 1:200 (immunohistochemistry)), chicken anti-GFP (Aves Labs, GFP-1010, 1:250), mouse anti-human cytokeratin (AE1/AE3) (Agilent Technologies, M351529-2, 1:100), rabbit anti-STING (D2P2F) (Cell Signaling Technologies, 13647, 1:250), goat anti-CCL5/RANTES (Novus Biologicals, AF278 (human), AF478 (mouse), 1:40), rabbit anti-CD3ε (D4V8L) (Cell Signaling Technologies 99940S, 1:200), goat anti-mouse NKp46/NCR1 (R&D Systems, AF2225, 1:250), rat anti-cytokeratin 8 (TROMA-1) (Millipore Sigma, MABT329, 1:100), rat anti-SOX2 (Btjce) (Thermo Fisher Scientific, 14-9811-82, 1:200), rabbit anti-SOX9 (Millipore Sigma, AB5535, 1:300), rabbit anti-mCherry (Abcam, ab167453, 1:500), goat anti-chicken 488 (Thermo Fisher Scientific, A-11039, 1:500), goat anti-rat 647 (Thermo Fisher Scientific, A-21247, 1:500), goat anti-rabbit 594 (Thermo Fisher Scientific, A-11012, 1:500), goat anti-mouse 488 (Thermo Fisher Scientific, A-11001, 1:500), donkey anti-mouse 488 (Thermo Fisher Scientific, A-21202, 1:500), donkey anti-rat 647 (Abcam, ab150155, 1:500), donkey anti-goat 594 (Thermo Fisher Scientific, A-11058, 1:500), donkey anti-chicken 488 (Biotium, 20166, 1:500).

RT–qPCR analysis

RNA was extracted from cells using the RNeasy Mini Kit (Qiagen, 74106). cDNA was generated using the Transcriptor First Strand cDNA Synthesis Kit (Roche, 04379012001). Relative gene expression was determined using Taqman or SYBR green assays (Life Technologies). Quantitative PCR was performed on the ViiA 7 Real-Time PCR System (Life Technologies). The housekeeping gene *ACTB* encoding β-actin was used as the internal control for calculating relative gene expression. Taqman assays used for human genes were: *STING* (Hs00736955_g1), *IFNB* (Hs01077958_s1), *SMAD7* (Hs00998193_m1), *SNAI1* (Hs00195591_m1), *cGAS* (Hs00403553_m1) and *ACTB* (Hs01060665_g1). Taqman assays used for mouse genes were: *Sting* (Mm01158117_m1), *Ifnb1* (Mm00439552_s1), *Ccl5* (Mm01302427_m1), *Cxcl10* (Mm00445235_m1), *Actb* (Mm01205647_g1). Primers used for SYBR green assays (human genes) are: *ACTB* (forward GTTGTCGACGACGAGCG; reverse GCACAGAGCCTCGCCTT), *IFNB* (forward CAGGAGAGCAATTTGGAGGA; reverse CTTTCGAAGCCTTTGCTCTG), *CCL5* (forward TGTACTCCCGAACCCATTTC; reverse TACACCAGTGGCAAGTGCTC), *CXCL10* (forward GCTGATGCAGGTACAGCGT; reverse GAGCCTACAGCAGAGGAACC).

Targeted next-generation bisulfite sequencing analysis

Sample preparation. H2087 cell pellets freshly isolated and sorted from metastases in athymic nude mice or NSG mice were frozen in −80 °C and analysed at EpigenDx. The promoter (H3K4me3 containing region) and 3′ enhancer (H3K4me1 and H3K27ac containing region) sequences of *STING* were acquired from the Ensembl genome browser and annotated. The target sequences were re-evaluated against the UCSC genome browser for repeat sequences including LINE, SINE, and LTR elements. Sequences containing repetitive elements, low sequence complexity, high thymidine content, and high CpG density were excluded from the in silico design process. Cell pellets were lysed using M-digestion buffer (ZymoResearch, D5021-9) and 5–10 µl of protease K (20mg ml^{-1}), with a final M-digestion concentration of 2×. The samples were incubated at 65 °C for a minimum of 2 h. 20 µl of the supernatant from the sample extracts were bisulfite modified using the EZ-96 DNA Methylation-Direct Kit (ZymoResearch, D5023) as per the manufacturer's protocol with minor modification. The bisulfite modified DNA samples were eluted using M-elution buffer in 46 µl.

Multiplex PCR. All bisulfite modified DNA samples were amplified using separate multiplex or simplex PCR reactions. PCR reactions included 0.5 units of HotStarTaq (Qiagen, 203205), 0.2 µM primers, and 3 µl of bisulfite-treated DNA in a 20 µl reaction. All PCR products were verified using the Qiagen QIAxcel Advanced System (v 1.0.6). Prior to library preparation, PCR products from the same sample were pooled and then purified using the QIAquick PCR Purification Kit columns or plates (Qiagen, 28106 or 28183). PCR settings included initial denaturation at 95 °C for 15 min; then 95 °C for 30 s, specific annealing temperature for each primer for 30 s, 68 °C for 30 s for 45 cycles; and extension at 65 °C for 5 min. Samples were run alongside established reference DNA samples created by mixing high- and low-methylated DNA to obtain samples with 0%, 5%, 10%, 25%, 50%, 75%, and 100% methylation. The high-methylated DNA was enzymatically methylated gDNA with >85% methylation. The low-methylated DNA was chemically and enzymatically treated to contain <5% methylation. Both were tested on numerous gene-specific and global methylation assays using pyrosequencing.

Library preparation and sequencing. Libraries were prepared using a custom library preparation method created by EpigenDx and purified using Agencourt AMPure XP beads (Beckman Coulter, A63882). Barcoded samples were then pooled in an equimolar fashion before template preparation and enrichment were performed on the Ion Chef system using Ion 520 and Ion 530 ExT Chef reagents (Thermo Fisher Scientific, A30670). Following this, enriched, template-positive library molecules were sequenced on the Ion S5 sequencer using an Ion 530 sequencing chip (A27764).

Data analysis. FASTQ files from the Ion Torrent S5 server were aligned to a local reference database using the open-source Bismark Bisulfite Read Mapper program (v 0.12.2) with the Bowtie2 alignment algorithm (v 2.2.3). Methylation levels were calculated in Bismark by dividing the number of methylated reads by the total number of reads. An R-squared value (RSQ) was calculated from the controls set at known methylation levels to test for PCR bias.

Chromatin immunoprecipitation analysis

For chromatin immunoprecipitation analysis (ChIP–seq and ChIP–PCR), cells were crosslinked with 1% formaldehyde (Millipore Sigma, F8775) for 10 min and quenched with 0.125 M glycine for 5 min at room

temperature. ChIP was performed using the ChIP assay kit (Millipore Sigma, 17-295) according to the manufacturer's instructions. Antibodies against H3K4me3 (Millipore Sigma, 05-745, 5 µg per sample), H3K27me3 (Millipore Sigma, 07-449, 10 µg per sample), H3K4me1 (Abcam, ab8895, 5 µg per sample), H3K27Ac (Active Motif, 39133, 5 µg per sample), DNMT1 (Abcam, ab13537, 5 µg per sample), DNMT3B (Cell Signaling Technologies, 57868S, 5 µg per sample) were used. Immunoprecipitated DNA was purified using the QIAquick PCR Purification Kit (Qiagen).

For ChIP–seq, immunoprecipitated DNA was quantified by PicoGreen and the size was evaluated by Agilent BioAnalyzer. When possible, fragments between 100 and 600 bp were size-selected using AMPure XP beads (Beckman Coulter, A63882) and Illumina sequencing libraries were prepared using the KAPA HTP Library Preparation Kit (Kapa Biosystems KK8234) according to the manufacturer's instructions, with an undetectable mass to 10 ng input DNA and 10 cycles of PCR. Barcoded libraries were run on the NovaSeq 6000 in a PE100 run, using the NovaSeq 6000 S4 Reagent Kit (200 Cycles) (Illumina). An average of 45 million paired reads were generated per sample. For mapping and visualization, paired-end (50/50 bp) FASTQ reads were mapped to human genome hg19 using Bowtie2 (v 2.1.0) with default filtering criteria[72]. Resulted SAM files were converted to BAM files though Samtools (v 1.9)[73]. BAM files were sorted and indexed with Samtools (v 1.9)[73]. BAM files were normalized, converted to bigwig files using bamCoverage-deepTools (v3.3.2)[23] and displayed with IGV browser (v 2.14.1). Peak calling from BAM files was performed with MACS (v 2.2.7.1).

For ChIP–PCR, DNA samples were amplified by real-time PCR using specific primers. The amplification product was calculated as the percentage of the input, then normalized to the control experiment for each condition. ChIP–PCR primers for the *STING* promoter are forward AGAAACACTCACCGCAGTC and reverse GGAGTCCTGCTCAGGTGTTA. ChIP–PCR primers for the *STING* 3′ enhancer are forward CATGGCAT CATTTGTGTGCTG and reverse GTCCTTTCAGTGCCTTTCTCT.

MeDIP analysis

MeDIP was performed as described in Karpova et al.[74] gDNA was extracted from cells using the QIAamp DNA Mini Kit (Qiagen, 51304), following the manufacturer's instructions. 9 µg DNA in 1 ml of immunoprecipitation (IP) buffer (10 mM sodium phosphate pH 7.0, 0.14 M NaCl, 0.05% v/v Triton X-100) was sonicated (the range of DNA fragment is 200–500 bp), then denatured at 99 °C for 10 min. Four micrograms of DNA was then incubated at 4 °C overnight shaking in IP buffer containing either mouse (G3A1) IgG1 isotype control (Cell Signaling Technologies, 5415, 3 µg per sample) or 5-methylcytosine, clone 33D3 (Diagenode, C15200081-100, 3 µg per sample) antibody. The following day, the DNA-antibody complex was incubated with Dynabeads Protein G for Immunoprecipitation (Thermo Fisher Scientific, 10003D) at 4 °C for 2 h. DNA combined with beads was washed three times in IP buffer, and DNA was eluted from beads in proteinase K digestion buffer (60 µg proteinase K, 50 mM Tris pH 8.0, 10 mM EDTA, 0.5% SDS) at 56 °C while shaking for 2 h. DNA was purified using the QIAquick PCR Purification Kit (Qiagen, 28106), followed by quantitative PCR analysis. 20% input was used as control. The amplification product was calculated as the percentage of the input, then normalized to the H2087-LCC control. PCR primers for the *STING* promoter (forward ACCAGTAAAGCTGCG GTTTG; reverse CTGCTCTGGATGATGACGAG) were obtained from a previous study[34]. PCR primers for the *STING* 3′ enhancer were CATG GCATCATTTGTGTGCTG (forward) and GTCCTTTCAGTGCCTTTCTCT (reverse).

Immunoblotting

Cells were lysed using RIPA cell lysis buffer (Cell Signaling Technology, 9806S) supplemented with protease inhibitors (Roche, cOmplete, mini, EDTA-free protease inhibitor tablets, 11836170001) and phosphatase inhibitor (Thermo Scientific, Halt Phosphatase Inhibitor Cocktail, 78427, 1:1,000). Protein concentration was measured using the BCA Protein Assay Kit (Pierce). Protein was then mixed with NuPage LDS sample buffer (Thermo Fisher Scientific, NP0007) supplemented with NuPAGE Sample Reducing Agent (Thermo Fisher Scientific, NP0009), heated at 95 °C for 10 min, briefly sonicated, then loaded in NuPAGE Novex 4-12% Bis-Tris gels (Thermo Fisher Scientific) using 1× MOPS SDS running buffer (Thermo Fisher Scientific, NP0001) and transferred to nitrocellulose membranes after electrophoresis. Membranes were blocked with Odyssey blocking buffer (Tris-buffered saline) (LI-COR Biosciences, 927–60001) and incubated overnight with primary antibodies against STING (Cell Signaling Technology, 13647, 1:1,000) or β-actin (Cell Signaling Technology, 3700, 1:5,000). After washing in PBS + 0.1% Tween (PBST) three times, membranes were incubated with IRDye 680RD goat anti-mouse (LI-COR Biosciences, 926–68070, 1:10,000) or IRDye 800CW goat anti-rabbit (LI-COR Biosciences, 926–32211, 1:10,000) secondary antibodies. Signal was detected using an Odyssey CLx imager (LI-COR Biosciences) and analysed using Image-StudioLite (LI-COR Biosciences, v3.1.4).

Cytokine array

Cells were plated in triplicate in 6-well plates and treated for 3 days with or without 1 µg ml^{-1} doxycycline hydrochloride (Thermo Fisher Scientific, BP2653-5) in 2 ml medium. Conditioned medium was collected and aliquots (75 µl) were then analysed using the Mouse Cytokine/Chemokine 44-Plex Discovery Assay Array from Eve Technologies.

Other assays

EdU incorporation assay was performed with Click-iT Plus EdU Alexa Fluor 647 Flow Cytometry Assay Kit (Thermo Fisher Scientific, C10634), following the manufacturer's instructions. Cells were plated in triplicates in 6-well plates and incubated with 10 µM EdU for 1.5–2 h, followed by flow cytometric analysis.

For cell viability assays, H2087-LCC cells were plated in four replicates in 96-well plates and incubated with 100 pM TGFβ1 or 2 µM CDK4/6 inhibitor palbociclib (Selleckchem, S1116) in culture medium. Cell proliferation was quantified at the indicated time points using the CellTiter-Glo Luminescent Cell Viability Assay (Promega, G7572), following the manufacturer's instructions. Samples were analysed using the Synergy H1 Hybrid microplate reader (Agilent).

For determinations of 2′,3′-cGAMP, 5×10^5 cells were lysed using M-PER mammalian protein extraction reagent (Thermo Fisher Scientific, 78503). 2′,3′-cGAMP content was measured with a 2′,3′-cGAMP ELISA kit (Cayman Chemical Company, 501700) following the manufacturer's instructions.

Statistics and reproducibility

Statistical analyses and number of samples (*n*) are given in each figure panel. Mann–Whitney *U*-tests, *t*-tests and log-rank tests were performed in Graphpad Prism (v 9.0.0.). No statistical method was used to predetermine the sample size for in vivo experiments. Sample sizes were chosen based on prior experience and pilot experiments for detecting statistically significant differences between conditions. For in vivo treatment assays with STING agonists, doxycycline and immune cell depleting antibodies, mice were distributed into treatment groups with approximately equal bioluminescent intensities. For other experiments, samples were randomly assigned to each group. Analysis of protein expression from immunohistochemistry or immunofluorescence images were blindly conducted using scripts of ImageJ batch analysis. Immunohistochemistry staining of STING expression in patient specimens was confirmed by a pathologist as a blinded reviewer. Investigators were blinded to conduct and analyse CRISPR screen assays. Investigators were not blinded to treatment groups for other in vivo or in vitro studies, as knowledge of this information was essential to conduct the studies.

Schematics

Schematics were prepared using Office 365 (Microsoft, v 16.57), Adobe Illustrator (v 25.0.1), and BioRender.com with permissions to publish (Figs. 1a,d, 2e, 4g and 5a and Extended Data Figs. 3h, 4a, 9d and 11a).

Reporting summary

Further information on research design is available in the Nature Portfolio Reporting Summary linked to this article.

Data availability

The raw sequencing data corresponding to CRISPR screens and targeted bisulfite sequencing have been deposited in the NCBI Sequence Read Archive under accessions PRJNA786579 and PRJNA867723, respectively. ChIP–seq data have been deposited in the Gene Expression Omnibus under accession GSE210946. Source data are provided with this paper.

Code availability

Custom code used in this study are available at Zenodo: https://doi.org/10.5281/zenodo.7618821.

51. Tello-Lafoz, M. et al. Cytotoxic lymphocytes target characteristic biophysical vulnerabilities in cancer. *Immunity* **54**, 1037–1054.e1037 (2021).
52. DuPage, M., Dooley, A. L. & Jacks, T. Conditional mouse lung cancer models using adenoviral or lentiviral delivery of Cre recombinase. *Nat. Protoc.* **4**, 1064–1072 (2009).
53. Girardin, S. E. et al. Nod1 detects a unique muropeptide from Gram-negative bacterial peptidoglycan. *Science* **300**, 1584–1587 (2003).
54. Wang, Q. et al. The E3 ubiquitin ligase AMFR and INSIG1 bridge the activation of TBK1 kinase by modifying the adaptor STING. *Immunity* **41**, 919–933 (2014).
55. Soto-Feliciano, Y. M. et al. A molecular switch between mammalian MLL complexes dictates response to Menin–MLL inhibition. *Cancer Discov.* **13**, 146–169 (2022).
56. Doench, J. G. et al. Optimized sgRNA design to maximize activity and minimize off-target effects of CRISPR–Cas9. *Nat. Biotechnol.* **34**, 184–191 (2016).
57. Michlits, G. et al. Multilayered VBC score predicts sgRNAs that efficiently generate loss-of-function alleles. *Nat. Methods* **17**, 708–716 (2020).
58. Sánchez-Rivera, F. J. et al. A base editing sensor streamlines high-throughput guide validation and engineering of cancer associated variants. *Nat. Biotechnol.* **40**, 862–873 (2022).
59. Dow, L. E. et al. Inducible in vivo genome editing with CRISPR–Cas9. *Nat. Biotechnol.* **33**, 390–394 (2015).
60. Minn, A. J. et al. Distinct organ-specific metastatic potential of individual breast cancer cells and primary tumors. *J. Clin. Invest.* **115**, 44–55 (2005).
61. Ebright, R. Y. et al. Deregulation of ribosomal protein expression and translation promotes breast cancer metastasis. *Science* **367**, 1468–1473 (2020).
62. Oshimori, N., Oristian, D. & Fuchs, E. TGF-β promotes heterogeneity and drug resistance in squamous cell carcinoma. *Cell* **160**, 963–976 (2015).
63. Ahn, J., Gutman, D., Saijo, S. & Barber, G. N. STING manifests self DNA-dependent inflammatory disease. *Proc. Natl Acad. Sci. USA* **109**, 19386–19391 (2012).
64. Setty, M. et al. Characterization of cell fate probabilities in single-cell data with Palantir. *Nat. Biotechnol.* **37**, 451–460 (2019).
65. McInnes, L., Healy, J. & Melville, J. UMAP: uniform manifold approximation and projection for dimension reduction. Preprint at https://arxiv.org/abs/1802.03426 (2018).
66. Finak, G. et al. MAST: a flexible statistical framework for assessing transcriptional changes and characterizing heterogeneity in single-cell RNA sequencing data. *Genome Biol.* **16**, 278 (2015).
67. Subramanian, A. et al. Gene set enrichment analysis: a knowledge-based approach for interpreting genome-wide expression profiles. *Proc. Natl Acad. Sci. USA* **102**, 15545–15550 (2005).
68. Mootha, V. K. et al. PGC-1α-responsive genes involved in oxidative phosphorylation are coordinately downregulated in human diabetes. *Nat. Genet.* **34**, 267–273 (2003).
69. Liberzon, A. et al. The Molecular Signatures Database (MSigDB) hallmark gene set collection. *Cell Syst.* **1**, 417–425 (2015).
70. Neri, S., Mariani, E., Meneghetti, A., Cattini, L. & Facchini, A. Calcein-acetyoxymethyl cytotoxicity assay: standardization of a method allowing additional analyses on recovered effector cells and supernatants. *Clin. Diagn. Lab. Immunol.* **8**, 1131–1135 (2001).
71. Chava, S., Bugide, S., Gupta, R. & Wajapeyee, N. Measurement of natural killer cell-mediated cytotoxicity and migration in the context of hepatic tumor cells. *J. Vis. Exp.* https://doi.org/10.3791/60714 (2020).
72. Langmead, B. & Salzberg, S. L. Fast gapped-read alignment with Bowtie 2. *Nat. Methods* **9**, 357–359 (2012).
73. Li, H. et al. The Sequence Alignment/Map format and SAMtools. *Bioinformatics* **25**, 2078–2079 (2009).
74. Karpova, N. N. & Umemori, J. Protocol for methylated DNA immunoprecipitation (MeDIP) analysis. *Epigenetic Methods Neurosci. Res.* **105**, 97–114 (2016).

Acknowledgements The authors thank the Thoracic Oncology Service, the Pathology Core Facility, the Flow Cytometry Core, the Molecular Cytology Core, the Genomic Editing and Screening Core, the Single-cell Analysis Innovation Lab, the Integrated Genomics Operation, and the Research Animal Resource Center at MSKCC for their assistance; the tissue donors at MSKCC for participating in this study; E. Er for early guidance with metastasis assays; C. Rudin for assistance in the procurement of tumour tissue samples; and Z. Zhang, H.-A. Chen and V. Tem for technical assistance. This work was supported by NIH grants R35-CA252978 and P01-CA129243 (J.M.), U54-CA209975 (J.M. and D.P.), K08-CA230213 (K.G.), P30 CA008748 (MSKCC), the Alan and Sandra Gerry Metastasis and Tumor Ecosystems Center at MSKCC (J.H., F.J.S.-R., Z.W., K.G., D.P. and J.M.), the Agilent Technologies Thought Leader Award (S.W.L.), and postdoctoral fellowships from the Terri Brodeur Breast Cancer Foundation (J.H.), the Translational Research Oncology Training Program 5T32CA160001 (F.J.S.-R.), and the Damon Runyon Quantitative Biology Program (S.G.). F.J.S.-R. is a HHMI Hanna Gray Fellow. D.P. and S.W.L. are HHMI Investigators.

Author contributions J.H. and J.M. conceived studies, designed experiments, interpreted results and wrote the manuscript. J.H. performed experiments and analysed data. F.J.S.-R., Y.-j.H. and S.W.L. designed and analysed CRISPR screens. S.G., S.K. and D.P. performed scRNA-seq data analysis. G.N.J. and J.P.H. provided technical assistance with experiments. Z.W. generated and characterized TGFβ-reporter and *TGFBR2*-knockout cell lines and performed immunohistochemistry analysis. K.G. established the KPad1 cell line. K.G., S.U. and C.A.I.-D. procured patient-derived tumour samples and validated the STING immunohistochemistry scoring. A.M.M., R.B.D. and J.C.S. performed immune phenotyping and NK cell cytotoxicity experiments. H.Z. and E.d.S. conducted drug treatment experiments in mice.

Competing interests S.W.L. received funding and research support from Agilent Technologies for the purposes of massively parallel oligonucleotide synthesis to generate the sgRNA libraries described in this Article.

Additional information
Supplementary information The online version contains supplementary material available at https://doi.org/10.1038/s41586-023-05880-5.

Correspondence and requests for materials should be addressed to Joan Massagué.

Peer review information *Nature* thanks Melanie Werner-Klein and the other, anonymous, reviewer(s) for their contribution to the peer review of this work. Peer reviewer reports are available.

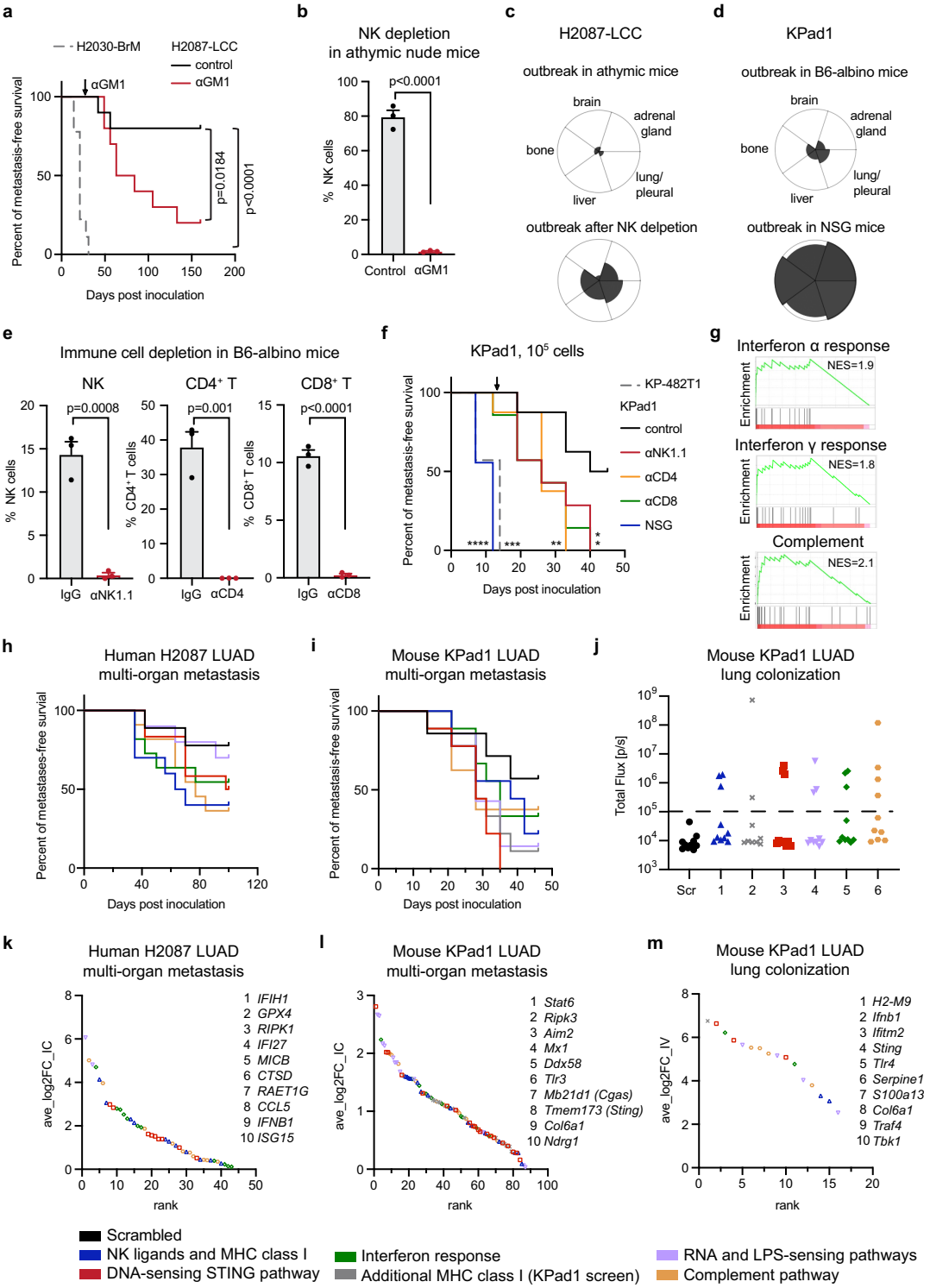

Extended Data Fig. 1 | See next page for caption.

Extended Data Fig. 1 | *In vivo* CRISPR screen for cell-autonomous immune regulators of dormant metastasis. (a) Metastasis-free survival Kaplan-Meier plots of athymic mice intracardially inoculated with 1×10^5 H2030-BrM or H2087-LCC cells. One set of mice inoculated with H2087-LCC cells was treated with anti-asialo-GM1 antibody to deplete NK cells 30 days after cell inoculation. *n* = 9 (H2030-BrM) or 10 (H2087-LCC) mice per group, log-rank test. **(b)** Flow cytometry analysis of Lineage$^-$CD45$^+$NKP46$^+$ NK cells in blood from athymic mice that were treated with IgG control or anti-asialo-GM1 antibody for 4 days. Lineage$^-$: TCRβ$^-$CD3$^-$CD19$^-$B220$^-$CD11c$^-$Ly6G$^-$F4/80$^-$. *n* = 3 mice per group. Mean ± s.e.m., two-sided unpaired t-test. **(c)** Petal charts of metastasis incidence in specific organs of 10 athymic mice intracardially inoculated with 1×10^5 H2087-LCC cells, treated with or without anti-asialo-GM1 antibody. Metastasis progression was monitored by BLI for 160 days after cell inoculation. **(d)** Petal charts of metastasis incidence in specific organs after intracardiac inoculation of 2×10^4 KPad1 cells into 8-9 B6-albino mice or NSG mice. Metastasis progression was monitored by BLI for 60 days (B6-albino mice) or 28 days (NSG mice) after cell inoculation. **(e)** Flow cytometry analysis of Lineage$^-$CD45$^+$NKP46$^+$ NK cells, CD45$^+$CD3$^+$CD4$^+$, and CD45$^+$CD3$^+$CD8$^+$ T cells in blood from B6-albino mice that were treated for 3 days with IgG control, anti-NK1.1, anti-CD4, or anti-CD8 antibodies. *n* = 3 mice per group. Mean ± s.e.m., two-sided unpaired t-test. **(f)** Metastasis-free survival Kaplan-Meier plots of NSG mice inoculated intracardially with KPad1 cells, or B6-albino mice inoculated intracardially with KPad1 cells or KP-482T1 cells, and treated with the indicated antibodies to deplete specific types of immune cells. 1×10^5 cells were inoculated per mouse. Antibody treatments started 12 days after inoculation. *n* = 8 (KPad1/control, KPad1/αCD4), 7 (KPad1/αNK1.1, KPad1/αCD8, KP-482T1), or 9 (NSG) mice per group, log-rank test. *, p = 0.03 (KPad1/αNK1.1 vs. KPad1/control), *, p = 0.0146 (KPad1/αCD8 vs. KPad1/control), **, p = 0.0094 (KPad1/αCD4 vs. KPad1/control), ***, p = 0.0002 (KP-482T1 vs. KPad1/control), ****, p < 0.0001 (KPad1/NSG vs. KPad1/control in B6-albino). **(g)** Gene set enrichment analysis (GSEA) showing pathways enriched in dormant H2087-LCC cells that were induced to proliferate in culture compared to cells from spontaneous metastatic outbreaks, analyzed from previous scRNA-seq data sets. **(h–i)** Metastasis-free survival of athymic mice (h) or B6-albino mice (i) intracardially inoculated with 2.5×10^5 H2087-LCC (h) or KPad1 cells (i), expressing a scrambled RNA control or various sgRNA pools. *n* = 9 (Scrambled), 10 (NK ligands and MHC class I), 12 (STING pathway), 10 (LPS and RNA-sensing pathways), or 11 (Interferon response, Complement pathway) mice per group (h); *n* = 7 (Scrambled, LPS and RNA-sensing pathways), 8 (Complement pathway), or 9 (other groups) mice per group (i). **(j)** BLI quantification of lung metastatic colonies after intravenous inoculation of 2.5×10^5 KPad1 cells expressing a scrambled control or different sgRNA pools in B6-albino mice. Tissues above the dotted line were harvested 57 days after cell inoculation, then subjected to sgRNA recovery and analysis. *n* = 9 (Additional MHC class I) or 10 (other groups) mice per group. **(k–l)** Gene rank based on the average fold enrichment of sgRNAs in multi-organ metastases from H2087-LCC (k) or KPad1 (l) cells. **(m)** Gene rank based on average fold change of sgRNAs enriched in the lung colonies formed after tail-vein inoculation of 2.5×10^5 KPad1 cells into B6-albino mice. For k-m, genes with average log2FC >0 are plotted and genes targeted by the top 10 enriched sgRNAs are listed.

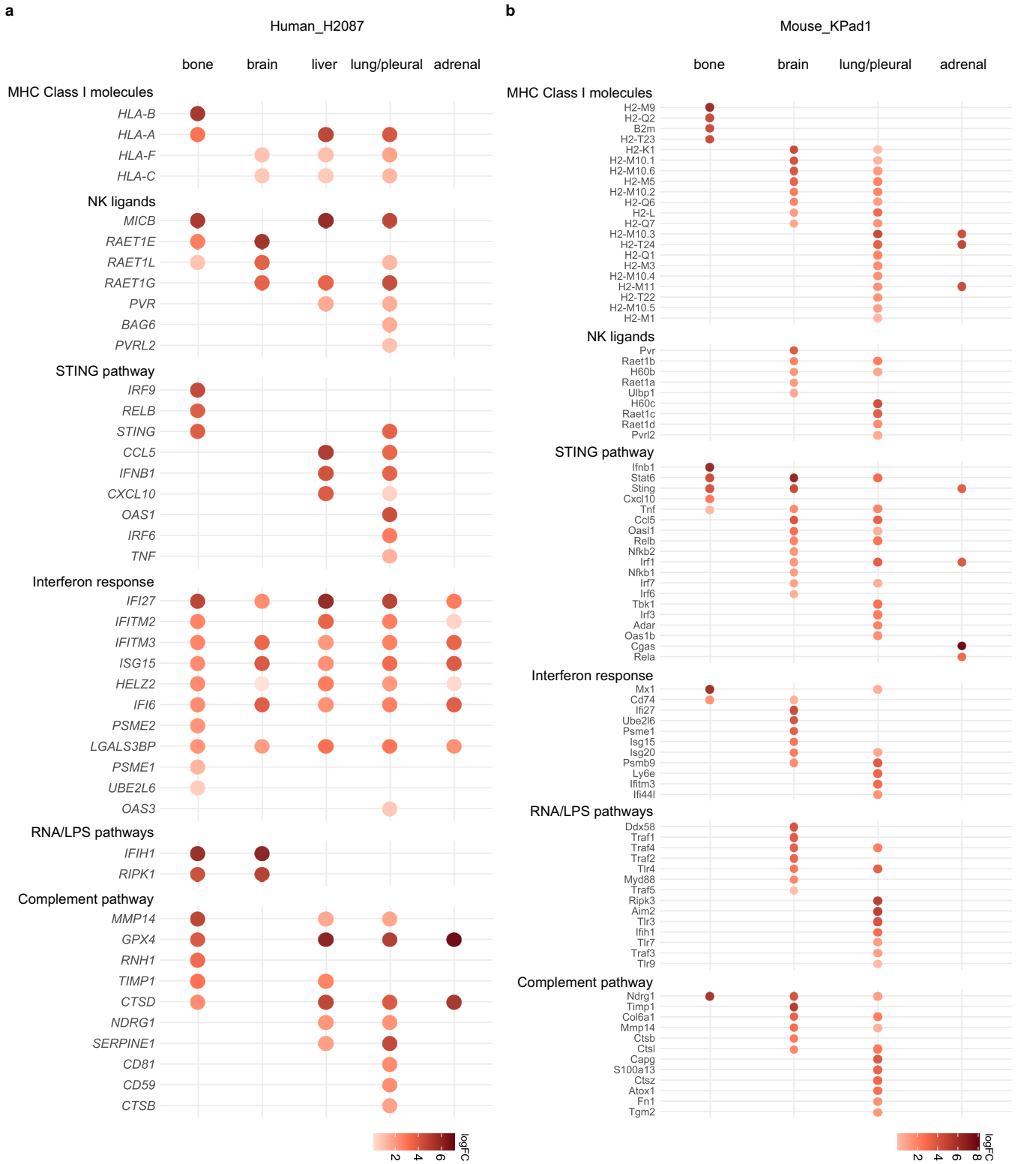

Extended Data Fig. 2 | sgRNAs enriched in metastases of specific organs. **(a–b)** Dot plots showing genes targeted by the enriched sgRNAs in metastases of the indicated organs after intracardiac inoculation of 2.5×10^5 H2087-LCC cells into athymic mice (a) or 2.5×10^5 KPad1 cells into B6-albino mice (b). Genes with average log2FC >0 are plotted.

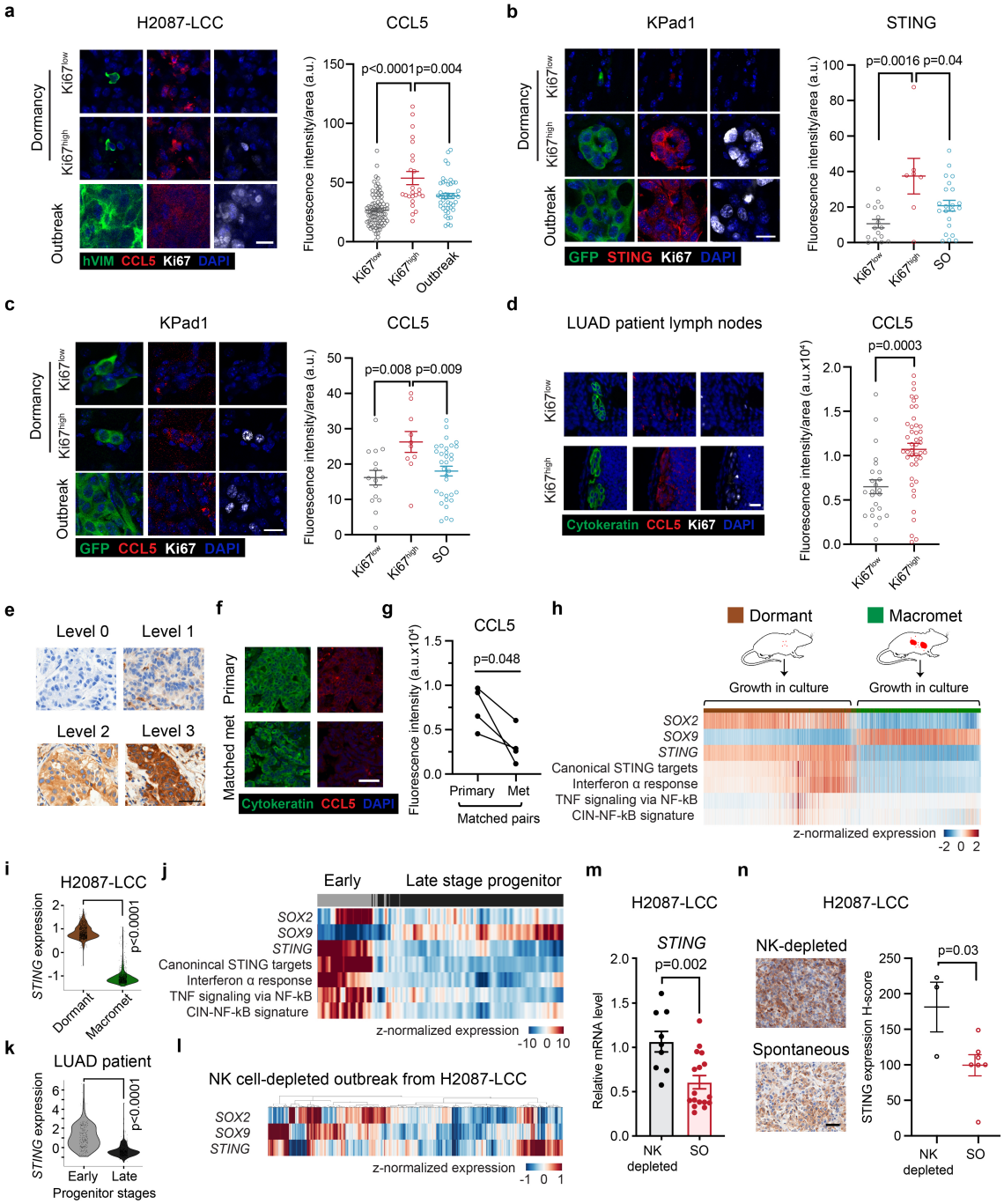

Extended Data Fig. 3 | See next page for caption.

Extended Data Fig. 3 | STING in dormant and reactivated metastatic progenitors and progenies. (a) As in Fig. 2a, representative IF images of single quiescent (Ki67^{low}) and proliferative (Ki67^{high}) cells during dormancy, and spontaneous outbreaks (SO) from H2087-LCC, stained for CCL5 IF (*red*), human vimentin (*green*), Ki67 IF (*white*), and DAPI (*blue*). The staining signal intensity of CCL5 in vimentin-positive cells was quantified and plotted (a.u., arbitrary units). Scale bar: 10 µm. *n* = 89 cells (Ki67^{low}), 24 cells (Ki67^{high}), or 45 regions (outbreaks), from 5 mice per group. Mean ± s.e.m, two-sided unpaired t-test. **(b–c)** Representative IF staining images of KPad1 cells (GFP, *green*) in brains of B6-albino mice that were intracardially inoculated with 1 x 10^5 KPad1 cells. Organs were harvested 25 days after inoculation to capture the dormant state, and 43–61 days after inoculation to capture spontaneous outbreaks. Tissue sections were stained for STING (b, *red*), CCL5 (c, *red*), Ki67 (b and c, *white*), and DAPI (b and c, *blue*), and the staining signal intensity of STING (b) and CCL5 (c) in GFP-positive cells was quantified and plotted (a.u., arbitrary units). Scale bar: 20 µm. *n* = 16 cells (Ki67^{low}), 7 cells (Ki67^{high}), or 22 lesions (outbreaks), from 4 mice per group in (b); *n* = 15 cells (Ki67^{low}), 10 cells (Ki67^{high}), or 33 lesions (outbreaks), from 4 mice per group in (c). Mean ± s.e.m, two-sided unpaired t-test. **(d)** Representative images of micrometastatic cells (cytokeratin AE1/AE3, *green*) in lymph nodes from stage II and stage III LUAD patients, stained for CCL5 IF (*red*), Ki67 (*white*), and DAPI (*blue*). The signal intensity of CCL5 in cytokeratin-positive cells was quantified and plotted. Scale bar: 20 µm. *n* = 24 (Ki67^{low}) or 44 (Ki67^{high}) regions, from 14 lymph nodes of 9 patients. Mean ± s.e.m., two-sided unpaired t-test. **(e)** Representative images of STING IHC intensity levels (0, none; 1, weak; 2, moderate; 3, strong) in patient-derived lung adenocarcinoma tissue samples. STING expression H-scores were calculated based on the intensity levels, representative of 2 independent experiments. Scale bar: 50 µm. **(f–g)** IF staining (f) and quantification (g) of CCL5 expression in patient-derived LUAD metastases compared to matched primary tumors. Tissue sections were stained for cytokeratin AE1/AE3 IF (*green*), CCL5 IF (*red*), and DAPI (*blue*), and the staining signal intensity of CCL5 in cytokeratin-positive areas was quantified and plotted (a.u., arbitrary units). Scale bar: 50 µm. *n* = 4 matched pairs, two-tailed paired t-test. **(h)** Expression of *SOX* transcription factors specifying early (SOX2) and late (SOX9) lung epithelial progenitor states, *STING*, canonical STING pathway targets, hallmark_ interferon α response genes (GSEA), canonical and non-canonical NF-kB target genes (rows) across H2087-LCC single cells isolated from dormant metastases or spontaneous macrometastases in athymic mice, and cultured under growth-promoting conditions. STING pathway targets refers to the mean expression of the genes shown in Extended Data Fig. 4. For each gene, imputed expression was z-normalized across all cells. In the top row, cells (columns) are colored and labeled by source. *n* = 2245 cells isolated from 3 mice. **(i)** Violin plots showing imputed and z-normalized expression of *STING* in H2087-LCC cells from the data set used in (h). *n* = 2245 cells isolated from 3 mice. Two-sided Mann-Whitney U-test. **(j)** Expression of SOX transcription factors, *STING*, canonical STING pathway targets, hallmark interferon α response genes (GSEA), canonical and non-canonical NF-kB target genes (rows) across patient-derived metastatic tumor cells assigned to early or late-stage progenitor states. STING pathway targets refers to the mean expression of the genes shown in Extended Data Fig. 4. For each gene, imputed expression was z-normalized across all cells and smoothed using a 20-cell moving average window. Individual cells (columns) are ranked left to right by average lung epithelial development score. *n* = 991 cells isolated from 5 patients. **(k)** Violin plots showing imputed and z-normalized expression of *STING* across patient-derived tumor cells assigned to early or late-stage progenitor states from the data set used in (**j**). *n* = 991 cells isolated from 5 patients. Two-sided Mann-Whitney U-test. **(l)** Clustered heatmap showing expression of *SOX2*, *SOX9*, and *STING* in H2087-LCC cells isolated from metastases formed after NK cell depletion by anti-asialo-GM1 antibody treatment in athymic mice. For each gene, imputed expression was z-normalized across all cells. n = 6073 cells isolated from 5 mice. **(m)** qRT-PCR analysis of *STING* mRNA levels in H2087-LCC cell cultures derived from spontaneous outbreaks (SO) compared to those derived from outbreaks following depletion of NK cells. NK cells were depleted by treating mice with anti-asialo-GM1 antibody 30 days after cancer cell inoculation. *n* = 9 H2087-LCC cell lines from 4 mice after NK cell depletion or *n* = 17 cell lines from 8 mice with spontaneous outbreaks. Mean ± s.e.m., two-sided unpaired t-test. **(n)** IHC staining and quantification of STING expression (H-score) in H2087-LCC spontaneous outbreaks and outbreaks following NK cell depletion in multiple organs from athymic mice. Scale bar: 50 µm. *n* = 3 organs from 3 mice (NK depletion) or 7 organs from 3 mice (spontaneous). Mean ± s.e.m., two-sided unpaired t-test.

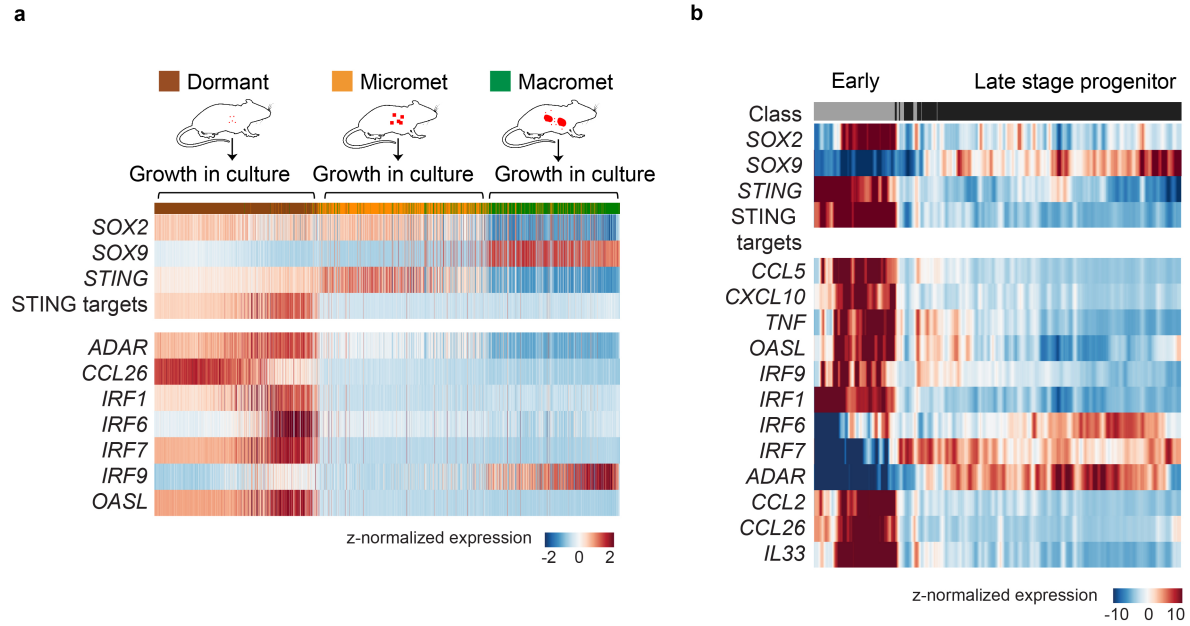

Extended Data Fig. 4 | Expression of canonical STING pathway targets from scRNA-seq datasets. (a) Expression of SOX transcription factors specifying early (SOX2) and late (SOX9) lung epithelial progenitor states, STING and canonical STING pathway targets (rows) across H2087-LCC single cells isolated from dormant metastases, or spontaneous macrometastases in athymic nude mice, and cultured under growth-promoting conditions. STING pathway targets refers to the mean expression of the genes shown in the bottom heatmap panel. For each gene, imputed expression was z-normalized across all cells. In the top row, cells (columns) are colored and labeled by source. $n = 2245$ cells isolated from 3 mice. **(b)** Expression of SOX transcription factors, STING and canonical STING pathway targets (rows) across patient-derived metastatic tumor cells assigned to early or late-stage progenitor states. STING pathway targets refers to the mean expression of the genes shown in the bottom heatmap panel. For each gene, imputed expression was z-normalized across all cells and smoothed using a 20-cell moving average window. Individual cells (columns) are ranked left to right by average lung epithelial development score, as in Laughney et al. $n = 991$ cells isolated from 5 patients.

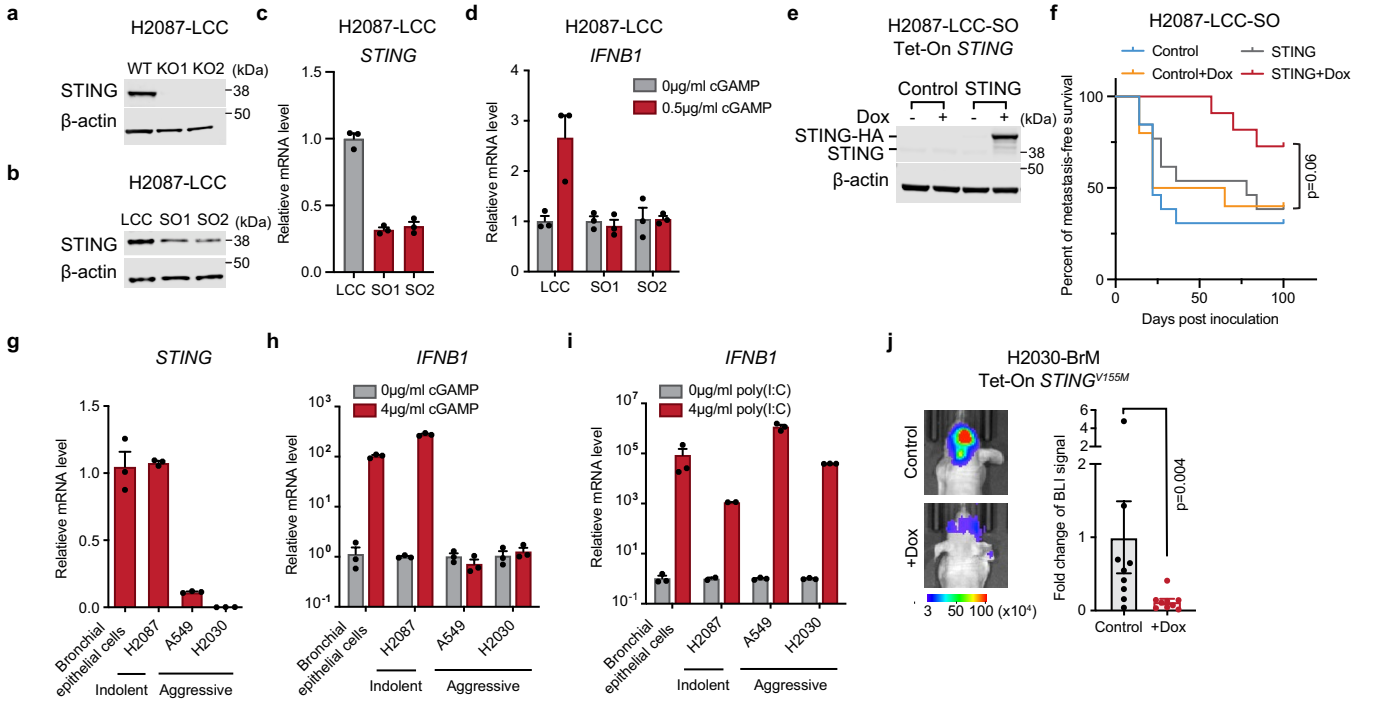

Extended Data Fig. 5 | Perturbation of STING activity in human LUAD models. (a) Western immunoblot analysis of STING and β-actin in WT and *STING* knockout H2087-LCC cells, representative of 2 independent experiments. **(b–c)** Immunoblotting (b) and qRT-PCR analyses (c) of STING expression in parental H2087-LCC cells and the spontaneous outbreak derivatives SO1 and SO2. Mean ± s.e.m, representative of 2 independent experiments. In (c), each dot represents a technical replicate of the assay. **(d)** qRT-PCR analysis of *IFNB1* expression after cGAMP treatment of H2087-LCC, SO1, and SO2 cells. Mean ± s.e.m, representative of 2 independent experiments. Each dot represents a technical replicate of the assay. **(e)** Western immunoblot analysis of STING (endogenous STING and HA-tagged STING) and β-actin in H2087-LCC-SO cells inducibly expressing STING-HA under doxycycline (Dox) treatment for 24 h. Representative of 2 independent experiments. **(f)** Metastasis-free survival plots of athymic mice inoculated intracardially with 1×10^5 H2087-LCC-SO cells. Cells were transduced with a vector control or a Dox-inducible STING expression vector. Dox treatment started 7 days after cell inoculation. $n = 13$ (Control, STING), 10 (Control+Dox), 11 (STING+Dox) mice per group, log-rank test. **(g)** qRT-PCR analysis of *STING* mRNA levels in human primary bronchial epithelial cells, H2087, A549, and H2030 LUAD cell lines. Mean ± s.e.m, representative of 3 independent experiments. Each dot represents a technical replicate of the assay. **(h–i)** qRT-PCR analysis of *IFNB1* mRNA expression in human primary bronchial epithelial cells and lung adenocarcinoma cell lines treated with cGAMP (h) or poly(I:C) (i). Mean ± s.e.m, representative of 3 independent experiments. Each dot represents a technical replicate of the assay. **(j)** BLI and quantification of metastases formed by H2030-BrM cells inducibly expressing activated STING-V155M, starting the day after intracardiac inoculation of 1×10^5 cells in athymic mice. Metastases were quantified 21 days after inoculation. $n = 9$ mice per group. Mean ± s.e.m., two-sided Mann-Whitney U-test. For gel source data, see Supplemental Fig. 1.

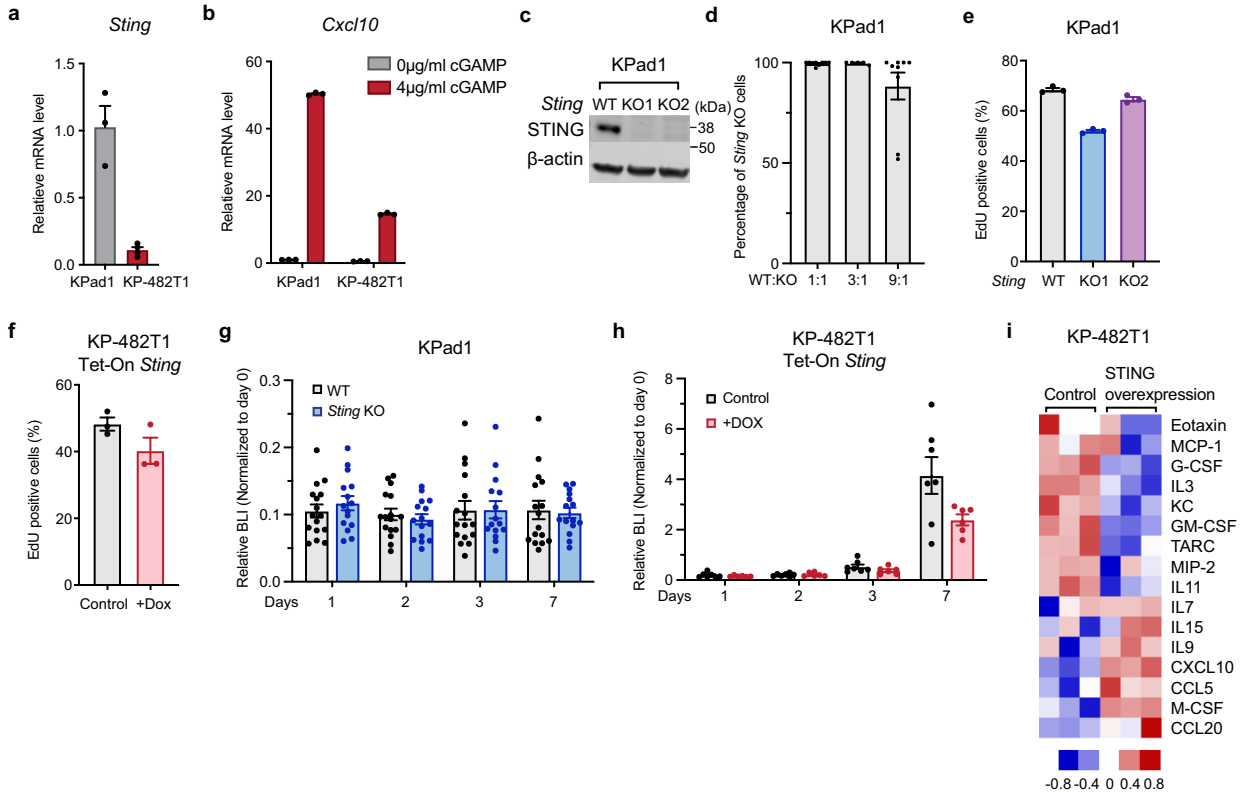

Extended Data Fig. 6 | STING activity in mouse lung adenocarcinoma cells. **(a-b)** qRT-PCR analysis of *Sting* (a) and *Cxcl10* (b) mRNA levels after cGAMP treatment in KPad1 and KP-482T1 cells. Mean ± s.e.m, representative of 2 independent experiments. Each dot represents a technical replicate of the assay. **(c)** Western immunoblotting of STING and β-actin in parental and *Sting* knockout KPad1 cells. Representative of 2 independent experiments. For gel source data, see Supplemental Fig. 1. **(d)** RFP-positive WT KPad1 cells and GFP-positive *Sting* KO KPad1 cells were mixed at the indicated ratios and intracardially inoculated (1×10^5 cells) in B6-albino mice. Metastases-bearing organs were harvested 4-17 weeks after inoculation and the percentage of GFP-positive cells and RFP-positive cells was determined by flow cytometry. $n = 9$ (1:1, 9:1) or 5 (3:1) lesions from 3-5 mice per group. Mean ± s.e.m. **(e)** Percentage of EdU positive cells of WT or *Sting* knockout KPad1 cells incubated with EdU for 2 h. $n = 3$ per group. Mean ± s.e.m. **(f)** Percentage of EdU positive cells in KP-482T1 Tet-On *Sting* cultures treated with Dox for 24 h and then incubated with EdU for 2 h. $n = 3$ per group. Mean ± s.e.m. **(g–h)** BLI signal intensity at the indicated time points after intracardiac inoculation of 1×10^5 WT or *Sting* knockout KPad1 cells (g) or KP-482T1 cells with induced overexpression of STING (h) in B6-albino mice. $n = 16$ (WT) or 15 (KO) mice (g); $n = 7$ (control) or 6 (Dox) mice (h). Mean ± s.e.m. **(i)** Heatmap representation of cytokine array analysis of culture supernatant from KP-482T1 cells transduced with a vector control or a *Sting* overexpression vector. $n = 3$ for each condition.

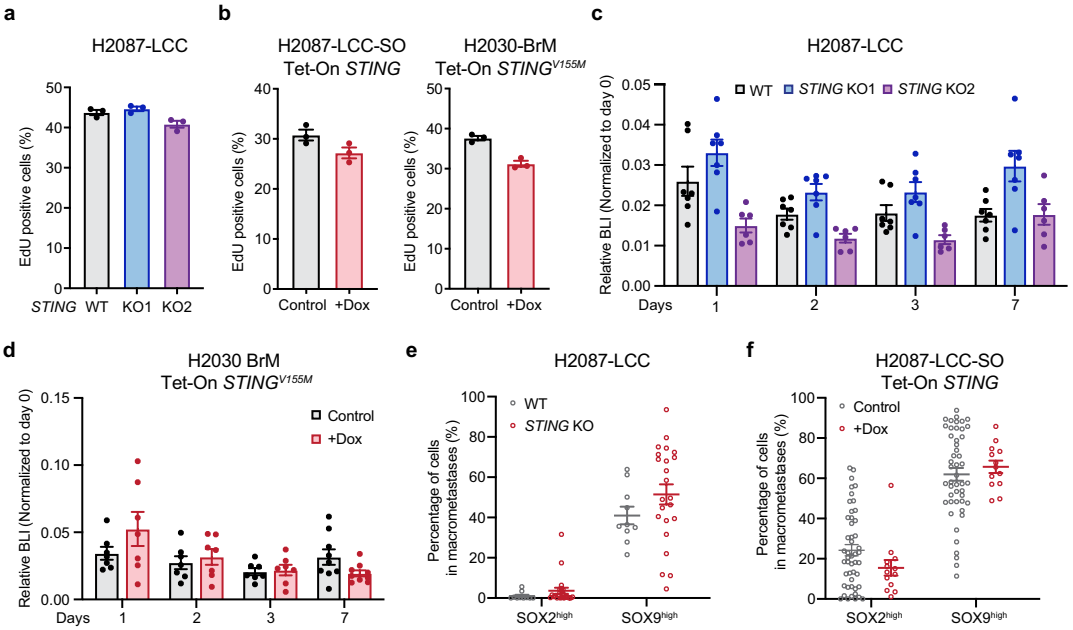

Extended Data Fig. 7 | STING knockout and overexpression effects on growth and differentiation of metastatic progenitors. (a) Percentage of EdU positive cells of WT or *STING* knockout H2087-LCC cells incubated with EdU for 2 h. $n = 3$ per group. Mean ± s.e.m. **(b)** Percentage of EdU positive cells in H2087-LCC-SO Tet-On *STING* or H2030-BrM Tet-On $STING^{V155M}$ cultures treated with Dox for 24 h, and then incubated with EdU for 2 h. $n = 3$ per group. Mean ± s.e.m. **(c-d)** BLI signal intensity at the indicated time points after intracardiac inoculation of 1×10^5 WT or *STING* knockout H2087-LCC cells (c) or H2030-BrM cells with Dox-induced overexpression of $STING^{V155M}$ (d) in athymic mice. $n = 7$ (WT, KO1) or 6 (KO2) mice per group (c); $n = 9$ (7 days) or 7 (other groups) mice per group (d). Mean ± s.e.m. **(e)** IF staining analysis showing percentage of $SOX2^{high}$ and $SOX9^{high}$ cells in spontaneous metastases formed after intracardiac inoculation of 1×10^5 WT or *STING* knockout (KO) H2087-LCC cells in athymic mice. Organs were harvested 12 weeks after inoculation. $n = 10$ lesions (WT) or 23 lesions (*STING* KO). Mean ± s.e.m. **(f)** IF staining analysis showing percentage of $SOX2^{high}$ and $SOX9^{high}$ cells in metastases formed after intracardiac inoculation of 1×10^5 H2087-LCC-SO cells inducibly overexpressing STING in athymic mice. Organs were harvested 7–13 weeks after inoculation for the control cells and 18 weeks after inoculation for the STING overexpressing cells. $n = 48$ images from 5 mice (control) or 13 images from 3 mice (Dox). Mean ± s.e.m.

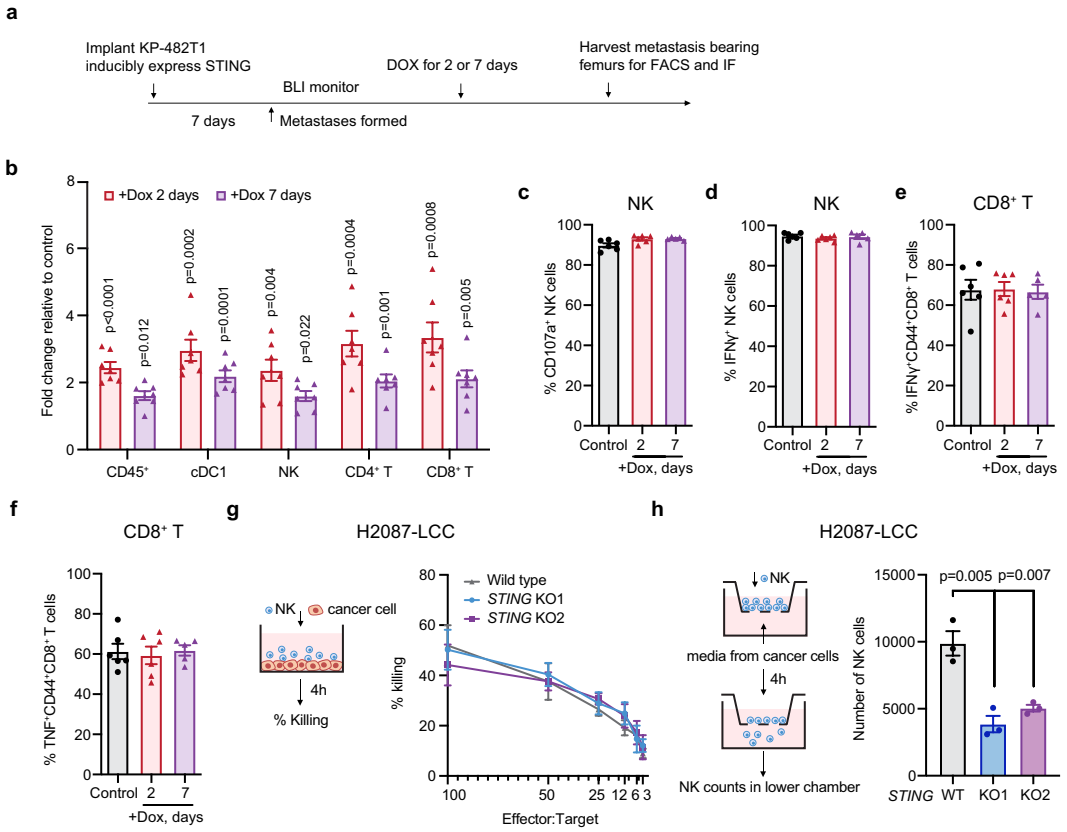

Extended Data Fig. 8 | Cancer cell STING increases NK and T cell levels in metastases. (a) Schematic of flow cytometry or immunofluorescence analysis of immune cells in bone metastasis. **(b)** Flow cytometry analysis and quantification of CD45$^+$ leukocytes, CD45$^+$CD19$^-$TCRβ$^-$XCR1$^+$CD11c$^+$ cDC1 cells, CD45$^+$NK1.1$^+$TCRβ$^-$CD49b$^+$NKp46$^+$ NK cells, CD45$^+$TCRβ$^+$NK1.1$^-$CD8$^+$ T cells, and CD45$^+$TCRβ$^+$NK1.1$^-$CD4$^+$ T cells in KP-482T1 metastasis-bearing femurs after Dox-induced expression of STING for 2 days or 7 days. Cell numbers per gram of femur tissue were counted and normalized to control (-Dox). Metastasis-bearing femurs were collected 2 weeks after intracardiac inoculation of 2×10^4 KP-482T1 cells in B6-albino mice. $n = 7$ mice per group. Mean ± s.e.m., two-sided unpaired t-test. p values comparing each Dox treatment group with control (−Dox). **(c–f)** Percentage of NK cells degranulating (CD107a$^+$) (c) or producing IFNγ (d), and percentage of CD44$^+$CD8$^+$ T cells producing IFNγ (e) or TNF (f), isolated from KP-482T1 metastasis-bearing femurs after Dox-induced expression of STING for 2 days or 7 days, and then cultured *ex vivo* with phorbol 12-myristate 13-acetate (PMA) and ionomycin for 4h. $n = 5$ (+Dox 7 days) or 6 (other groups) mice per group. Mean ± s.e.m. **(g)** Schematic of the NK cell-mediated killing assay, and the percentage of WT or *STING* KO H2087-LCC cells killed by incubation with naïve NK cells for 4h at the indicated effector:target ratios. $n = 3$ per group. Mean ± s.e.m. **(h)** Schematic of the trans-well migration assay, and the number of NK cells migrated into cell culture media conditioned by WT or *STING* knockout H2087-LCC cells. $n = 3$ per group. Mean ± s.e.m., two-sided unpaired t-test.

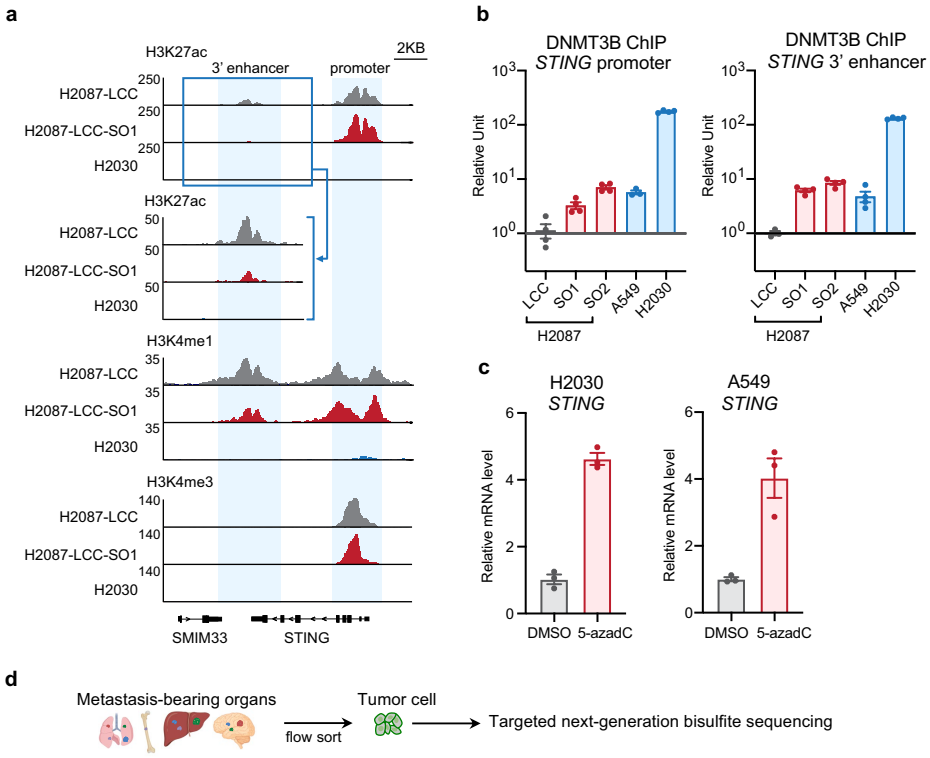

Extended Data Fig. 9 | *STING* locus regulation during metastatic progression. (a) Gene track view for H3K27ac, H3K4me1, and H3K4me3 ChIP-Seq tags at the *STING* locus in H2087-LCC, spontaneous outbreak derivative H2087-LCC-SO1, and H2030 cells. **(b)** ChIP-PCR analysis of DNMT3B binding to the *STING* promoter or 3′ enhancer regions in parental H2087-LCC, H2087-LCC-SO1, H2087-LCC-SO2, and in A549 and H2030 cells. Mean ± s.e.m., representative of 2 independent experiments. Each dot represents a technical replicate of the assay. **(c)** qRT-PCR analysis of *STING* mRNA levels in H2030 and A549 cells after a 3-day treatment with 100nM 5-aza-2′deoxycytidine (5-azadC) in culture. Mean ± s.e.m., representative of 3 independent experiments. Each dot represents a technical replicate of the assay. **(d)** Schematic of targeted bisulfite sequencing analysis of the *STING* locus in metastatic cells of interest.

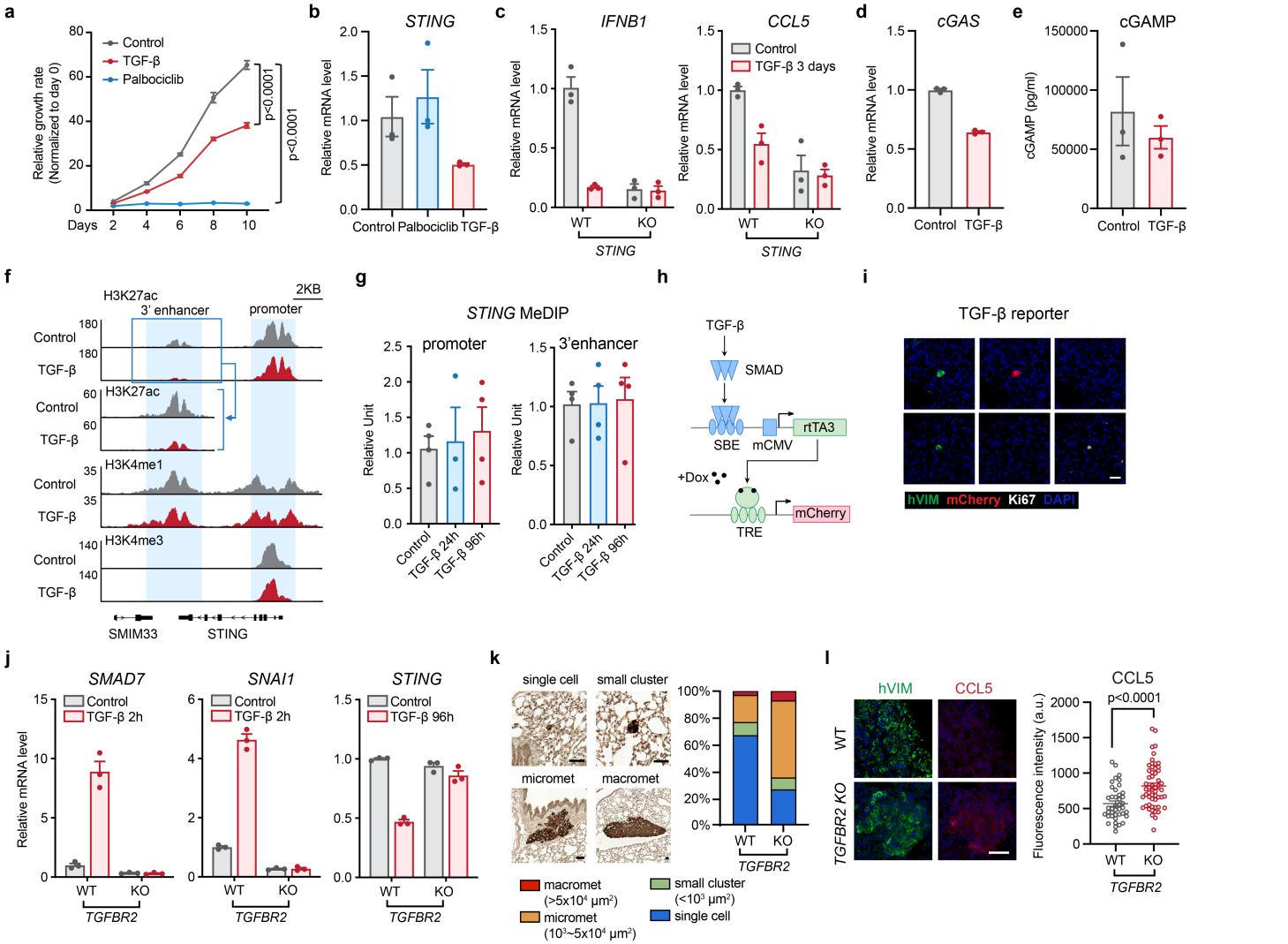

Extended Data Fig. 10 | TGF-β mediated suppression of STING expression. **(a)** Growth rate of H2087-LCC cells treated with TGF-β or CDK4/6 inhibitor palbociclib for the indicated times. $n = 4$. Mean ± s.e.m., two-way ANOVA analysis. **(b)** qRT-PCR analysis of *STING* mRNA levels in H2087-LCC cells treated with TGF-β or palbociclib for 7 days. Mean ± s.e.m., representative of 3 independent experiments. Each dot represents a technical replicate of the assay. **(c)** qRT-PCR analysis of *IFNB1* and *CCL5* expression in WT or *STING* knockout H2087-LCC cells treated with TGF-β for 3 days. Mean ± s.e.m., representative of 2 independent experiments. Each dot represents a technical replicate of the assay. **(d)** qRT-PCR analysis of *cGAS* mRNA levels in H2087-LCC cells treated with TGF-β for 7 days. Mean ± s.e.m., representative of 3 independent experiments. Each dot represents a technical replicate of the assay. **(e)** ELISA analysis of cGAMP levels in H2087-LCC cells treated with TGF-β for 5 days. $n = 3$ per group. Mean ± s.e.m. **(f)** Gene track view of H3K27ac, H3K4me1, and H3K4me3 ChIP-Seq tags at the *STING* locus in H2087-LCC cells treated with TGF-β for 4 days. **(g)** PCR based quantitation of methylated *STING* promoter and 3′ enhancer sequences in MeDIP samples from H2087-LCC cells that were treated with TGF-β for the indicated times. Mean ± s.e.m., representative of 3 independent experiments. Each dot represents a technical replicate of the assay. **(h)** Schematic of the TGF-β and SMAD-dependent transcriptional reporter. SBE: Smad Binding Element. mCMV: minimal CMV promoter. TRE: Tetracycline-Responsive promoter Element. **(i)** Representative IF staining images of H2087-LCC cells (human vimentin, *green*) expressing SMAD-responsive mCherry reporter in the lungs of athymic mice intravenously inoculated with $1x10^5$ cells. Organs were harvested 8 weeks after inoculation. Disseminated cancer cells were present as single quiescent ($Ki67^{low}$) or proliferative cells ($Ki67^{high}$, *white*). Representative of 2 independent experiments. Scale bar: 20 μm. **(j)** qRT-PCR analysis of *SMAD7*, *SNAI1* and *STING* expression in H2087-LCC cells treated with TGF-β or no additions for 2 h or 96 h, respectively. Mean ± s.e.m., representative of 2 independent experiments. Each dot represents a technical replicate of the assay. **(k)** Representative IHC images (left) and quantification (right) of the proportion of H2087-LCC single cells, small clusters, micrometastases, and macrometastases in the lungs of NSG mice 7 weeks after intravenous injection of $1x10^5$ cells. Scale bar: 50 μm. $n = 102$ (WT) or 33 (KO) single cells, 17 (WT) or 12 (KO) small clusters, 31 (WT) or 71 (KO) micrometastases, and 5 (WT) or 9 (KO) macrometastases. **(l)** IF staining of human vimentin (*green*), DAPI (*blue*), and CCL5 (*red*), in lung metastases generated 7 weeks after intravenous inoculation of $1x10^5$ WT or *TGFBR2* knockout H2087-LCC cells in NSG mice. The IF staining intensity in vimentin-positive areas was quantified. Scale bar: 50 μm. $n = 41$ (WT) or 55 (KO) lesions from 5 mice. Mean ± s.e.m., two-sided unpaired t-test.

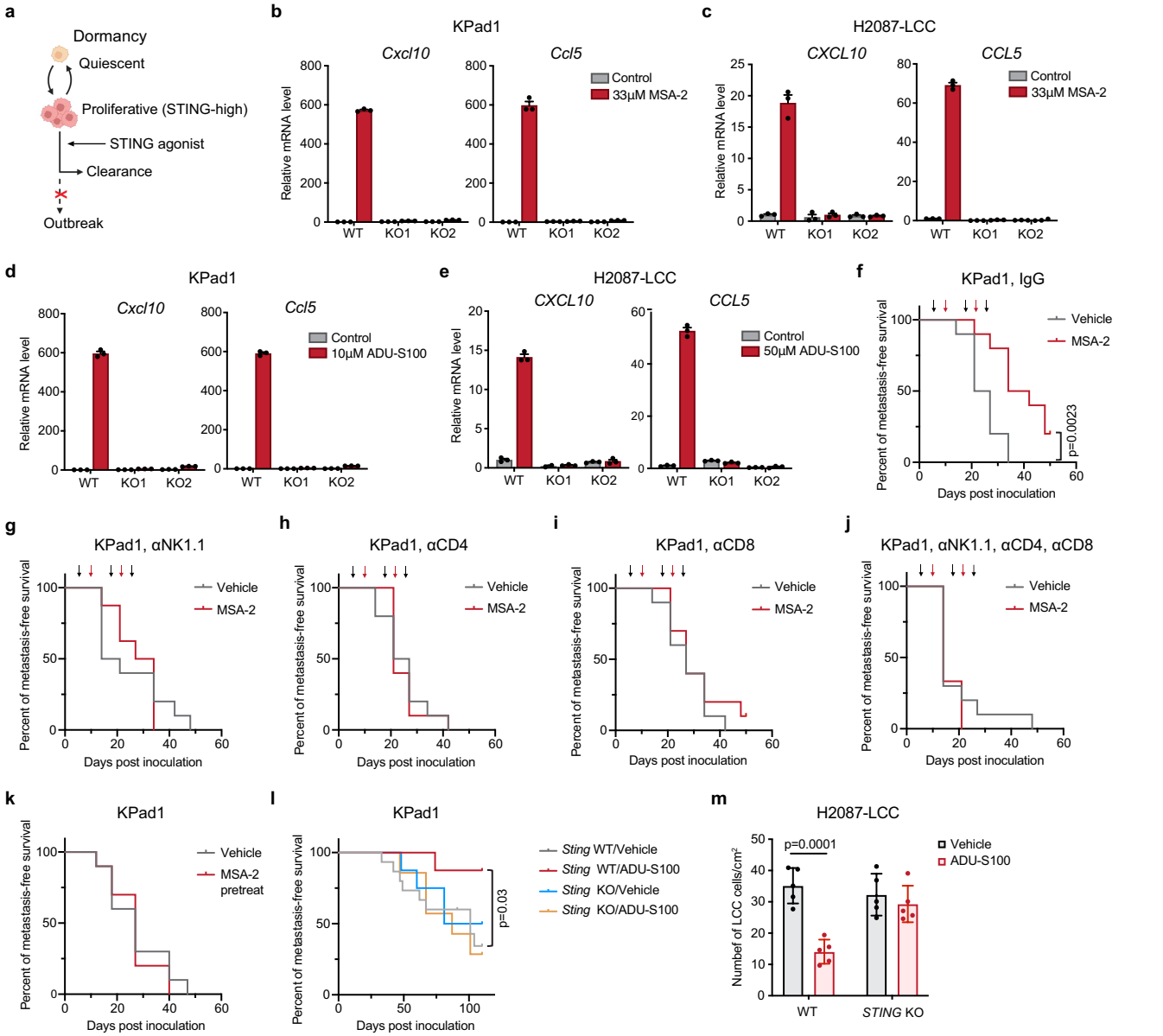

Extended Data Fig. 11 | Immune cell dependence of STING agonist-mediated suppression of metastasis reactivation. (a) Rationale for experimental design. **(b-c)** qRT-PCR analysis of *CXCL10* and *CCL5* mRNA levels in WT or *STING* knockout KPad1 (b) or H2087-LCC (c) cells treated with 33 μM MSA-2 for 4 h. Mean ± s.e.m., representative of 2 independent experiments. Each dot represents a technical replicate of the assay. **(d–e)** Treatment was performed as in (b, c) but with 10 μM (KPad1) or 50 μM (H2087-LCC) ADU-S100. Mean ± s.e.m., representative of 2 independent experiments. Each dot represents a technical replicate of the assay. **(f-j)** Metastasis-free survival plots of B6-albino mice intracardially inoculated with $2.5x10^5$ KPad1 cells, treated with both MSA-2 and IgG control (f, $n = 10$ mice) or individual antibodies to deplete NK cells (g, $n = 10$ mice for vehicle or 8 mice for MSA-2), $CD4^+$ T cells (h, $n = 10$ mice), $CD8^+$ T cells (i, $n = 10$ mice), or a combination of these antibodies (j, $n = 10$ mice for vehicle or 9 mice for MSA-2). Mice were administered antibodies (200 μg/mouse) once weekly for 3 weeks starting 6 days after cell inoculation, and vehicle or MSA-2 (50 mg/kg of body weight) once weekly for 2 weeks starting 9 days after cell inoculation. Log-rank test. **(k)** Metastasis-free survival plots of B6-albino mice intracardially inoculated with 2.5×10^5 KPad1 cells pre-treated with 33 μM MSA-2 for 24h before inoculation. $n = 10$ mice per group. **(l)** Metastasis-free survival plots of C57BL/6J mice intravenously inoculated with 2.5×10^5 WT or *Sting* knockout KPad1 cells and treated with vehicle or ADU-S100 (1.25 mg/kg of body weight) once weekly by intratracheal delivery until the study endpoint. ADU-S100 treatment started 5 days after cell inoculation. $n = 15$ mice (control) or 8 mice (ADU-S100). Log-rank test. **(m)** Quantification of WT or *STING* knockout H2087-LCC cell numbers in lungs from athymic mice treated with vehicle or ADU-S100 (6.25 mg/kg of body weight) once weekly for 4 weeks by intratracheal delivery. ADU-S100 treatment started 1 week after intravenous inoculation of 1×10^5 cells. Lungs were harvested 5 weeks after inoculation. $n = 5$ mice per group. Mean ± s.e.m., two-sided unpaired t-test.

nature portfolio

Corresponding author(s): Joan Massagué

Last updated by author(s): Feb 6, 2023

Reporting Summary

Nature Portfolio wishes to improve the reproducibility of the work that we publish. This form provides structure for consistency and transparency in reporting. For further information on Nature Portfolio policies, see our Editorial Policies and the Editorial Policy Checklist.

Statistics

For all statistical analyses, confirm that the following items are present in the figure legend, table legend, main text, or Methods section.

n/a	Confirmed
☐	☒ The exact sample size (*n*) for each experimental group/condition, given as a discrete number and unit of measurement
☐	☒ A statement on whether measurements were taken from distinct samples or whether the same sample was measured repeatedly
☐	☒ The statistical test(s) used AND whether they are one- or two-sided *Only common tests should be described solely by name; describe more complex techniques in the Methods section.*
☒	☐ A description of all covariates tested
☐	☒ A description of any assumptions or corrections, such as tests of normality and adjustment for multiple comparisons
☐	☒ A full description of the statistical parameters including central tendency (e.g. means) or other basic estimates (e.g. regression coefficient) AND variation (e.g. standard deviation) or associated estimates of uncertainty (e.g. confidence intervals)
☐	☒ For null hypothesis testing, the test statistic (e.g. *F*, *t*, *r*) with confidence intervals, effect sizes, degrees of freedom and *P* value noted *Give P values as exact values whenever suitable.*
☒	☐ For Bayesian analysis, information on the choice of priors and Markov chain Monte Carlo settings
☒	☐ For hierarchical and complex designs, identification of the appropriate level for tests and full reporting of outcomes
☒	☐ Estimates of effect sizes (e.g. Cohen's *d*, Pearson's *r*), indicating how they were calculated

Our web collection on statistics for biologists contains articles on many of the points above.

Software and code

Policy information about availability of computer code

Data collection

Bioluminescence imaging (BLI) data was acquired using IVIS Spectrum Xenogen instrument (PerkinElmer). Histology data for H&E and IHC were acquired using Mirax scanner (Carl Zeiss). Immunofluorescence imaging data was acquired using SP5 confocal microscope (Leica Microsystems) or Zeiss Imager.Z1 fluorescence microscope (Carl Zeiss). qRT-PCR data was acquired using ViiA 7 real-time PCR system (Life Technologies). Western blot data was acquired using Odyssey CLx imager (LI-COR Biosciences). Flow cytometry analysis was acquired using LSRFortessa (BD Biosciences) and Cytek Aurora (Cytek Biosciences) instruments. Cell sorting was performed using either FACS Aria II or Aria III cytometer (BD Biosciences). Bisulfite sequencing products were verified on Qiagen QIAxcel Advanced System (Qiagen, v1.0.6) and template enrichment was done on Ion ChefTM system (Thermo Fisher). Immunoprecipitated DNA utilized in ChIP-Seq was evaluated by BioAnalyzer (Agilent), and barcoded libraries were run on NovaSeq 6000 (Illumina). NK cell cytotoxicity assay data was collected using EnVision Robot Plate Reader (Perkin Elmer). CellTiter-Glo® and ELISA data was collected using Synergy H1 Hybrid microplate reader (Agilent).

Data analysis

Statistical analysis: GraphPad Prism v 9.0.0
Image processing and analysis: ImageJ v 2.1.0/1.53c
BLI data analysis: Living Image software v 4.5.0
Flow cytometry data analysis: FlowJo v 10.6.2
Western blot images and analysis: ImageStudioLite v 3.1.4
Genome-sequencing analysis for CRISPR screens: MAGeCK (v 0.5.9.4) and R (v 4.0.5).
scRNA-seq analysis: Statistical analysis and visualizations were performed in Python (v 3.8.8). The following open-source algorithms were used: SEQC (v 0.2.1), MAGIC (v 0.1.1), Phenograph (v 1.5.2), MAST (v 1.0.1), Pandas (v 1.4.3), Numpy (v 1.21.5), Scipy (v 1.7.3), Scikit-learn (v 1.1.1), Matplotlib (v 3.5.1), and Palantir (v 1.0.0).
ChIP-seq analysis: Bowtie2 (v 2.1.0), Samtools (v 1.9), bamCoverage-deepTools (v 3.3.2), MACS (v 2.2.7.1) and IGV (v 2.14.1)
Targeted bisulfite sequencing analysis: Bismark Bisulfite Read Mapper program (v 0.12.2) with the Bowtie2 alignment algorithm (v 2.2.3).
Schematics: Office 365 (Microsoft, v 16.57), Adobe Illustrator (v 25.0.1).

Custom code are available at Zenodo under DOI 10.5281/zenodo.7618821.

For manuscripts utilizing custom algorithms or software that are central to the research but not yet described in published literature, software must be made available to editors and reviewers. We strongly encourage code deposition in a community repository (e.g. GitHub). See the Nature Portfolio guidelines for submitting code & software for further information.

Data

Policy information about availability of data

All manuscripts must include a data availability statement. This statement should provide the following information, where applicable:

- Accession codes, unique identifiers, or web links for publicly available datasets
- A description of any restrictions on data availability
- For clinical datasets or third party data, please ensure that the statement adheres to our policy

The raw sequencing data corresponding to CRISPR screens, and targeted bisulfite sequencing have been deposited in the NCBI SRA under accession number PRJNA786579 and PRJNA867723, respectively. ChIP-seq data have been deposited in the GEO under accession number GSE210946. scRNA-seq data of human LUAD specimens and mouse H2087-LCC model were reanalyzed from Laughney et al (GSE123904). Custom code are available at Zenodo under DOI 10.5281/zenodo.7618821.

Field-specific reporting

Please select the one below that is the best fit for your research. If you are not sure, read the appropriate sections before making your selection.

☒ Life sciences ☐ Behavioural & social sciences ☐ Ecological, evolutionary & environmental sciences

For a reference copy of the document with all sections, see nature.com/documents/nr-reporting-summary-flat.pdf

Life sciences study design

All studies must disclose on these points even when the disclosure is negative.

Sample size	For CRISPR screens, animal numbers were chosen based on the calculations of the number of guides each pool and the number of cells inoculated into each mouse, in order to reach >500x library representation. Based on previous reports, <5% of cancer cells survive after seeding in distant organs. We injected 2.5x10^5 cells into each mouse and assumed that 2-3% of cells would survive. Therefore, around 5-7.5x10^3 cells survive during metastatic dormancy in each mouse. As there are 100 gRNAs in each library pool, 5x10^4 cells in total are required to express each pool and reach 500x library representation. 7-10 mice were chosen for each experimental group based on the following calculation: 5x10^4 (cells in total) divided by 5-7.5x10^3 (cells surviving per mouse). For in vivo experiments, no statistical method was used to predetermine the sample size. Sample sizes were chosen based on prior experience and pilot experiments for detecting statistically significant differences between conditions. In compliance with IACUC guidelines, a minimal number of animals for a statistically significant result was used.
Data exclusions	No data was excluded from the studies.
Replication	All attempts at replication were successful. Biological replicates of each experiment is stated under each figure legend and all attempts were successful. Furthermore, the key findings were verified independently by multiple models.
Randomization	For in vivo treatment assays with STING agonists, doxycycline, and immune cell depleting antibodies, mice were distributed into treatment groups with approximately equal bioluminescent intensities. For all other experiments, samples were randomly assigned to each group.
Blinding	Analysis of protein expression from IHC or IF images were blindly conducted using scripts of ImageJ batch analysis. IHC staining of STING expression in patient specimens was confirmed by a pathologist as a blinded reviewer. Investigators were blinded to conduct and analyze CRISPR screen assays. Investigators were not blinded to treatment groups for other in vivo or in vitro studies, as knowledge of this information was essential to conduct the studies.

Reporting for specific materials, systems and methods

We require information from authors about some types of materials, experimental systems and methods used in many studies. Here, indicate whether each material, system or method listed is relevant to your study. If you are not sure if a list item applies to your research, read the appropriate section before selecting a response.

Materials & experimental systems

n/a	Involved in the study
☐	☒ Antibodies
☐	☒ Eukaryotic cell lines
☒	☐ Palaeontology and archaeology
☐	☒ Animals and other organisms
☐	☒ Human research participants
☒	☐ Clinical data
☒	☐ Dual use research of concern

Methods

n/a	Involved in the study
☐	☒ ChIP-seq
☐	☒ Flow cytometry
☒	☐ MRI-based neuroimaging

Antibodies

Antibodies used

antibody application supplier name catalog number clone name lot number dilution fluorophore
anti-mouse NKp46 Flow cytometry Biolegend Cat# 137612 29A1.4 B336719 1:50 BV421
anti-mouse CD44 Flow cytometry Biolegend Cat# 103057 IM7 B323846 1:400 BV421
anti-mouse XCR1 Flow cytometry Biolegend Cat# 148220 ZET B340831 1:100 BV650
anti-mouse TCRb Flow cytometry Southern Biotech Cat# 1785-16 H57-597 L0416-NA71X 1:200 PECy5.5
anti-mouse TCRb Flow cytometry Biolegend Cat# 109220 H57-597 B361176 1:400 APC-Cy7
anti-mouse CD11c Flow cytometry Biolegend Cat# 117318 N418 B303302 1:400 PeCy7
anti-mouse CD19 Flow cytometry Biolegend Cat# 115530 6D5 B356278 1:400 APC-Cy7
anti-mouse TNFa Flow cytometry Biolegend Cat# 506308 MP6-XT22 B319666 1:100 APC
anti-mouse CD49b Flow cytometry BD Biosciences Cat# 741523 HMa2 2336685 1:200 BUV661
anti-mouse NK1.1 Flow cytometry BD Biosciences Cat# 741926 PK136 2346045 1:200 BUV805
anti-mouse CD8a Flow cytometry BD Biosciences Cat# 748535 53-6.7 2130169 1:200 BUV563
anti-mouse CD4 Flow cytometry BD Biosciences Cat# 565974 GK1.5 2018458 1:200 BUV395
anti-mouse IFN-g Flow cytometry Thermo Fisher Cat# 48-7311-82 XMG1.2 2446926 1:100 eFluor450
anti-mouse CD45 Flow cytometry Tonbo Cat# 80-0451-U100 30-F11 C0451012119803 1:200 redFluor710
anti-mouse CD107a (LAMP-1) Flow cytometry Biolegend Cat# 121624 1D4B B323778 1:100 PE/Dazzle 594
anti-mouse Ly6G NK enrichment Bio X Cell Cat# BE0075-1 1A8 1:100
anti-mouse CD19 NK enrichment Bio X Cell Cat# BE0150 1D3 1:100
anti-mouse CD3ε NK enrichment Bio X Cell Cat# BE0002 17A2 1:100
anti-mouse CD8α NK enrichment Bio X Cell Cat# BE0061 2.43 1:100
anti-mouse CD4 NK enrichment Bio X Cell Cat# BE0003-1 GK1.5 1:100
anti-mouse Ter-119 NK enrichment Bio X Cell Cat# BE0183 TER-119 1:100
anti-mouse NK1.1 Flow cytometry Tonbo Cat# 65-5941 PK136 CSa41071720653 1:100 PECy5.5
anti-mouse NKp46 Flow cytometry Biolegend Cat# 137604 29A1.4 B336719 1:100 PE
anti-mouse CD49b Flow cytometry BioLegend Cat# 108918 DX5 B34a580 1:100 Pacific Blue
Rat anti-mouse CD16/CD32 Flow cytometry BD Biosciences Cat# 553142 clone 2.4G2 (RUO) 6148596 1/1000
Rat anti-Ki67 IF Invitrogen Cat# 14-5698-80 SolA15 2496198 1:100
Mouse anti-Vimentin IF, IHC Abcam Cat# ab8069 V9 GR3379996-2 1:500 (IF), 1:200 (IHC)
Chicken anti-GFP IF Aves Labs Cat# GFP-1010 GFP3717982 1:250
Rabbit anti-STING IF, IHC, western blot Cell Signaling Technologies Cat# 13647 D2P2F 5 1:500 (IHC), 1:250 (IF)
Goat anti-CCL5/RANTES IF Novus Biologicals Cat# AF278(human), AF478 (mouse) "mouse: AD50520061
human: WJ0519061" 1:40
Rabbit anti-CD3ε IF Cell Signaling Technologies Cat# 99940S D4V8L 1 1:200
Goat anti-mouse NKp46/NCR1 IF R&D Systems Cat#AF2225 KWW0418011 1:250
Rat anti-Cytokeratin 8 IF Millipore Sigma Cat# MABT329 TROMA-1 3855211 1:100
goat anti-chicken 488 IF Thermo Fisher Scientific Cat# A-11039 1555387 1:500
goat anti-rat 647 IF Thermo Fisher Scientific Cat# A-21247 2420724 1:500
goat anti-rabbit 594 IF Thermo Fisher Scientific Cat# A-11012 2433881 1:500
goat anti-mouse 488 IF Thermo Fisher Scientific Cat# A-11001 1789729 1:500
donkey anti-mouse 488 IF Thermo Fisher Scientific Cat# A-21202 2090565 1:500
donkey anti-rat 647 IF Abcam Cat# ab150155 WB322626 1:500
donkey anti-goat 594 IF Thermo Fisher Scientific Cat# A-11058 2045324 1:500
donkey anti-chicken 488 IF Biotium Cat# 20166 20C1016 1:500
β-actin western blot Cell Signaling Technologies Cat# 3700 8H10D10 15 1:500
mouse anti-human cytokeratin (AE1/AE3) IF Agilent Technologies Cat# M351529-2 AE1/AE3 11313304 1:100
rat anti-SOX2 IF Thermo Fisher Scientific Cat# 14-9811-82 Btjce 2357438 1:200
rabbit anti-SOX9 IF Millipore Sigma Cat# AB5535 3813922 1:300
rabbit anti-mCherry IF Abcam Cat# ab167453 GR3297302-3 1:500
Rabbit Anti-trimethyl-Histone H3 (Lys4) CHIP Millipore Sigma Cat# 05-745 15-10C-E4 3158071 5ug/sample
Rabbit Anti-trimethyl-Histone H3 (Lys27) CHIP Millipore Sigma Cat# 07-449 2194165 10ug/sample
Rabbit anti-Histone H3 (mono methyl K4) CHIP Abcam Cat# ab8895 GR3283215-1 5ug/sample
Rabbit Anti-H3K27ac CHIP Active Cat# 39133 6921014 5ug/sample
mouse Anti-DNMT1 CHIP Abcam Cat# ab13537 60B1220.1 5ug/sample
rabbit anti-DNMT3B CHIP Cell Signaling Technologies Cat# 57868S E8A8A 1 5ug/sample
anti-mouse NK1.1 Immune depletion in mouse Bio X Cell Cat# BE0036 clone PK136 796521N1 200ug/mouse
anti-mouse CD4 Immune depletion in mouse Bio X Cell Cat# BE0003-1 clone GK1.5 798421M1B 200ug/mouse
anti-mouse CD8α Immune depletion in mouse Bio X Cell Cat# BE0004-1 clone 53-6.7 792821J3 200ug/mouse
anti-mouse IgG2a control Immune depletion in mouse Bio X Cell Cat# BE0089 clone 2A3 815021S1 200ug/mouse

rabbit anti-asialo-GM1 Immune depletion in mouse Wako Chemical Cat# 986-10001 AQK0011 33ug/mouse
mouse IgG1 isotype control meDIP Cell Signaling Technologies Cat# 5415 G3A1 10 3ug/sample
mouse 5-methylcytosine meDIP Diagenode C15200081-100 clone 33D3 RD-005 3ug/sample
IRDye 680RD goat anti-mouse Western blot LI-COR Biosciences Cat# 926-68070 D20427-25 1:10000
IRDye 800CW goat anti-rabbit Western blot LI-COR Biosciences Cat# 926-32211 D20621-05 1:10000

Validation

Validation statement for each primary antibody is provided on the manufacturer's website.
antibody website
anti-mouse NKp46 https://www.biolegend.com/nl-be/products/brilliant-violet-421-anti-mouse-cd335-nkp46-antibody-7506?GroupID=BLG8849
anti-mouse CD44 https://www.biolegend.com/nl-nl/search-results/brilliant-violet-711-anti-mouse-human-cd44-antibody-10316
anti-mouse XCR1 https://www.biolegend.com/fr-fr/products/brilliant-violet-650-anti-mouse-rat-xcr1-antibody-12421
anti-mouse TCRb https://www.southernbiotech.com/hamster-anti-mouse-tcrb-pe-cy5-5-h57-597-1785-16
anti-mouse TCRb https://www.biolegend.com/en-us/products/apc-cyanine7-anti-mouse-tcr-beta-chain-antibody-4137?GroupID=BLG6994
anti-mouse CD11c https://www.biolegend.com/fr-ch/products/pe-cyanine7-anti-mouse-cd11c-antibody-3086
anti-mouse CD19 https://www.biolegend.com/en-us/search-results/apc-cyanine7-anti-mouse-cd19-antibody-3903
anti-mouse TNFa https://www.biolegend.com/nl-be/sean-tuckers-tests/apc-anti-mouse-tnf-alpha-antibody-975
anti-mouse CD49b https://www.bdbiosciences.com/en-us/products/reagents/flow-cytometry-reagents/research-reagents/single-color-antibodies-ruo/BUV661-Hamster-Anti-Mouse-CD49b.741523
anti-mouse NK1.1 https://www.bdbiosciences.com/en-us/products/reagents/flow-cytometry-reagents/research-reagents/single-color-antibodies-ruo/buv805-mouse-anti-mouse-nk-1-1.741926
anti-mouse CD8a https://www.bdbiosciences.com/en-us/products/reagents/flow-cytometry-reagents/research-reagents/single-color-antibodies-ruo/buv563-rat-anti-mouse-cd8a.748535
anti-mouse CD4 https://www.bdbiosciences.com/en-us/products/reagents/flow-cytometry-reagents/research-reagents/single-color-antibodies-ruo/buv395-rat-anti-mouse-cd4.565974
anti-mouse IFN-g https://www.thermofisher.com/antibody/product/IFN-gamma-Antibody-clone-XMG1-2-Monoclonal/48-7311-82
anti-mouse CD45 https://tonbobio.com/products/redfluor-710-anti-mouse-cd45-30-f11
anti-mouse CD107a (LAMP-1) https://www.biolegend.com/nl-nl/products/pe-dazzle-594-anti-mouse-cd107a-lamp-1-antibody-13156

anti-mouse Ly6G https://bioxcell.com/invivomab-anti-mouse-ly6g-be0075-1
anti-mouse CD19 https://bioxcell.com/invivomab-anti-mouse-cd19-be0150
anti-mouse CD3ε https://bioxcell.com/invivomab-anti-mouse-cd3-be0002
anti-mouse CD8α https://bioxcell.com/invivomab-anti-mouse-cd8a-be0061
anti-mouse CD4 https://bioxcell.com/invivomab-anti-mouse-cd4-be0003-1
anti-mouse Ter-119 https://bioxcell.com/invivomab-anti-mouse-ter-119-be0183
anti-mouse NK1.1 https://cytekbio.com/products/percp-cyanine5-5-anti-mouse-nk1-1-cd161-pk136?variant=40581194285092
anti-mouse NKp46 https://www.biolegend.com/en-us/products/pe-anti-mouse-cd335-nkp46-antibody-6523
anti-mouse CD49b https://www.biolegend.com/fr-lu/products/pacific-blue-anti-mouse-cd49b-pan-nk-cells-antibody-6571?GroupID=BLG4896
Rat anti-mouse CD16/CD32 https://www.bdbiosciences.com/en-us/products/reagents/flow-cytometry-reagents/research-reagents/single-color-antibodies-ruo/purified-rat-anti-mouse-cd16-cd32-mouse-bd-fc-block.553142
Rat anti-Ki67 https://www.thermofisher.com/antibody/product/Ki-67-Antibody-clone-SolA15-Monoclonal/14-5698-82
Mouse anti-Vimentin https://www.abcam.com/vimentin-antibody-v9-cytoskeleton-marker-ab8069.html
Chicken anti-GFP https://www.aveslabs.com/products/anti-green-fluorescent-protein-antibody-gfp
Rabbit anti-STING https://www.cellsignal.com/products/primary-antibodies/sting-d2p2f-rabbit-mab/13647
Goat anti-CCL5/RANTES https://www.rndsystems.com/products/mouse-ccl5-rantes-antibody_af478, https://www.rndsystems.com/products/human-ccl5-rantes-antibody_af-278-na
Rabbit anti-CD3ε https://www.cellsignal.com/products/primary-antibodies/cd3e-d4v8l-rabbit-mab/99940
Goat anti-mouse NKp46/NCR1 https://www.rndsystems.com/products/mouse-nkp46-ncr1-antibody_af2225
Rat anti-Cytokeratin 8 https://www.emdmillipore.com/US/en/product/Anti-Cytokeratin-8-Antibody-clone-TROMA-1,MM_NF-MABT329
goat anti-chicken 488 https://www.thermofisher.com/antibody/product/Goat-anti-Chicken-IgY-H-L-Secondary-Antibody-Polyclonal/A-11039
goat anti-rat 647 https://www.thermofisher.com/antibody/product/Goat-anti-Rat-IgG-H-L-Cross-Adsorbed-Secondary-Antibody-Polyclonal/A-21247
goat anti-rabbit 594 https://www.thermofisher.com/antibody/product/Goat-anti-Rabbit-IgG-H-L-Cross-Adsorbed-Secondary-Antibody-Polyclonal/A-11012
goat anti-mouse 488 https://www.thermofisher.com/antibody/product/Goat-anti-Mouse-IgG-H-L-Cross-Adsorbed-Secondary-Antibody-Polyclonal/A-11001
donkey anti-mouse 488 https://www.thermofisher.com/antibody/product/Donkey-anti-Mouse-IgG-H-L-Highly-Cross-Adsorbed-Secondary-Antibody-Polyclonal/A-21202
donkey anti-rat 647 https://www.abcam.com/donkey-rat-igg-hl-alexa-fluor-647-preadsorbed-ab150155.html
donkey anti-goat 594 https://www.thermofisher.com/antibody/product/Donkey-anti-Goat-IgG-H-L-Cross-Adsorbed-Secondary-Antibody-Polyclonal/A-11058
donkey anti-chicken 488 https://biotium.com/product/donkey-anti-chicken-igy-igg-hl-highly-cross-adsorbed/
β-actin https://www.cellsignal.com/products/primary-antibodies/b-actin-8h10d10-mouse-mab/3700
mouse anti-human cytokeratin (AE1/AE3) https://www.agilent.com/en/product/immunohistochemistry/antibodies-controls/primary-antibodies/cytokeratin-%28concentrate%29-76562
rat anti-SOX2 https://www.thermofisher.com/antibody/product/SOX2-Antibody-clone-Btjce-Monoclonal/14-9811-82
rabbit anti-SOX9 https://www.emdmillipore.com/US/en/product/Anti-Sox9-Antibody,MM_NF-AB5535
rabbit anti-mCherry https://www.abcam.com/mcherry-antibody-ab167453.html
Rabbit Anti-trimethyl-Histone H3 (Lys4) https://www.emdmillipore.com/US/en/product/Anti-trimethyl-Histone-H3-Lys4-Antibody-clone-15-10C-E4-rabbit-monoclonal,MM_NF-05-745R?ReferrerURL=https%3A%2F%2Fwww.google.com%2F
Rabbit Anti-trimethyl-Histone H3 (Lys27) https://www.emdmillipore.com/US/en/product/Anti-trimethyl-Histone-H3-Lys27-Antibody,MM_NF-07-449
Rabbit anti-Histone H3 (mono methyl K4) https://www.abcam.com/histone-h3-mono-methyl-k4-antibody-chip-grade-ab8895.html?productWallTab=ShowAll
Rabbit Anti-H3K27ac https://www.activemotif.com/catalog/details/39133/histone-h3-acetyl-lys27-antibody-pab
mouse Anti-DNMT1 https://www.abcam.com/dnmt1-antibody-60b12201-ab13537.html
rabbit anti-DNMT3B https://www.cellsignal.com/products/primary-antibodies/dnmt3b-e8a8a-xp-rabbit-mab/57868
anti-mouse NK1.1 https://bioxcell.com/invivomab-anti-mouse-nk1-1-be0036
anti-mouse CD4 https://bioxcell.com/invivomab-anti-mouse-cd4-be0003-1
anti-mouse CD8α https://bioxcell.com/invivomab-anti-mouse-cd8a-be0004-1
anti-mouse IgG2a control https://bioxcell.com/invivomab-rat-igg2a-isotype-control-anti-trinitrophenol-be0089
rabbit anti-asialo-GM1 https://labchem-wako.fujifilm.com/us/product/detail/W01W0198-1000.html
mouse IgG1 isotype control https://www.cellsignal.com/products/primary-antibodies/mouse-g3a1-mab-igg1-isotype-control/5415
mouse 5-methylcytosine https://www.diagenode.com/en/p/5-mc-monoclonal-antibody-33d3-premium-100-ug-50-ul
IRDye 680RD goat anti-mouse https://www.licor.com/bio/reagents/irdye-680rd-goat-anti-mouse-igg-secondary-antibody
IRDye 800CW goat anti-rabbit https://www.licor.com/bio/reagents/irdye-800cw-goat-anti-rabbit-igg-secondary-antibody

Eukaryotic cell lines

Policy information about cell lines

Cell line source(s)	Mouse lung cancer cell line KP-482T1 was a gift from T. Jacks (MIT). Mouse KPad1 cell line was generated from KrasLSL-G12D/+;Trp53flox/flox mice. Human bronchial/tracheal epithelial cells (NHBE) were purchased from Lonza (Cat# CC-2540). A549 cells were purchased from ATCC. H2087 (ATCC)-LCC derivatives were isolated as described in Malladi et al. 2016, Cell. H2030 (ATCC)-BrM derivative was isolated as described in Nguyen et al. 2009, Cell. H2087-LCC derived spontaneous outbreak cell lines (SO) were generated from spontaneous metastases in mice inoculated intracardially with H2087-LCC cells.
Authentication	KPad1 and KP-482T1 cell lines were genotyped to verify the presence of KrasG12D and Tp53 mutations using PCR amplification. A549, H2087-LCC, and H2030-BrM cells were authenticated with STR profiling. Human bronchial/tracheal epithelial cells (NHBE) was not authenticated.

Mycoplasma contamination	All cell lines tested negative for mycoplasma contamination.
Commonly misidentified lines (See ICLAC register)	None of the cell lines used are listed as commonly misidentified lines in the ICLAC database.

Animals and other organisms

Policy information about studies involving animals; ARRIVE guidelines recommended for reporting animal research

Laboratory animals	Athymic nude (Foxn1nu, stock 069) mice were obtained from Envigo. NSG (NOD.Cg-PrkdcscidIL2rgtm1Wjl/SzJ, stock 005557), C57BL/6J (stock 000664), and B6(Cg)-Tyrc-2J/J (B6-albino, stock 000058) mouse strains were obtained from The Jackson Laboratory. Female mice from 6 to 8 weeks of age were used for the study. Animals were housed under the following conditions: temperatures of 21.1-22.2 °C (70-72 °F), 30%-70% humidity, 10-15 fresh air exchanges hourly, and a 12-12 hour light-dark cycle (lights were on from 0600-1800).
Wild animals	The study did not involve wild animals.
Field-collected samples	The study did not involve samples collected in the field.
Ethics oversight	All animal experiments were performed in accordance with protocols approved by the Memorial Sloan Kettering Cancer Center Institutional Animal Care and Use Committee (IACUC).

Note that full information on the approval of the study protocol must also be provided in the manuscript.

Human research participants

Policy information about studies involving human research participants

Population characteristics	Lung cancer primary tumor and metastatic samples were obtained from patients confirmed Stage II, III, or IV lung cancer. Patients were both male and female, with an age range of 56-81 at recruitment. Four pairs of tissues from primary tumor and metastases were collected at autopsy (non-human subject by NIH definition). Patients/samples were selected based on the availability of a sufficient quantity of formalin-fixed paraffin-embedded tissue from patients who had given preoperative consent to tissue utilization for research purposes.
Recruitment	There were no recruitment biases to impact the results of our analyses
Ethics oversight	Human specimens were obtained and approved under Memorial Sloan Kettering Cancer Center Institutional Review Board biospecimen research protocol 17-239. All patients provided pre-procedure informed consent.

Note that full information on the approval of the study protocol must also be provided in the manuscript.

ChIP-seq

Data deposition

☒ Confirm that both raw and final processed data have been deposited in a public database such as GEO.

☒ Confirm that you have deposited or provided access to graph files (e.g. BED files) for the called peaks.

Data access links *May remain private before publication.*	ChIP-seq data have been deposited in the GEO under accession number GSE210946.
Files in database submission	RAW FILES: H2087-LCC_H3K27ac_bio rep 1_IGO_08749_C_31_S164_L003_R1_001.fastq.gz H2087-LCC_H3K27ac_bio rep 2_IGO_08749_D_1_S133_L003_R1_001.fastq.gz H2087-LCC_H3K4me1_IGO_08749_C_1_S266_L004_R1_001.fastq.gz H2087-LCC_H3K4me3_IGO_08749_C_7_S273_L004_R1_001.fastq.gz H2087-LCC_input_bio rep 1_IGO_08749_C_25_S85_L003_R1_001.fastq.gz H2087-LCC_input_bio rep 2_IGO_08749_D_5_S129_L003_R1_001.fastq.gz H2087-LCC-TGFb_H3K27ac_IGO_08749_D_2_S128_L003_R1_001.fastq.gz H2087-LCC-TGFb_H3K4me1_IGO_08749_C_2_S268_L004_R1_001.fastq.gz H2087-LCC-TGFb_H3K4me3_IGO_08749_C_8_S274_L004_R1_001.fastq.gz H2087-LCC-TGFb_input_IGO_08749_C_26_S86_L003_R1_001.fastq.gz H2087-LCC-SO1_H3K27ac_IGO_08749_C_15_S262_L004_R1_001.fastq.gz H2087-LCC-SO1_H3K4me1_IGO_08749_C_3_S269_L004_R1_001.fastq.gz H2087-LCC-SO1_H3K4me3_IGO_08749_C_9_S275_L004_R1_001.fastq.gz H2087-LCC-SO1_input_IGO_08749_C_27_S87_L003_R1_001.fastq.gz H2030_H3K27ac_IGO_08749_C_16_S263_L004_R1_001.fastq.gz H2030_H3K4me1_IGO_08749_C_4_S270_L004_R1_001.fastq.gz H2030_H3K4me3_IGO_08749_C_10_S258_L004_R1_001.fastq.gz H2030_input_IGO_08749_C_28_S88_L003_R1_001.fastq.gz H2087-LCC_H3K27ac_bio rep 1_IGO_08749_C_31_S164_L003_R2_001.fastq.gz

H2087-LCC_H3K27ac_bio rep 2_IGO_08749_D_1_S133_L003_R2_001.fastq.gz
H2087-LCC_H3K4me1_IGO_08749_C_1_S266_L004_R2_001.fastq.gz
H2087-LCC_H3K4me3_IGO_08749_C_7_S273_L004_R2_001.fastq.gz
H2087-LCC_input_bio rep 1_IGO_08749_C_25_S85_L003_R2_001.fastq.gz
H2087-LCC_input_bio rep 2_IGO_08749_D_5_S129_L003_R2_001.fastq.gz
H2087-LCC-TGFb_H3K27ac_IGO_08749_D_2_S128_L003_R2_001.fastq.gz
H2087-LCC-TGFb_H3K4me1_IGO_08749_C_2_S268_L004_R2_001.fastq.gz
H2087-LCC-TGFb_H3K4me3_IGO_08749_C_8_S274_L004_R2_001.fastq.gz
H2087-LCC-TGFb_input_IGO_08749_C_26_S86_L003_R2_001.fastq.gz
H2087-LCC-SO1_H3K27ac_IGO_08749_C_15_S262_L004_R2_001.fastq.gz
H2087-LCC-SO1_H3K4me1_IGO_08749_C_3_S269_L004_R2_001.fastq.gz
H2087-LCC-SO1_H3K4me3_IGO_08749_C_9_S275_L004_R2_001.fastq.gz
H2087-LCC-SO1_input_IGO_08749_C_27_S87_L003_R2_001.fastq.gz
H2030_H3K27ac_IGO_08749_C_16_S263_L004_R2_001.fastq.gz
H2030_H3K4me1_IGO_08749_C_4_S270_L004_R2_001.fastq.gz
H2030_H3K4me3_IGO_08749_C_10_S258_L004_R2_001.fastq.gz
H2030_input_IGO_08749_C_28_S88_L003_R2_001.fastq.gz

PROCESSED DATA FILES:
H2087-LCC_H3K27ac_bio rep 1.bigwig
H2087-LCC_H3K27ac_bio rep 2.bigwig
H2087-LCC_H3K4me1.bigwig
H2087-LCC_H3K4me3.bigwig
H2087-LCC_input_bio rep 1.bigwig
H2087-LCC_Input_bio rep 2.bigwig
H2087-LCC-TGFb_H3K27ac.bigwig
H2087-LCC_TGFb_H3K4me1.bigwig
H2087-LCC_TGFb_H3K4me3.bigwig
H2087-LCC_TGFb_input.bigwig
H2087-LCC-SO1_H3K27ac.bigwig
H2087-LCC-SO1_H3K4me1.bigwig
H2087-LCC-SO1_H3K4me3.bigwig
H2087-LCC-SO1_input.bigwig
H2030_H3K27ac.bigwig
H2030_H3K4me1.bigwig
H2030_H3K4me3.bigwig
H2030_input.bigwig

H2087-LCC_H3K27ac_bio rep 1_summits.bed
H2087-LCC_H3K27ac_bio rep 2_summits.bed
H2087-LCC_H3K4me1_C_summits.bed
H2087-LCC_H3K4me3_C_summits.bed
H2087-LCC_TGFb_H3K27ac_summits.bed
H2087-LCC_TGFb_H3K4me1_summits.bed
H2087-LCC_TGFb_H3K4me3_summits.bed
H2087-LCC-SO1_H3K27ac_summits.bed
H2087-LCC-SO1_H3K4me1_summits.bed
H2087-LCC-SO1_H3K4me3_summits.bed
H2030_H3K27ac_summits.bed
H2030_H3K4me1_summits.bed
H2030_H3K4me3_summits.bed

Genome browser session
(e.g. UCSC)

N/A

Methodology

Replicates

ChIP-seq experiments were performed 1 or 2 times, and confirmed with ChIP-PCR.

Sequencing depth

50 bp paired-end sequencing was performed to obtain 45 million read depth.

Antibodies

Antibodies against H3K4me3 (Millipore Sigma, Cat# 05-745, 5 µg per sample), H3K4me1 (Abcam, Cat# ab8895, 5 µg per sample), H3K27Ac (Active Motif, Cat# 39133, 5 µg per sample), DNMT1 (Abcam, Cat# ab13537, 5 µg per sample), DNMT3B (Cell Signaling Technologies, Cat# 57868S, 5 µg per sample)

Peak calling parameters

For mapping and visualization, paired-end (50/50 bp) FASTQ reads were mapped to human genome hg19 using Bowtie2 with default filtering criteria. Resulted SAM files were converted to BAM files though Samtools. BAM files were sorted and indexed with Samtools. BAM files were normalized, converted to bigwig files using bamCoverage-deepTools and displayed with IGV browser. Peak calling from BAM files was performed with MACS v 2.2.7.1.

Data quality

Details of data analysis and quality assurance are in the methods section.

Software

For QC: FastQC
For alignment: Bowtie2

For ChIPseq sorting, normalization, and visualization: Samtools, bamCoverage-deepTools & IGV
For peak calling: MACS

Flow Cytometry

Plots

Confirm that:

☒ The axis labels state the marker and fluorochrome used (e.g. CD4-FITC).

☒ The axis scales are clearly visible. Include numbers along axes only for bottom left plot of group (a 'group' is an analysis of identical markers).

☒ All plots are contour plots with outliers or pseudocolor plots.

☒ A numerical value for number of cells or percentage (with statistics) is provided.

Methodology

Sample preparation	For immune phenotyping of metastases-bearing femurs, tissues were washed in PBS, then chopped into small pieces using a sterile razor blade and resuspended in 5 mL of digestion buffer containing 1 mg/mL collagenase D (Millipore Sigma, Cat# 11088866001) and 0.05 mg/mL DNase in RPMI media. After incubation at 37°C for 40 min, the tissue sample was passed through a 70 µm strainer, spun down, and processed in 1x eBioscience™ 10X red blood cell lysis buffer (Thermo Fisher Scientific, Cat# 00-4300-54). Cells were washed and resuspended with stain media (PBS supplemented with 2% FBS) that contained fixable viability dye eFluor 506 (Thermo Fisher Scientific, Cat# 65-0866-14), anti-mouse CD16/32 antibodies (clone 2.4G2, BioXCell, Cat# BE0307), and antibodies specific for proteins of interest. Cells were stained for surface proteins for 25 min at 4C, washed, and stained for intracellular proteins according to the FoxP3/Transcription Factor Staining Buffer Set instructions (Thermo Fisher Scientific, Cat# 00-5523-00). Stained cells were washed and resuspended in stain media that contained a known number of 123count eBeads (Thermo Fisher Scientific, Cat# 01-1234-42) to calculate absolute cell number.
Instrument	Analysis was performed on a BD Fortessa (BD Biosciences) or a Cytek Aurora instrument (Cytek Biosciences). Flow sorting was performed using a BD FACSAria II or BD Aria III cytometer (BD Bosciences) fitted with a 100 µm nozzle.
Software	Data were analyzed using FlowJo.
Cell population abundance	For sorting experiments, if performed, post-sort purity was >90%.
Gating strategy	Leukocytes were gated as CD45+ cells, cDC1 cells were gated as CD45+CD19-TCRβ-XCR1+CD11c+ cells, NK cells were gated as CD45+NK1.1+TCRβ-CD49b+NKp46+ cells, T cells were gated as CD45+TCRβ+NK1.1-CD8+ T cells, or CD45+TCRβ+NK1.1-CD4+ T cells.

☒ Tick this box to confirm that a figure exemplifying the gating strategy is provided in the Supplementary Information.